Order number: 41871

Design Methodology of Antennas Based on Metamaterials and the Theory of Characteristic Modes: Application to Cognitive Radio

DOCTORAL THESIS[1]

Presented in partial fulfilment of the requirements for the degree of Doctor of Philosophy in

Lille University of Science and Technology

By

M.Hassanein RABAH

Defense on 24 November 2015

THESIS COMMITTEE

Christophe CRAEYE	*Prof. at Polytechnic School of Louvain*	—Reviewer
Xavier BEGAUD	*Prof. at TELECOM Paris Tech*	—Reviewer
Marta CABEDO FABRÈS	*Prof. at the Polytechnic University of Valencia*	—Examiner
Jalal JOMAAH	*Prof. at the Lebanease University*	—Examiner
Eddy JEHAMY	*Dr.-Ing at Altair Engineering, Inc.*	—Invited
Divitha SEETHARAMDOO	*Researcher at IFSTTAR*	—Thesis Supervisor
André DE LUSTRAC	*Prof. at Paris Sud University*	—Thesis Director
Marion BERBINEAU	*Research Director at IFSTTAR*	—Thesis Director

[1]Doctoral School: Sciences Pour Ingénieur (EDSPI 072)
Diploma title: Micro and Nano Technologies, Acoustics and Telecommunications

© 2015 Tous droits réservés.

−Abstract

The rise of wireless communication systems and the big demand of high bit rate links have entailed researches to move towards new diverse communications systems. With this diversity of wireless systems, flexibility for operating between different standards is strongly needed. Cognitive radio (CR) consists the future system that can offer this flexibility. The requirements of CR systems induce several challenges for antenna designers such as miniaturization, isolation and bandwidth enhancement. Especially when the geometry of the antenna becomes more complex in order to fit the terminal chassis. In this thesis we consider the use of metamaterials (MTM) to overcome physical limitations to address these challenges. The analysis of MTM in the presence of radiating elements such as antennas proves to be a challenge. We propose a new approach to address these challenges. It is based on a modal concept using the theory of characteristic modes (TCM). It is applied to analyse and design electrically small antenna (ESA), metamaterial-inspired antennas and metamaterial-based antennas. The same approach is used to evaluate the antenna performances when surrounded by complex artificial materials by proposing closed-form formulas for the quality factor. A novel approach for systematic design of metamaterial inspired antenna has been introduced and validated on canonical antennas. Finally, it is applied to improve the efficiency of an extremely-wide-band antenna for underlay CR (sensing antenna) in the electrically small regime. The antenna has been fabricated and tested experimentally.

Keywords: Artificial magnetism, theory of characteristic modes, antenna miniaturization, metamaterials, cognitive radio, extremely-wide-band antenna, small antennas, spectrum sensing antenna, TVWS, arbitrary-shaped antenna, Q factor.

© 2015 Tous droits réservés.

Thèse de Mhamad Hassanein Rabah, Lille 1, 2015

−Résumé

C'est dans la course au débit que de differentes systèmes de communications sans fil sont proposés aujourd'hui. À ce jour il n'existe pas de technologie ou de standard unique pour remplacer toutes les autres technologies radio tout en satisfaisant l'ensemble des besoins de services et d'usages. Les futurs systèmes de communications devront donc permettre l'interopérabilité entre les différents standards au niveau européen et mondial. L'émergence des technologies de la radio intelligente constitue aujourd'hui une solution originale et prometteuse pour répondre à ce defi. Cependant, le déploiement de ces systèmes soulève encore de nombreux défis techniques notamment au niveau des antennes. Ces dernières doivent en particulier être capables de modifier leurs réponses en fréquences ou bien avoir une très large bande tout en minimisant la déformation des formes d'ondes. Elles doivent répondre aux besoins de cohabitation multi-systèmes et de miniaturisation. Or la miniaturisation et la largeur de bande sont limités par des contraintes physiques et les caractéristiques des matériaux les constituant. Les métamatériaux, des composites électromagnétiques artificiels, peuvent permettre la conception d'éléments rayonnants pour la radio intelligente avec un plus grand degré de liberté et à moindre coût. Cependant l'analyse de l'association des métamatériaux à des antennes ou éléments rayonnants n'est pas aisé, surtout quand les antennes prennent une forme arbitraire. En effet, les techniques classiques de conception d'antennes peuvent être très longue a mettre en oeuvre. Pour cela, nous proposons dans ce travail une approche basée sur le concept modale se basant sur la théorie des modes caractéristiques. Cette approche présente un potentiel remarquable dans la conception des antennes éléctriquement petites ainsi que les antennes basées/inspirées des métamatériaux. En outre, l'évaluation des performances d'antennes à formes arbitraires en fonction des paramètres géométriques à été démontré sans considérer d'éxcitation. Ceci offre un énorme avantage pour les techniques basées sur l'optimisation des formes d'antennes. Une technique de conception systématique d'antennes inspirées des métamatériaux est proposée et validée sur des antennes canoniques. Finalement, elle est appliquée à une antenne très large bande dediée au sondage du spectre. L'approche modale a été utilisée afin de garantir un diagramme du rayonnement stable sur toute la bande de fréquence ainsi qu'une bonne efficacité dans le régime éléctriquement petit. Plusieurs validations expérimentales sont également presentées.

Mots Clef: Radio intelligente, radio cognitive, antennes éléctriquement petites, métamatériaux, modes caractéristiques, magnétisme artificiel, facteur de qualité.

© 2015 Tous droits réservés. doc.univ-lille1.fr

Thèse de Mhamad Hassanein Rabah, Lille 1, 2015

Related publications

Patents

1. **M.H. RABAH**, D. SEETHARAMDOO; H. Srour, M. BERBINEAU, "Antenne très large bande à efficacité améliorée par l'utilisation de métamatériau : procédé de conception et prototype", (Pending).

Journal papers

1. **M.H. RABAH**, D. SEETHARAMDOO, R. ADDACI, M. BERBINEAU, "Novel miniature extremely-wide-band antenna with stable radiation pattern for spectrum sensing applications" **IEEE Antennas and Wireless Propagation Letters**, vol., no.99, pp.1,1, 2015.

2. **M.H. RABAH**, D. SEETHARAMDOO, A. DE LUSTRAC, M. BERBINEAU, "New Metrics for Artificial Magnetism from Metal-dielectric Metamaterial Based on The Theory of Characteristic Modes", **IEEE Antennas and Wireless Propagation Letters**. 10.1109/LAWP.2015.2452269 (InPress).

3. **M.H. RABAH**, D. SEETHARAMDOO, A. DE LUSTRAC, M. BERBINEAU, "Analysis of Miniature Metamaterial and Magneto-Dielectric Arbitrary Shaped Patch Antennas Using Characteristic Modes: Evaluation of the Q-Factor" Submitted on July 2015 to **IEEE Transactions on Antennas and Propagation** (Under Review).

4. **M.H. RABAH**, D. SEETHARAMDOO, A. DE LUSTRAC, M. BERBINEAU, "On the Association of Arbitrary Shaped Driven Antennas with Resonant Parasitic Metamaterial Inclusions" Manuscript in Preparation for Submission to **IEEE Transactions on Antennas and Propagation**.

5. **M.H. RABAH**, D. SEETHARAMDOO, A. DE LUSTRAC, M. BERBINEAU, "Q-Factor calculation of a Totally Arbitrary Shaped Antennas" Manuscript in Preparation for Submission to **IET Electronics letters**.

© 2015 Tous droits réservés.

doc.univ-lille1.fr

Communications

1. **M.H. Rabah** and D. Seetharamdoo "Calculation of the Total Q-Factor for Electrically Small Antennas with Metamaterials Using Characteristic Modes" accepted for presentation at the **Antennas and Propagation (EuCAP), 2016 10th European Conference** in Davos, Switzerland, April 2016.

2. **M.H. Rabah** and D. Seetharamdoo: "Analysis of Metamaterial Inclusions Using Characteristic Modes", **International Workshop on Metamaterials-by-Design** 03 December 2015. Supelec, Saclay-Paris.

3. **M.H. RABAH**, D. SEETHARAMDOO, M. BERBINEAU, "Modal Study of Electrically Small Patch Antennas on Dielectric, Magnetic and Reactive Impedance Metamaterial Substrates" 2014 **Loughborough Antennas & Propagation Conference 10th & 11th November 2014** Burleigh Court International Conference Centre pp. 545-548, Loughborough, UK.

4. **M.H. RABAH**, D. SEETHARAMDOO, A. DE LUSTRAC, M. BERBINEAU, "Analysis of metamaterial inclusions for association with radiating elements using the theory of characteristic modes," **Antennas and Propagation (EuCAP), 2014 8th European Conference**, vol., no., pp.927, 930, 6-11 April 2014.

5. **M.H. RABAH**, D. SEETHARAMDOO, R. ADDACI, M. BERBINEAU, "Future Communication Systems: Cognitive radios from antenna Point of View". **20th Conference of the Lebanese association for advanced sciences, LAAS20**, Hadath, Lebanon.

6. **M.H. RABAH**, D. SEETHARAMDOO, R. ADDACI, M. BERBINEAU, "A Miniaturized EWB Antenna for spectrum sensing applications" **Antennas and Propagation Society International Symposium (APSURSI), 2013 IEEE**, vol., no., pp.1750, 1751, 7-13 July 2013.

7. **M.H. RABAH**, D. SEETHARAMDOO, M. BERBINEAU, "Antennes miniatures pour la radio intelligente: sondage de spectre et liaison de communication", **secondes journées FRANCO-LIBANAISES, Avancées de la Recherche et de ses Applications**, 22-25 Octobre 2013, Université du Littoral Côte d'Opale-Dunkerque, France. 1p. (hal-00971737)

8. **M.H. RABAH**, D. SEETHARAMDOO, R. ADDACI, M. BERBINEAU, "Analysis and design of miniaturized extremely wide band antenna using characteristic mode theory", **Journées scientifiques de l'URSI-France 2013**, Paris 26-27 Mai 2013.

© 2015 Tous droits réservés.

Acknowledgements

Firstly, I would like to thank my thesis reviewers: Prof. Christophe Craeye from Université Catholique de Louvain and Prof. Xavier Begaud Télécom Paris Tech for their insightful comments and encouragement. I am also grateful to have them in my thesis committee.

Particular thanks goes to Prof. Marta Cabedo Fabrés from Universitat Politècnica de València for accepting to be a member of my PhD committee. I thanks here on behalf of me and many researchers for her contributions in the modern application of the theory of characteristic modes (the heart of this thesis) to antenna problems.

I thanks Prof. Jalal Jomaah from the Lebanese university for accepting to be an examiner of my thesis. I am grateful for the collaboration we have installed together with him and Dr. Hussam Ayad from the Lebanese university through the co-supervision of two Masters thesis.

Thanks for Dr. Eddy Jehamy from Altair engineering for being a member of my thesis committee. I thanks Eddy for advising me like my big brother since I was a Master student and during my internship with him at TRW-AUTOCRUISE.

It is my pleasant privilege to offer my sincere thanks to my supervisor and my friend Dr. Divitha Seetharamdoo from the French Institute of Science and Technology for Transport, Development and Networks (IFSTTAR) for the continuous support of my Ph.D study and related research, for her motivation, deep knowledge of Electromagnetics and demanding a high quality of work in all my endeavour. Her guidance helped me in all the time of research and writing of this thesis.

My thanks goes to the advisor of my thesis Prof. Marion Berbineau from IFSTTAR for providing me the intellectual freedom in my work, and supporting my attendance at various national and international conferences.

My thanks also goes to the co-advisor of my thesis Prof. André DE-LUSTRAC from Paris Sud university. I thanks him for his fruitful discussions and suggestions during meetings and conferences.

I would like to thank further the two Masters students I have supervised during my Ph.D: Hussein Srour and Maher Ayoub. Thank you for your contributions in the different research topics of this Ph.D.

I am also grateful to Jean Pierre Ghys from IFSTTAR, Lamine Koné and Pierre Laly from University Lille 1 for the technical support and for fabricating many antenna prototypes as well as performing measurements.

© 2015 Tous droits réservés.

doc.univ-lille1.fr

Thèse de Mhamad Hassanein Rabah, Lille 1, 2015

Thanks to the IFSTTAR , and the french region Nord-Pas-de-Calais for funding my Ph.D scholarship.

I thanks my colleagues in my Lab for the stimulating discussions, for the time we were working together before deadlines, and for all the fun we have had in the last three years. I particularly thanks Rafik, Cristophe, Liu, Adil, Nadjah, Owais, Raouf, Pierre and other PhD students in the Lab. Thanks also for all the members of ASP (Association des Sportives des Personnelles) Lille 1 for sharing football games every Wednesday!

Last but not the least, I would like to thank my family: my brothers and sister for supporting me spiritually throughout writing this thesis and my life in general.

Thank you Linda!

© 2015 Tous droits réservés.

doc.univ-lille1.fr

Contents

Abstract i

Résumé ii

Acknowledgements v

List of Figures x

List of Tables xvii

Abbreviations xviii

1 General Introduction 1
Cognitive radio and Antennas: 2
Objectives of this work 4
Organisation of the dissertation 5

2 Review of Cognitive Radio Antenna Solutions and Associated Physical Limitations 7
2.1 Introduction 7
2.2 Antenna Challenges in CR Systems 8
2.3 Review of CR Antenna Solutions 12
2.3.1 Review of antennas for spectrum interweave CR 12
2.3.2 Review of antennas for spectrum underlay CR 13
2.3.3 Summary 20
2.4 Physical limitations of Antennas 20
2.5 Metamaterial Based Antennas 22
2.6 Metamaterial Inspired Antennas 26
2.6.1 Magnetic-Based MTM Inspired Antenna 27
2.6.2 Electric-based MTM Inspired Antenna 28
2.7 Existing Antenna Solutions Using the Theory of Characteristic Modes . 29
2.8 Conclusion 31

3 Introducing TCM for Metamaterial Inclusions 32
3.1 Introduction 32
3.2 Formulations of The Theory of Characteristic modes and Computation Assumptions 33

© 2015 Tous droits réservés.

doc.univ-lille1.fr

3.2.1 Characteristic fields Orthogonality 34
3.2.2 Surface Current Decomposition and Associated Metrics 36
3.2.3 Active and Reactive Modal Powers 37
3.2.4 Characteristic Modes Computations and Assumptions 38
CMs for PEC objects: 39
CMs for composite (dielectric+metallic) objects: 39
Characteristic modes tracking: 40
3.3 New metrics validation for metamaterial inclusions 41
3.3.1 Application of new metrics to demonstrate an equivalence between magnetic artificial media 45
3.3.1.1 Discussion 46
3.4 Conclusion 47

4 Quality Factor Computation for ESAs using the TCM: Application to Metamaterial-Based and Arbitrary-Shaped Antennas 48
4.1 Introduction 48
4.2 State of the art on Electrically Small Antennas Quality Factor Calculation 50
4.3 State of the Art (Continued): Q Factor Based on TCM 54
4.4 Beyond State of The art: New Q Factor expression based -only- on Eigenvalues 60
4.5 Validation Of The Proposed Q Factor Expression For Arbitrary-Shaped Antenna 62
4.5.1 Modal Q Calculation for the IFSTTAR Antenna 63
4.5.2 Excitation of the IFSTTAR Antenna 65
4.6 Characteristic Modes Analysis of Patch Antennas over Metamaterial and Magneto-Dielectric Substrates 68
4.6.1 Considered Patch Antennas 68
4.6.2 Modal Significances Evaluation and Comparaison 71
4.6.3 Modal Q Factors Evaluation and Comparaison 73
4.6.3.1 Impact of the losses on $Q_{1,f_{1,res}}$ 74
4.7 Discussion 78
4.8 Conclusion 78

5 Metamaterial Inspired Antennas: Systematic Design Based on Characteristic Modes 80
5.1 Introduction 80
5.2 Methodology Proposed for the Design and Analysis of Metamaterial Inspired Antennas 81
5.2.1 Modes Selection 81
5.2.2 Near Field Dominant Energy Identification 82
5.2.3 Inclusion Analysis and Selection 83
5.3 Modal Study of Metamaterial Inspired Antennas 86
5.3.1 Modal Study of 2D Electric Based Antennas 86
5.3.1.1 Isolated Monopole 86
5.3.1.2 Isolated Meander Line 88
5.3.1.3 Monopole and Meander Line 89
5.3.1.4 Power and Quality Factor Calculations for the 2D Antenna 93

© 2015 Tous droits réservés.

Thèse de Mhamad Hassanein Rabah, Lille 1, 2015

5.3.2 Modal Study of 3D Magnetic Based Antennas 96
5.3.2.1 Isolated Semi-Loop 96
5.3.2.2 Isolated Capacitively-Loaded Loop 98
5.3.2.3 Semi-Loop with a Capacitively-Loaded Loop 99
5.3.2.4 Power and Quality Factor Calculations for the 3D Antenna 102
5.4 Discussion 104
5.5 Conclusion 105

6 Design of a Spectrum Sensing Antenna Using TCM 106
6.1 Introduction 106
6.2 Bandwidth Enhancement of a Spectrum Sensing Antenna Using TCM . 107
6.3 Power pattern stability enhancement of a spectrum sensing antenna using TCM 111
6.3.1 Experimental Results and Discussion: Part 1 113
6.4 Efficiency Enhancement With Metamaterials: EWB-MTM Antenna . . . 115
6.4.1 CMA of the EWB Antenna 116
6.4.2 Searching For the Right Inclusion 117
6.4.3 Experimental Results and Discussion: Part 2 121
6.5 Conclusion 125

7 Conclusions and Future Work 127
7.1 Main Contributions of the Thesis 127
7.2 Some Limitations 128
7.3 Further Work 129

Bibliography 130

© 2015 Tous droits réservés. doc.univ-lille1.fr

List of Figures

1.1 Classical cognitive radio cycle 2

2.1 Solutions proposed by FCC to the spectrum underutilization problem. 8
2.2 Schematic of whitespaces in the spectrum. 9
2.3 CR scenarios: (a) Spectrum Interweave, and (b) Spectrum Underlay, [1] 10
2.4 Interweave cognitive radio architecture with parallel sensing and communications. 11
2.5 Underlay cognitive radio architecture with combined sensing and communications. 11
2.6 Half-wave dipole antenna. 20
2.7 Illustration of the smallest sphere a containing an antenna. 20
2.8 (a) Electric dipole enclosed in a shell ($r_1 = 10\ mm$) made up of metamaterial of frequency independent negative permittivity ($\epsilon_r = -3$), (b) Associated radiated power ratio for different values of loss tangent of the permittivity of the metamaterial shell [2]. 23
2.9 (a) Bulk periodic metamaterial, (b) Patch antenna with metamaterial substrate, (c) Reflection coefficient of the metamaterial antenna and the reference antenna with respect to frequency, (d) Radiation pattern of the metamaterial antenna for the E and H planes [3]. 24
2.10 (a) Permittivity and permeability of the metamaterial with respect to frequency. The dashed lines represent the imaginary part and solid lines real parts. The inset show a picture of the antenna with the metamaterial substrate (b) Schematic of the metasolenoid metamaterial, (c) Reflection coefficient of the metamaterial and reference antenna with respect to frequency [4]. 24
2.11 (a) Metamaterial reactive impedance substrate, (b) Normalized surface impedance with respect to frequency, (c) Patch antenna on a reactive impedance substrate, (d) Reflection coefficient with respect to frequency for a conventional patch antenna and the reactive impedance metamaterial antenna [5]. 25
2.12 Illustration of the coupling and radiation behavior of the near-field metamaterial-inspired small antenna. The driven element (capacitor) represents a monopole/dipole antenna which stores electric energy in his near-field. The parasitic element, replaces the need for an external matching network. 27
2.13 3D magnetic based antenna presented in [6]: (a) 3D view and (b) 2D cross-sectional view. The driven element is an electrically small loop antenna and the resonant parasitic element is the capacitively coupled loop [7]. 27

© 2015 Tous droits réservés. doc.univ-lille1.fr

2.14 **S_{11} (right) and complex input impedance (left) of the 3D magnetic-based antenna presented in [6]. The input reactance behave like magnetic dipole resonant antenna. The anti-resonance occurs when the reactance crosses zero from positive to negative.** 28
2.15 **2D Electric based antenna presented in [6]: (a) 3D view and (b) 2D cross-sectional view. The driven element is an electrically small monopole antenna and the resonant parasitic element is a meander line.** 28
2.16 **S_{11} (right) and complex input impedance (left) of the 2D electric-based antenna presented in [6]. The input reactance presents a monopole like resonance behaviour. The resonance occurs when the reactance cross zero from negative to positive.** 29
2.17 **The first four eigencurrents and eigenvalues for a vehicle modelled with FEKO in order to find the optimum antenna placement [8, 9].** . . 30
2.18 **The first four eigencurrents and eigenfields for ring antenna used for 2×2 MIMO system [10].** 30

3.1 **Arbitrary PEC object S in an impressed field E and the induced surface current J.** 33
3.2 **Schematic of the considered BC-SRR structure. The dimensions are: $D = 11.25$ mm, $W = 1$ mm, $g = 1.95$ mm, the substrate height $h = 1.08$ mm with relative permittivity $\epsilon_r = 2.2$. The load admittance Y_{load} represents the gap admittance and Y_{loop} is the loop input admittance.** 41
3.3 **First four eigenvalues of the considered BCSRR printed over both substrate faces.** 43
3.4 **(a) Characteristic angles for the first three eigenmodes ϕ_0, ϕ_1 and ϕ_2. (b) Normalized polarizability $a_{mm} \cdot 3/(4\pi\epsilon_0 r^3)$ from equation (3.29) and the transmission coefficient from conventional unit-cell analysis.** 43
3.5 **First three eigencurrents profiles of the considered BC-SRR.** 44
3.6 **Modal weighting coefficients (from equation 3.18) of the 1st, 2nd and 3rd modes of the considered broadside-coupled split-ring-resonator in presence of a perpendicular (left) and parallel (right) magnetic excitation. J_0 and J_1 have higher weighting coefficients at their resonances, when the magnetic field is perpendicular to the ring. The third mode J_2 has a weighting coefficient close to zero for both configurations since its is not a resonant mode. When the magnetic field is parallel to the plane of the ring, J_1 (electric) is more reactive than J_0. Nonetheless, J_0 (magnetic) is the most reactive when the magnetic field is perpendicular to the ring.** 45
3.7 **Characteristic angles of the first five modes of a 4×4 reactive impedance substrate as depicted. The dimensions are $a = 12$ mm, $\Delta_x = \Delta_y = 18$ mm, $h = 4$ mm and $\epsilon_r = 25$ (Ref.[5]).** 45
3.8 **Modal weighting coefficients of the $1^{st}$and 2nd modes of the considered 4×4 reactive impedance substrate in presence of a perpendicular (left) and parallel (right) magnetic excitation. Modes 1 and 2 are more reactive when the magnetic field is parallel to the substrate.** 46

4.1 **Equivalent circuit of TM_n spherical wave, proposed by Chu [11].** . . . 51
4.2 **Portion of an antenna in the vicinity of a feeding gap. The modal impedance is calculated using the computed $I_{n,in}$ and V_n^i.** 55

© 2015 Tous droits réservés.

Thèse de Mhamad Hassanein Rabah, Lille 1, 2015

4.3 **Illustration of an eigenvalue curve with respect to the frequency crossing zero line. The modal derivative $\frac{\partial \lambda_n}{\partial f_n}$ is defined at the mode resonance using particular eigenvalues. The choice of these eigenvalues depends on the linearity region near to the resonance in order to ensure that $[X] >> [R]$ condition.** 61
4.4 **Schematic of the optimised arbitrary star-like shaped antenna. The antenna is printed over an Arlon substrate with $\epsilon_r = 10.7$ and the height $h = 1.5\ mm$.** 63
4.5 **Modal significance with respect to the frequency of the first five modes on the arbitrary-shaped antenna.** 64
4.6 **Eigenvalue with respect to the frequency of mode 1 with indication of the used values to calculate the first modal slope $\mathrm{Slope}_{1,f_{res}}$. In this case $\gamma = 10$.** 64
4.7 **Profiles of the first two eigencurrents of the proposed IFSTTAR antenna.** 65
4.8 **Position of the optimum feeding in order to excite mode 1 at 0.7 GHz.** 65
4.9 **(a) Photo of the fabricated prototype of the arbitrary-shaped IFSTTAR antenna. (b) Measurements setup of the reflexion coefficient using an HP8720D vector network analyser.** 66
4.10 **(a) Reflection coefficient of the arbitrary-shaped IFSTTAR antenna fed by a coaxial cable as in Fig. 4.8. (b) Simulated complex input impedance used for the calculation of the Yaghjian-Best original Q_Z.** 67
4.11 **(a) Schematic a patch antenna over a substrate representing classical, magneto-dielectric or metamaterial substrate. (b, c, d) Profiles of the first three calculated eigencurrents, respectively. Modes profiles are frequency independent. The eigencurrents are calculated only on the metallic patch, since an infinite substrate (multi-layered green function) is considered. The same current profiles have been found in all considered cases.** 69
4.12 **Characteristic angles with respect to the frequency of the first three eigenmodes for a patch antenna resonating at 1.85 GHz.** 69
4.13 **(a) Schematic of a miniaturized patch antenna over two substrates: classical substrate ($\epsilon_r = 6$) and RIS. (b,c) Schematic of a 4×4 reactive impedance substrate. The dimensions are $a = 12$ mm, $\Delta_x = \Delta_y = 18$ mm, $h = 4$ mm and $\epsilon_r = 25$, [5].** 70
4.14 **Configuration of studied designs over different substrates. Except for design A, patch dimensions are 20×16 mm. These dimensions are identical to the considered patch antenna in [5].** 71
4.15 **Modal significance with respect to the frequency of the first mode for the studied cases: the MS_1 is close to unity at the resonance frequency (1.85 GHz) for all cases because it is a radiating mode. The width of the curve varies between cases because it is proportional to the mode bandwidth in each case.** 72
4.16 **Modal significance with respect to the frequency of the second mode for the studied cases: Similarly to the first active mode, MS_2 is close to unity at the resonance frequency (2.12 GHz) for all cases because it is a radiating mode. The width of the curve varies from case to another because it is proportional to the mode bandwidth in each case.** 73

© 2015 Tous droits réservés. doc.univ-lille1.fr

5.1 **Illustration of the problem of associating metamaterial inclusion to non-classical arbitrary shaped antennas.** 81
5.2 **Illustration of the threshold applied on the eigenvalues within a targeted frequency band in order to identify the dominant modes.** 82
5.3 **Design workflow for enhancing the efficiency of antennas using metamaterial inclusion based on the theory of characteristic modes.** 85
5.4 **Calculated eigenvalues (a), and eigenangles (b), of an isolated monopole. Any of the eigenvalues approaches zero since the modes are non-resonant in the studied frequency band. For the same reason, any characteristic angles cross the 180° line.** 87
5.5 **Profiles of the first three eigencurrents of an isolated monopole (2D view). The monopole is perpendicular to an infinite ground plane. The same scale is used for all modes.** 87
5.6 **Modal excitation coefficient V_n^i of the first three modes of an isolated monopole: the considered excitation here is an edge voltage source as depicted. The first mode is the most influenced by this excitation because of the mode configuration. Indeed the excitation is placed at the maximum surface current of this mode.** 88
5.7 **Calculated eigenvalues (a), and eigenangles (b), of an isolated meander line. The first eigenvalue cross zero at the first resonance while the second mode has a high positive eigen value and the third mode has a high negative eigenvalue. For the same reason, the first characteristic angle cross the 180° line at 1.481 GHz which is the resonance of the first mode.** 89
5.8 **Profiles of the first three eigencurrents of an isolated meander line. The first eigencurrent go straight following the meander line, similarly to a current in a coil. The second eigencurrent follow a path with two way direction, which will push the resonance toward higher frequencies. The third mode presents the same profile as the second one but they are out of phase.** 90
5.9 **Calculated eigenvalues (a), and eigenangles (b), of the system composed of the monopole and the meander line. The first eigenvalue crosses zero at the first resonance 1.442 GHz. This could also be seen from the first characteristic angle which crosses the 180° line at the same frequency. The second and third modes have high positive and negative eigenvalues, respectively. Both are bad radiators.** 91
5.10 **Normalized modal weighting coefficients [from Eq. (3.18)] for the first three eigencurrents of the meander line and monopole together: the first mode has the higher coefficient because it meets the resonance condition and has high modal excitation coefficient (Fig. 5.6).** 91
5.11 **Comparison of the first eigenvalue of the antenna system and the meander line alone. The isolated meander has a higher resonance than the system of monopole and meander. The difference is slight and is estimated to be 1%.** 92
5.12 **First eigencurrent profile of a monopole associated to a meander line: the profile on the meander remains unchanged from when it is isolated. The current profile on the monopole is modified compared to an isolated one, and seems to follow the paths of the meander line.** . 93

© 2015 Tous droits réservés.

Thèse de Mhamad Hassanein Rabah, Lille 1, 2015

5.13 **Full wave simulation: transmitted power to the structure. This power represents the power generated by the voltage source and transmitted to the monopole + meander line antenna system. The peak value is 6 mW.** . . . 93
5.14 **Modal active and reactive powers from Eq. (3.22) and (3.20), respectively, of the first three characteristic modes of the monopole associated to the meander line.** . . . 94
5.15 **Calculated eigenangles of an isolated semi-loop. Any of the characteristic angles cross the 180° line, since the modes are non-resonant in the studied frequency band.** . . . 96
5.16 **Profiles of the first two eigencurrent of an isolated semi-loop (2D view). The loop is mounted on an infinite ground plane.** . . . 97
5.17 **Modal excitation coefficient V_n^i of the first three modes of an isolated semi-loop: the considered excitation here is a wire port as depicted. The first mode is the most excited with a such excitation because of the mode configuration. Indeed the excitation is not placed at the maximum of the mode, then V_1^i is not the maximum at 300 MHz.** . . . 97
5.18 **Calculated eigenvalues (a), and eigenangles (b), of an isolated CLL. The first eigenvalue crosses zero at the first resonance while the second mode has a high negative eigenvalue and the third mode has a high positive eigenvalue. For the same reason, the first characteristic angle crosses the 180° line at 301 MHz which is the resonance of the first mode.** . . . 98
5.19 **Profiles of the first two eigencurrent of a CLL (3D view). The CLL is mounted on an infinite ground plane.** . . . 99
5.20 **Profiles of the first two eigencurrent of a CLL+ semi-loop antenna (3D view). The system is mounted on an infinite ground plane (not shown on the figure).** . . . 100
5.21 **Comparison of the first eigenvalue of the antenna system and an isolated CLL inclusion. The CLL alone has a slightly higher resonance than the system. The difference is very small and is estimated to be 0.55%.** . . . 101
5.22 **Normalized modal weighting coefficients (from Eq. (3.18)) for the first three eigencurrents of the semi-loop and the CLL together: the first mode has the higher coefficient because it meets the resonance condition and has considerable high modal excitation coefficient (Fig. 5.17). The two higher modes have $w_{c,1 \text{ and } 2}$ close to zero since they only store energy.** . . . 101
5.23 **Full wave simulation: transmitted power to the structure. This power represents the power generated by the voltage source and transmitted to the semi-loop + CLL antenna system. The peak value is 6 mW.** . . . 102
5.24 **Modal active and reactive power from Eq. (3.22) and (3.20), respectively, of the first three characteristic modes of the semi-loop associated to the capacitively-loaded loop.** . . . 102

6.1 **Miniaturized antenna configuration: optimized feeding system based on a CPW transmission line with a triangular ground plane.** . . . 107
6.2 **First six eigenvalues of the considered EWB antenna over the band 0−4 GHz.** . . . 108

© 2015 Tous droits réservés. doc.univ-lille1.fr

6.3 **Impact of the trident feed on the first two eigenvalues of the monopole.** 109
6.4 **Trident feed configuration and the surface current densities of the first two eigencurrents at 1 GHz. The first two current modes present higher current peripheral at their maxima (the circumference of the disk) when the trident feed is used, thus modes become better radiators at the corresponding frequency.** . . . 109
6.5 **Simulated VSWR proposed EWB antenna before modifying the radiator.** . . . 110
6.6 **Power pattern (YZ plane) for the described antenna without the V-shaped slot at different frequencies within the matched frequency band.** . . . 111
6.7 **V-shaped slot impact on the 6th current mode at 7.5 GHz: the dip in the main radiation axis is due to the low surface current density in the center of the disk. The V-shaped slot creates a new current maximum in the center instead of the two nulls. This results in a maximum in the main radiation axis.** . . . 112
6.8 **Miniaturized antenna configuration: optimized feeding system based on a CPW transmission line with a triangular ground plane, and an optimized slotted radiator for power pattern stabilisation.** . . . 112
6.9 **Power pattern (YZ plane) for the described antenna with the V-shaped slot at different frequencies within the matched frequency band.** . . . 113
6.10 **Simulated VSWR comparison for the proposed EWB antenna with and without V-Slot.** . . . 113
6.11 **Comparison between simulated and measured S_{11} parameters for the proposed antenna printed on an 0.787 mm thick Teflon substrate ($\epsilon = 3.2, tan(\delta) = 0.0002$).** . . . 114
6.12 **Measured radiation pattern of the fabricated antenna in the XZ plane (—), and YZ plane (−−), over the matched frequency band.** . . . 114
6.13 **Measurements setup of the power pattern of the proposed EWB antenna in the anechoic chamber [12].** . . . 115
6.14 **Schematic of the EWB antenna illustrating the question of searching the right metamaterial inclusion at a specific frequency (in our case 600 MHz), wether it should be inductive or capacitive ?** . . . 116
6.15 **First six eigenvalues of the considered EWB antenna over the band 0−4 GHz. A threshold of 500 is applied on the eigenvalues in order to limit the number of the considered modes within the electrically small regime.** . . . 116
6.16 **Schematic of a split ring composed of 2 elliptical semi-loops printed over both faces of a dielectric substrate, and connected via the substrate. The substrate has a thickness of 1.5 mm and relative permittivity of ϵ_r=10.7. The dimensions in mm are: R_1=17.595, R_2=16.15 and the loop width equals to 1.105 mm.** . . . 118
6.17 **First four eigenvalues of an elliptical loop printed over both substrate faces.** . . . 118
6.18 **New configuration of the EWB-MTM inspired antenna.** . . . 119
6.19 **First four eigenvalues of the considered EWB antenna associated with an elliptical loop in Fig. 6.16.** . . . 119

© 2015 Tous droits réservés.

6.20 **Impact of the loop on the first eigencurrent (J_1) profile at 600 MHz. The presence of the the loop makes the first eigencurrent emulating the same path of the current flowing on the loop.** 120
6.21 **Prototype of the modified EWB-MTM inspired antenna printed over Arlon10 substrate with relative permittivity $\epsilon_r = 10.7$, $tan(\delta) = 0.0023$ and height of 1.55 mm.** 121
6.22 **Comparison between simulation and measurement of the reflexion coefficient of the EWB antenna with and without the metamaterial loop inclusion.** 122
6.23 **Comparison between simulation and measurement of the reflexion coefficient of the EWB-MTM inspired antenna over the band 0–18 GHz** 122
6.24 **Measurements setup of the reflexion coefficient of the EWB-MTM Inspired antenna.** 123
6.25 **Comparison of the realized gain of the EWB antenna in the XZ plane, with and without the metamaterial inclusion at 600 MHz. The average difference over all the angles is about 10 dB.** 124
6.26 **Design methodology for the enhancement of the bandwidth, radiation pattern and efficiency of a planar monopole antenna.** 125

© 2015 Tous droits réservés. doc.univ-lille1.fr

List of Tables

2.1 **Overview on proposed antenna systems for spectrum interweave CR in the past years** 16
2.2 **Overview on proposed antennas for spectrum underlay and wide-band sensing operation in the past years** 18

4.1 **Summary of quality factor expressions proposed in literature.** 53
4.2 **Summary of quality factor expressions based on characteristic modes.** 59
4.3 Comparison between modal based, and conventional input impedance based total Q factor of the arbitrary-shaped antenna at 0.7 GHz. 67
4.4 **Specifications of the considered patch designs** 70
4.5 **Summary of the eigen slopes and modal quality factor -at the resonance- for mode 1 ($\gamma = 0.1, \tan\delta_e = 0.001$ and $\tan\delta_m = 0.1$)** 73
4.6 Impact of the losses on $Q_{1,f_{1,res}}$ 74
4.7 **Summary of the eigen slopes and modal quality factor -at the resonance- for mode 2 ($\gamma = 0.1, \tan\delta_e = 0.001$ and $\tan\delta_m = 0.1$)** 75
4.8 **Summary of the eigen slopes and modal quality factor -at the resonance- for mode 1 for different values of μ_r and ϵ_r, ($\gamma = 0.1, \tan\delta_e = 0.001$ and $\tan\delta_m = 0.1$)** 75
4.9 **Comparison Between The Classical Q Factor and The Proposed Q Factor Based on Eigenvalues, at 1850 MHz** 76
4.10 **Comparison Between The Classical Q Factor and The Proposed Q Factor Based on Eigenvalues, at 2120 MHz** 77

5.1 **Comparison between calculated quality factors of a 2D Electric Based Antenna (Monopole+Meander Line), based on modal and classical expressions.** 95
5.2 **Comparison between calculated quality factors of a 3D Magnetic Based Antenna (Semi-Loop+CLL), based on modal and classical expressions.** 103

6.1 **Dimensions of the miniaturized antenna [mm]** 108
6.2 **Efficiency of the proposed miniature EWB antenna.** 115
6.3 **Comparison of the radiation performances of the EWB antenna alone and the MTM Inspired EWB antenna.** 124

© 2015 Tous droits réservés. doc.univ-lille1.fr

Abbreviations

SDR	**S**oftware **D**efined **R**adio
CR	**C**ognitive **R**adio
ITS	**I**ntelligent **T**ransport **S**ystem
DVB-H	**D**igital **V**ideo **B**roadcast-**H**andled
UHF	**U**ltra **H**igh **F**requency
COM	**C**ommunication
IR	**I**mpulse **R**adar
ISM	**I**ndustrial **S**cientific **M**edical
QoS	**Q**quality **O**ver **S**service
PDA	**P**ersonal **D**igital **A**ssistant
MIMO	**M**ultiple **I**nput **M**ultiple **O**utput
RF	**R**adio **F**requency
EM	**E**electromagnetic
GPS	**G**lobal **P**ositioning **S**ystem
URC	**U**rbanisme des **R**adio **C**ommunications
CORRIDOR	**C**ognitive **R**adio for **R**aIlway through **D**ynamic and **O**pportunistic spectrum **R**euse
ESA	**E**lectrically **S**mall **A**ntenna
CM	**C**haracteristic **M**ode
TCM	**T**heory **C**harcteristic **M**odes
CMA	**C**haracteristic **M**odes **A**nalysis
ELC	**E**lectric **L** **C** resonator
MTM	**M**etamaterial
UWB	**U**ltra **W**ide **B**and
SRR	**S**plit **R**ing **R**esonator
CSRR	**C**omplemantary **S**plit **R**ing **R**esonator

© 2015 Tous droits réservés.

doc.univ-lille1.fr

Thèse de Mhamad Hassanein Rabah, Lille 1, 2015

BC-SRR	**B**road-side **C**oupled **S**plit **R**ing **R**esonator
EWB	**E**xtremely **W**ide **B**and
ENG	**E**lectric **N**egative
MNG	**M**agnetic **N**egative
DSA	**D**ynamic **S**pectrum **A**ccess
FCC	**F**ederal **C**ommunications **C**ommission
GSM-R	**G**lobal **S**ystem **M**obile for **R**ailway
WRAN	**W**wireless **R**ural **A**rea **N**etwork
WAVE	**W**wireless **A**ccess in **V**ehicular **E**nvironments
VSWR	**V**oltage **S**tanding in **W**ave **R**ation
CPW	**C**oPlanar **W**aveguide
EZ-Antennas	**E**rentok and **Z**iolkowski Antennas
MS	**M**odal **S**ignificance
PEC	**P**erfect **E**lectric **C**onductor
MoM	**M**oment method
RWG	**R**ao **W**ilton **G**lisson
SIE	**S**urface **I**ntegral **E**quation
EFIE	**E**lectrical **F**ield **I**ntegral **E**quation
MFIE	**M**agnetic **F**ield **I**ntegral **E**quation
CFIE	**C**ombined **F**ield **I**ntegral **E**quation
VIE	**V**olume **I**ntegral **E**quation
MPIE	**M**ixed **P**otential **I**ntegral **E**quation
CPM	**C**haracteristic **P**ort **M**odes
TM	**T**ransverse **M**agnetic
TE	**T**ransverse **E**lectric
RIS	**R**eactive **I**mpedance **S**ubstrate
EMC	**E**lectromagnetic **C**ompatibility
RCS	**R**adar **C**ross **S**ection
LUT	**L**ook **U**p **T**able
FDTD	**F**inite **D**ifference **T**ime **D**omain

© 2015 Tous droits réservés.

doc.univ-lille1.fr

To the soul of my parents...

© 2015 Tous droits réservés.

doc.univ-lille1.fr

Chapter 1

General Introduction

The rise of wireless communication systems and the big demand for high bit rate links have entailed research to move towards new diverse communications systems. With this diversity of wireless systems, flexibility for operating between different standards is strongly needed. Cognitive radio (CR) consists in the future system that can offer this flexibility. This will have significant effects on antenna requirements for applications ranging from mobile phones to satellite communications. Although the concept of software control of radio transceivers has been around for many decades, the current thrust in software defined radio (SDR) was first described by Mitola [13]. SDR is seen as an enabling technology for CR, which offers much promise to increase spectrum usage efficiencies to users and a wide variety of applications.

Three major features define a cognitive radio. A CR must be able to sense, decide, adapt, and learn from its environment. These are the characteristics that make CR unique from other spectrum sharing and wireless communication techniques.

Since being introduced by Mitola [14], the operation of cognitive radios has been frequently illustrated by the cognition cycle illustrated in Fig. 1.1. The cognition cycle is a state machine that resides in the cognitive radio and defines how the radio learns about and reacts to its operating environment.

It is expected that the concept of CR will lead to the deployment of cheaper RF modules. The emergence of CR will change the face of current commercial wireless products, such as cellular phones, PDAs, high speed internet, commercial radios, video conferencing, GPS, transport communications, etc. The major areas where CR will be most beneficial are: military applications, government and regulatory areas, public safety and transport environments. Cognitive radio technology is an important innovation for the future of communications and likely to be a part of the new wireless

© 2015 Tous droits réservés. doc.univ-lille1.fr

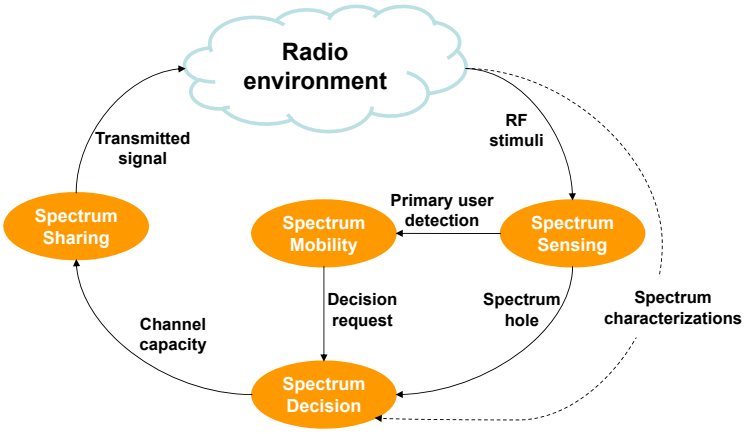

FIGURE 1.1: **Classical cognitive radio cycle**

standards, becoming almost a necessity for situations with large traffic and interoperability concerns [15].

The aspect of the interoperability refers to the ability of different types of wireless devices and applications to work together effectively, without prior communication, in order to exchange information in a useful and meaningful manner. As an example, a national emergency occurred in France when a high speed train (TGV) travelling from Paris to Limoges left the tracks and crashed in Brétigny. To respond to the disaster, all jurisdictions, civil and security services where communicating within the same geographic zone. This has saturated the capacity of the systems within the same frequency bands and prevented a seamlessly communication without interference. CR will become a must-have technology for situations as these with its frequency agility and/or flexibility, the ability to enhance interoperability between different radio standards, and the capability to sense the presence of interferers [15].

The existence of many wireless communications applications, especially in the band extending from 0.3 GHz to 3 GHz, has increased spectrum use, causing significant spectrum congestion [16, 17]. This has driven regulatory agencies have found new ways to use spectrum resources. There are a number of dynamic spectral access models possible, such as shared use by underlay methods, as in UWB systems, or overlay spectrum commons, as used in industrial, scientific, and medical bands (ISM) [17].

Cognitive radio and Antennas: At the hardware level, the implications for future antenna design are multiple. CR has two possible architectures: combined or parallel spectrum sensing and communications; in both architectures two types of antennas are needed [18]. One antenna is extremely wideband and omni-directional, feeding a receiver capable of both coarse and fine spectrum sensing over a broad bandwidth.

© 2015 Tous droits réservés.

Thèse de Mhamad Hassanein Rabah, Lille 1, 2015

The second antenna is directional and feeds, or is fed, by a frequency agile front end that can be tuned to the selected band.

Antenna research into this area has only just begun. Sensing antenna for example can not be a simple energy detector: we need to be able to detect both radiation angles and the availability of frequency bands.

For CR the goal is to incorporate, inexpensive RF components and cheaper processing [14]. This relies mostly on the antenna technology used in the devices. This is where antenna engineers can make an impact. How can we design truly reconfigurable antennas that can sense the entire spectrum of interest and minimize interference and multipath problems within several frequency bands? Do we design a wideband antenna, or use a number of antennas that can be used to sense, receive and transmit?

Moreover, as the antenna geometry gets more complicated, there is no closed formulation to analyze it. In addition, an antenna must take arbitrary shapes in order to be integrated in complex platforms such as a vehicle or a mobile phone chassis geometry. This adds an extra difficulty to the analysis as well as to the estimation of the figure of merit of an antenna, namely the quality factor Q. Modern design techniques rely on the the use of the theory of characteristic modes (TCM) to bring the physical interpretation to the designer in the industry [19]. TCM provides a systematic design tool by taking multiple constraints into consideration such as resonance conditions as well as current mode profiles. Furthermore, the physical insight provided by TCM makes it suitable for the industry since the Physics is put back into the simulation and can be easily exploited by engineers [20].

Terminals size miniaturization and the cohabitation of growing number of systems require antennas with small sizes and good performances. This has opened large interest in research and development of small antennas and antenna miniaturization techniques. Fundamental limitations of small antennas are still an active research area. Antenna size and performances are linked together; for instance the bandwidth is inversely proportional to the dimensions. An antenna does not radiate a wave whose wavelength is much greater than its size; it does not resonate at that corresponding frequency. However, to approach the physical limits while keeping acceptable radiation performances, new sophisticated techniques such as the use of metamaterials[2, 5] can be considered more and more. Metamaterials are artificial materials tailored to mold the flow of electromagnetic waves.

Implementing metamaterials into common antenna design is challenging. Indeed, the common classical approaches are insufficient to address this problem. In this context,

© 2015 Tous droits réservés. doc.univ-lille1.fr

Thèse de Mhamad Hassanein Rabah, Lille 1, 2015

our work will focus on the integration of these techniques into the antenna design using the theory of characteristic modes.

Objectives of this work

To address the above-mentioned challenges, simple antenna design techniques might be insufficient to take into consideration the different constraints as wideband operation, miniaturization and coupling limitation for multiple antenna operation. Thus, novel antenna concepts need to follow new methodologies and to use new materials such as artificial metamaterials. In this thesis, we will focus on the use of metamaterials (MTM) to address these challenges.

The use of MTM to enhance the performances of antennas or to overcome their fundamental limitations has been the subject of a big number of research works [5, 21]. It was suggested that MTM can prove to be useful in miniaturization without deterioration of the radiation performances for both planar patch antennas [22] and electrically small antennas (ESA) [23]. To ensure practical realizations, a novel approach was proposed by Erentok et *al.* [6]. The authors propose to insert a single tailored metamaterial inclusion as a parasitic element in the extreme near-field of an ESA to enhance the input impedance matching and radiation efficiency. The term metamaterial-inspired antennas has been coined for this approach to differentiate it from metamaterial-based antennas where bulk homogenous metamaterials are considered. Indeed, to use the bulk homogeneous metamaterial approach, effective permittivity and permeability (ϵ_{eff} and μ_{eff}) have first to be defined for plane wave interaction with all the associated difficulties, when resonant MTM are considered [24]. When this MTM is then associated to antennas as substrate or superstrate, physical insight in the interaction with the radiating element is not easy to provide.

Our aim in this work to propose a novel approach for the analysis of MTM inclusions which should help us to provide a deeper physical insight into the design of antennas using MTM and even should be useful in isolation problems. This approach should prove to be useful both for the metamaterial-based and metamaterial-inspired antenna approaches. It will then be generalized to account for different antenna types. It is based on the decomposition and analysis of the surface currents into real orthogonal sets called current modes. We believe that this approach should lead to systematic designs unlike the common trial & error approaches for antenna design.

To analyse the electromagnetic behaviour of metamaterial structures, we propose to use the analysis of the electrical and magnetic energy storage (W_{elec} and W_{mag}) over

© 2015 Tous droits réservés. doc.univ-lille1.fr

Thèse de Mhamad Hassanein Rabah, Lille 1, 2015

a frequency band and investigate the surface modal current densities. We highlight in this work the importance of this method for planar structures since it is based on the study of surface currents. This is done through the use of characteristic mode (CM) concept in the definition of metrics related to the nature of the stored energy in the structure together with the resonance conditions, and by decomposing the total surface currents onto a set of real orthogonal currents.
Providing such tools to analyse antennas and MTM from a physical point of view will be the key to meet CR antenna systems requirements in terms of cohabitation (i.e. isolation), bandwidth enhancement and miniaturization.

Organisation of the dissertation

In chapter 2, a state of the art on antennas proposed for CR systems will be presented. These designs are reconfigurable for interweave CR, or large-band for underlay CR. Also, we will present antenna designs when the TCM was used with a brief description of the TCM. In the literature, only a few antennas operating below 2 GHz with a small electrical size have been proposed for CRs.

The physical limitations associated to antennas, and especially when they become electrically small will be addressed. The use of metamaterials to overcome these limitations is reported in this chapter. A description of MTM based and MTM inspired antennas is provided. Furthermore, the use of the theory of characteristic modes for antenna design and integration is reported.

Chapter 3 introduces the mathematical formulation of the theory of characteristic modes. Computation assumptions considered in this work are detailed. Hence, we introduce new metrics to analyse MTM inspired structures based on the TCM. Indeed, to the best of our knowledge, no work on the use of the TCM with metamaterial structures has been done yet. An analysis of a particular MTM inclusion, the broad-side coupled split-ring-resonator (BC-SRR) with the TCM will be presented in order to validate the approach. Using the new metrics proposed, a reactive impedance substrate based on metal-dielectric metamaterial excited by a parallel magnetic field is shown to exhibit artificial magnetism. These metrics are shown to present good agreement with other analytical and numerical methods.

Chapter 4 deals mainly with ESAs. The different expressions proposed to evaluate the performances of an ESAs are reported and compared. A new expression based on the TCM is proposed in this chapter. This expression is based on the study of the eigenvalue variation of the dominant modes of the antenna. As an example of

© 2015 Tous droits réservés. doc.univ-lille1.fr

Thèse de Mhamad Hassanein Rabah, Lille 1, 2015

application, a detailed study of an electrically small patch antenna over classical and metamaterial substrates will be presented. It is demonstrated qualitatively as well as quantitatively how a non-classical substrate can miniaturise the antenna without the deterioration of the other antenna parameters (i.e. bandwidth, efficiency). We will show also an agreement between the proposed approach and other approaches from the literature.

In Chapter 5, a design methodology to apply the concept of metamaterial-inspired structure in order to improve the radiation efficiency will be presented. This methodology is based on the analysis of particular characteristic modes of the antenna and the metamaterial inclusion. These particular characteristic modes are selected with respect to their resonance conditions and their sensitivity to a particular external excitation. Then we apply this methodology to the previously published metamaterial-inspired antennas in order for validation.

In Chapter 6 the design of an extremely-wide-band (EWB) antenna for spectrum sensing applications based on TCM will be presented. The theory of characteristic modes is used to analyze and optimize the excitation and multimodal radiation of the monopole antenna. The total efficiency of the antenna has been improved by using the methodology proposed in Chapter 5 for the analysis of metamaterial-inspired antennas. In fact, an adequate metamaterial inclusion has been designed in order to improve the radiation performance of the EWB in the electrically small regime. An experimental validation of the EWB antenna performances will be presented.

Chapter 7 will summarise the findings of this thesis. Some limitations of the proposed approach will be emphasised. Perspectives for further potential investigation of these findings will be also be presented.

© 2015 Tous droits réservés. doc.univ-lille1.fr

Chapter 2

Review of Cognitive Radio Antenna Solutions and Associated Physical Limitations

2.1 Introduction

Cognitive radio systems have not been standardised yet over all existing frequency bands among countries. This has led to multiple CRs deployment scenarios and business directions. To support these scenarios, two CR architectures are involved. The first one combines spectrum sensing and communication within the same device, while the second one separates them. The main purpose of CRs is enabling the exploitation of the unoccupied channels that are possibly spread over a wide bandwidth. Before CRs are to perform, several challenges, researchers and operators are faced with, have to be solved. In CR systems, signal processing is moved as far as possible to the digital part. This makes from the physical interface one of the most challenging parts of the architecture.

In this chapter, different CR architectures are described. Key components of the front-end RF are identified with the antenna design challenges. Then, a state of the art of the most recent antenna systems proposed for CR is presented. It will be shown that strong constraints make antennas subject to several physical limitations which are going to be described in Section 2.4. Metamaterials have proved to be helpful for overcoming these limitations. Examples from the literature on metamaterial antennas are then presented. Finally, we show the need for new analysis tools for antennas when associated with such artificial materials, and that the theory of characteristic modes can prove to be a powerful tool for a such systematic design.

© 2015 Tous droits réservés. doc.univ-lille1.fr

Thèse de Mhamad Hassanein Rabah, Lille 1, 2015

2.2 Antenna Challenges in CR Systems

The need for higher data rates has led to a shortage in the radio frequency (RF) spectrum. One of the most important reasons for this shortage is the static frequency allocation which has caused a large portion of the spectrum to be underutilized. As a result, many dynamic spectrum access techniques have been developed to utilize the spectrum in a more efficient way. Three solutions have been suggested by the FCC to improve spectrum utilization: spectrum reallocation, spectrum leasing and spectrum sharing, as shown in Fig. 2.1 [25].

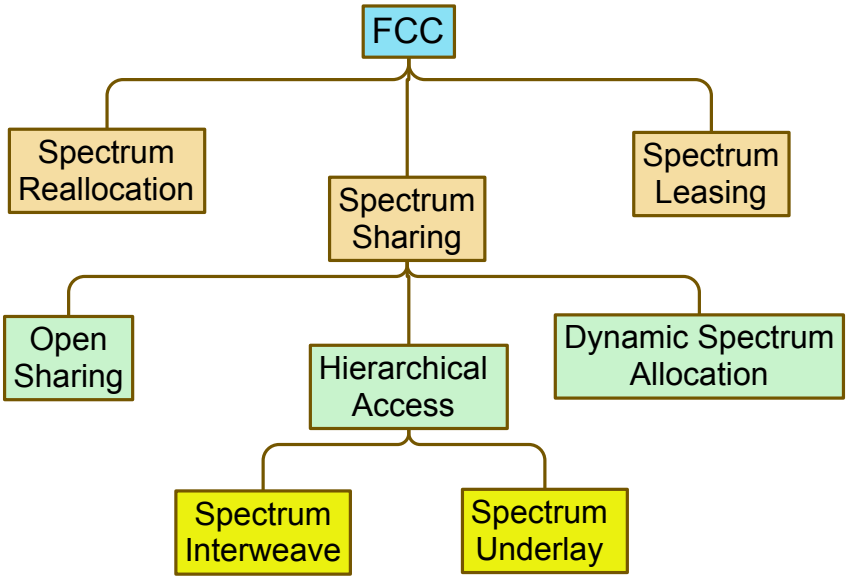

FIGURE 2.1: **Solutions proposed by FCC to the spectrum underutilization problem.**

Spectrum reallocation is a long-term solution and resulted in the opening of the TV band for CR operation. Spectrum leasing is an off- line solution. It allows frequency licensees to sell their channels to third parties. The last solution is spectrum sharing, has attracted the attention of many research activities. It is often known as dynamic spectrum access (DSA), [1]. Fig. 2.2 illustrates the presence of whitespace in the spectrum, and where dynamic spectrum access can be used.

Unlike the current static spectrum access, DSA enables users to dynamically access the spectrum with respect to the time and the frequency as shown in Fig. 2.2. The open sharing model enables all users to simultaneously access the spectrum with certain constraints on the transmitted power according to the used protocol. WiFi and Bluetooth are examples for this model. The dynamic spectrum allocation improves the spectrum efficiency in a certain region for a specific time by assigning frequency

© 2015 Tous droits réservés. doc.univ-lille1.fr

Thèse de Mhamad Hassanein Rabah, Lille 1, 2015

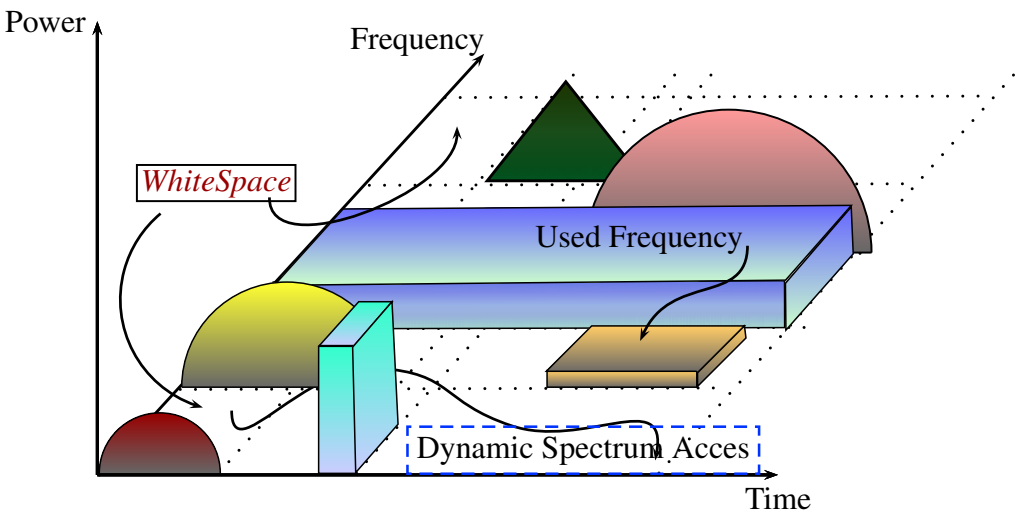

FIGURE 2.2: **Schematic of whitespaces in the spectrum**.

band dynamically to wireless services according to their spatial and temporal traffic statistics. The hierarchical model, which is the main concern of this chapter −because it remains to further antenna specifications− enables the secondary user to access the spectrum bands that are not fully utilized by the primary user [1]. The only constraint in this model is that the quality of service (QoS) of the primary user most not be affected. Two approaches are considered in this model: spectrum interweave and spectrum underlay. In the spectrum interweave approach, the secondary user avoids the primary user using spectrum sensing and adaptive allocation techniques, as shown in Fig. 2.3 (a). This approach known as interweave cognitive radio relies on the detection and exploitation of spectrum holes. While in the spectrum underlay approach, the secondary user operates under the noise floor of the primary user, as shown in Fig. 2.3(b). An example of this approach is the ultra-wide band (UWB) transmission, in which the transmitted signal of the secondary user is spread over an ultra-wide frequency band. This UWB transmission enables very short distance, high speed and low power communication. This approach does not depend on the detection of the spectrum holes and it is known as underlay cognitive radio.

From the antenna point of view, the spectrum interweave approach requires two antennas: sensing and reconfigurable antennas, while the spectrum underlay approach requires only one antenna for wideband operations. It should be mentioned that CR has not been standardised yet, and hence, different frequency bands are targeted by

[1] Users sharing certain spectrum are divided into two categories, primary and secondary. Primary user has a spectrum license for certain region (assigned by FCC on long-term). Secondary user does not have a spectrum license, yet, he is allowed to temporally use the spectrum as long as QoS of the primary user most not be affected.

© 2015 Tous droits réservés. doc.univ-lille1.fr

Thèse de Mhamad Hassanein Rabah, Lille 1, 2015

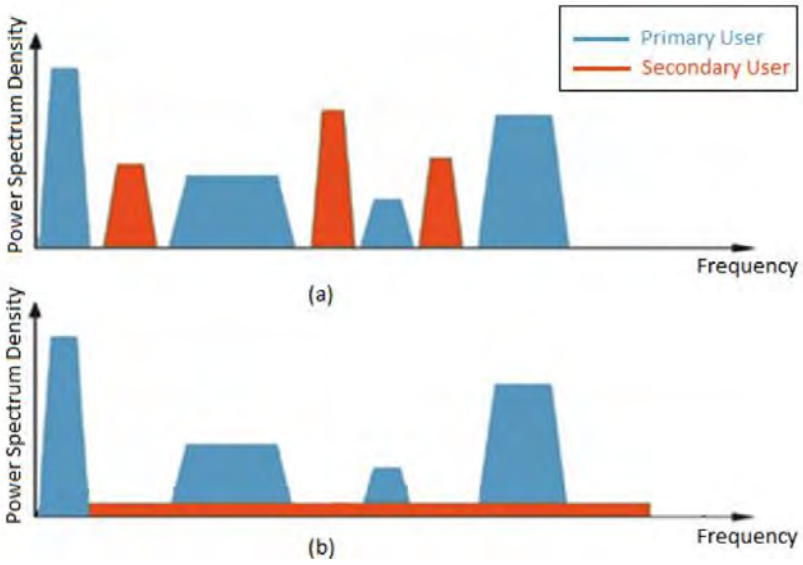

FIGURE 2.3: **CR scenarios: (a) Spectrum Interweave, and (b) Spectrum Underlay, [1]**

different research groups. In Section 2.3 we present examples of different techniques used to implement these systems.

In reviewing the requirements for and the state of the art in antennas for SDR and CR, it is evident that there are as yet no clear specifications. Hence, the focus of the actual work is narrowing around specific applications as potential systems emerge [26]. Applications of CR can be classified into different fields, namely Military, Regulatory and Public safety. Many of these fields can be covered at the same time.

The frequency ranges needed will be much wider than those covered by antennas in most current communication systems and this implies that extremely-wide-band and frequency reconfigurable antennas will become increasingly important as will smart and multiple antenna techniques both in the base station and in terminals.

CR networks can be categorised as those in which the decision making about spectrum allocation is made locally by individual terminals or a group of terminals sharing data, and those in which spectrum allocation is performed at a centre base station [27].

Interweave CR monitors continuously the spectrum usage in a process which runs in parallel with the communication link as shown in Fig. 2.4. Proposed interweave CR systems use two antennas [28]. One antenna is sideband and omni-directional, feeding a receiver capable of both coarse and fine spectrum sensing over a broad bandwidth. The second antenna feeds a frequency agile front end that can be tuned to the selected band. This category also includes single antenna system [29], where a single sideband antenna feeds both the spectrum sensing modules and the frequency agile front end.

© 2015 Tous droits réservés. doc.univ-lille1.fr

Thèse de Mhamad Hassanein Rabah, Lille 1, 2015

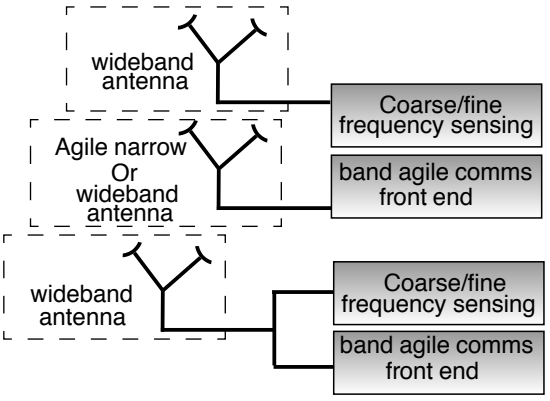

FIGURE 2.4: **Interweave cognitive radio architecture with parallel sensing and communications.**

Underlay CR assigns a single channel for both spectrum sensing and communication as shown in Fig. 2.5. The operations are separated by various time frames.

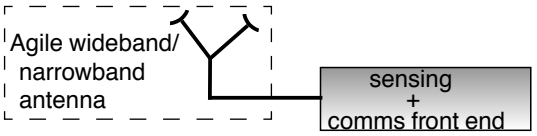

FIGURE 2.5: **Underlay cognitive radio architecture with combined sensing and communications.**

Spectrum sensing and radio reconfiguration are performed when the communication link quality fails below defined thresholds. In [30], two thresholds are defined. Link quality falling below the first threshold triggers spectrum sensing, so that a better system configuration can be identified in order to meet the link quality requirements. When the quality degrades below a second lower threshold; the system is reconfigured.

Whether both of these techniques are used will depend on the available space. In the case of a base station both spatial and spectral sensing may be used, but in the case of handheld terminals it is likely that only spectral sensing may be possible [27]. These issues have been further discussed in [31].

The most (relevant) significant antenna challenges are listed as below:

1. In general, wideband antennas dimensions are larger than narrowband ones which will be a significant problem. Miniaturization of wideband antennas is a main challenge for CR systems. The fundamental limits of electrically small antennas, in terms of bounds on Q factor and gain, also limit the instantaneous

© 2015 Tous droits réservés. doc.univ-lille1.fr

Thèse de Mhamad Hassanein Rabah, Lille 1, 2015

coverage that can be achieved [32]. Furthermore, the design of wideband arrays gives great difficulties in element spacing in base stations.

2. Combining the two bounds of the gain and Q factor implies that an antenna with an extremely-wide band will be very inefficient, if it is small compared to the wavelength. Thus, the efficiency of the antenna in the electrically small regime becomes a challenge.

3. The sensing and communication antennas should be enclosed within the same space, thus cohabitation between both antennas requires good isolation.

Antenna designers are always faced to the after-mentioned challenges. They combine multiple antennas within the same space and try to find a tradeoff between the bandwidth, miniaturization and the isolation. In the next section, we present some of the designs proposed in the context of CR.

2.3 Review of CR Antenna Solutions

2.3.1 Review of antennas for spectrum interweave CR

In the spectrum interweave CR, sensing and reconfigurable antennas are needed. The sensing antenna is a very-large-band antenna and used to sense the spectrum to find spectrum holes. Using these information, the reconfigurable antenna is tuned to transmit at the frequencies of these holes. The designers have to face several difficulties at the antenna level. First, minimising the area containing both antennas suffers from the physical limitations. Second, the coupling between the two antennas has an important impact on such a system, and therefore, isolation techniques should be considered to enhance the isolation. Furthermore, both antennas should also present an omni-directional radiation pattern.

Many works have been published in the frequency band from 2 to 10 GHz. In these publications, a complete spectrum interweave CR system was implemented (both sensing and reconfigurable antennas on the same substrate). However, no work has been published in the DVB-H or UHF bands (i.e. for frequencies below 1 GHz) this is due to a strong miniaturization challenge when the antenna becomes electrically small. It is important to note that there is an extensive literature available on this topic, meanwhile, we select the most relevant designs to this thesis.

In [33], both sensing and frequency reconfigurable antennas were presented on the same substrate. The sensing antenna is a modified egg-shaped monopole antenna

© 2015 Tous droits réservés. doc.univ-lille1.fr

Thèse de Mhamad Hassanein Rabah, Lille 1, 2015

which covers the frequency band 2 GHz – 10 GHz. The frequency tunability is achieved mechanically by rotating a circular substrate section holding five different antenna patches using a stepper motor. Using these five patch antennas, five bands could be achieved to cover the whole frequency range. Both sensing and reconfigurable antennas have an omnidirectional pattern with a planar structure of size 70×50 mm^2 which corresponds to $(0.46 \times 0.33)\lambda_l$[2] of electrical size.

In [34], an incorporated planar UWB/reconfigurable-slot antenna was proposed for cognitive radio applications. Again, UWB antenna was implemented using the egg-shaped monopole antenna to cover the frequency range from 2.5–12 GHz. A slot resonator was precisely embedded in the disc monopole radiator to achieve an individual narrowband antenna. A varactor diode was inserted across the slot, providing a reconfigurable frequency function in the range of 5–6 GHz. By controlling the voltage across the varactor (0–5 V), the varactor capacitance achieved values between 7.643–0.469 pF. The slot was fed by an off-centered microstrip line that creates the desired matching across the tunable frequency band. Both antennas had an omnidirectional radiation pattern with a planar structure of size 40×36 mm^2 which corresponds to a $(0.5 \times 0.44)\lambda_l$.

In [35], a unique combination of wide and narrow band antenna is proposed using uniplanar nature of coplanar waveguide. The antenna prototype consists of a notched Vivaldi printed antenna on a Rogers TMM6 laminate with relative dielectric permittivity of $\epsilon_r = 6$ and a printed dipole as a communication antenna which operates at 5.5 GHz. The antenna overall dimensions are 74×59 mm^2, thus its electrical size is $(0.64 \times 0.51)\lambda_l$. The antenna provides a $S_{11} \leq -10$ dB over a bandwidth from 2.6 to 11 GHz.

All of these antenna systems mostly present an omnidirectional power pattern to cover all the space and thus all possible orientation configurations of the device. Thereby, the stability of the power pattern remains a serious challenge for both CR categories.

2.3.2 Review of antennas for spectrum underlay CR

In the spectrum underlay CR, the secondary user is allowed to send signals with very low power over a large frequency band. Hence, he can simultaneously use the spectrum with the primary user. Only a wideband antenna is needed in this system. The main challenge is to minimize the antenna size, so it can be installed in portable devices. The miniaturization problem is not exclusive for mobile telecommunication terminals. However, the same challenge is proven for other systems such as

[2]The wavelength at the least matched frequency

© 2015 Tous droits réservés. doc.univ-lille1.fr

Thèse de Mhamad Hassanein Rabah, Lille 1, 2015

for railways communication systems where frequencies are very low (e.g at 50 MHz the wavelength is $\lambda = 6$ m).

The main challenge to design very large band antennas comes from the need of matching the energy stored by the antenna over the entire bandwidth. However, the traditional tradeoffs such as size vs. efficiency and size vs. bandwidth (Chu-Harrington limit) still influence the characteristics and performance of antennas. As reported in Chapter 1, those limitations can be overcome by using MTM [23] and will be presented in Sections 2.5 and 2.6. However, a non exhaustive review of techniques used to implement UWB antennas is presented here. These antennas can be used in the spectrum underlay CR as well as in the spectrum interweave CR (as a sensing antenna).

It is obvious that monopole antennas are the most appealing planar wideband antennas for nowadays designers, because they possess different features in their geometries as described in [36]. Therefore, we see that the majority of recent planar designs, which are dedicated to spectrum sensing antennas are based on monopole configurations. In 2007, Ray and Ranga [37] have proposed an elliptical monopole antenna with a detailed study on the impact of the feeding line position. The feeding line consists of a 50 Ω matched microstrip line. Authors show that positioning the feed line along the ellipse major axis could decrease the least matched frequency f_l while exciting along the minor axis increase this one against a wider overall matched bandwidth. The antenna with total dimensions of $(0.2 \times 0.18)\lambda_l$ achieve a bandwidth with $S_{11} \leq$-10 dB from 1.1–13.61 GHz.

Liu and Esselle [38, 39] have proposed an interesting antenna design in two versions. The first version is with a microstrip feeding system and the second one using a CPW. Both antennas are composed of a trapezoid ground plane and an elliptical monopole, which are etched on the top and the back surfaces of a 1.5 mm-thick Rogers 4350B substrate with relative permittivity of $\epsilon_r = 3.48$ and loss tangent $tan(\delta) = 0.002$. A tapered semi-ring feed has been used in order to increase the upper bound of the matched frequency band. The measured VSWR bandwidth extends from 1.08–27 GHz. The antenna total dimensions are 124×120 mm^2, thus, an electrical size of $(0.44 \times 0.43)\lambda_l$. The power patterns of these antennas seem to be stable with many dips in different directions.
This design can be a good candidate for spectrum underlay CR. In Chapter 6 we propose a novel design, based on that proposed in [39] with many improvements in terms of power pattern stability, miniaturization and efficiency using metamaterials and the theory of characteristic modes.

The literature is rich in antennas dedicated for diverse applications and can be used in the context of CRs. Indeed, Table 2.1 lists the presented antennas with others used

© 2015 Tous droits réservés. doc.univ-lille1.fr

Thèse de Mhamad Hassanein Rabah, Lille 1, 2015

for spectrum interweave CR and classify them in terms of the electrical size, coupling level and reconfigurability type. Table 2.2 lists some candidate antennas for spectrum underlay CR and emphasises on the efficiency and minimum gain.

© 2015 Tous droits réservés.

doc.univ-lille1.fr

Thèse de Mhamad Hassanein Rabah, Lille 1, 2015

TABLE 2.1: **Overview on proposed antenna systems for spectrum interweave CR in the past years**

Ref. capture	Year	Antenna operating frequency in [GHz]	Antenna Dimensions in [mm^2]	ϵ_r	Electrical size	Coupling	Gain/ Efficiency	Design configuration	Reconfigurability
[33]	2009	3.3–11	65.5 × 58	2.2	$(0.72 \times 0.64)\lambda_l$	≤-20 dB	7 dB	Slotted monopole in microstrip technology with a two positions triangular monopole	Mechanical : two positions triangular monopole.
[40]	2010	3.1–11	50 × 50	2.2	$(0.74 \times 0.74)\lambda_l$	≤-10 dB	4.7 dB	Egg-shaped monopole fed by a microstrip line	Electrical: Use of lumped element.
[41]	2011	2–10	70 × 50	2.2	$(0.46 \times 0.33)\lambda_l$	≤-10 dB	NA	Modified egg-shaped monopole fed by a tapered microstrip line	Mechanical: Five rotating shapes.
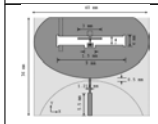 [34]	2012	2.5–12	40 × 36	3.48	$(0.55 \times 0.44)\lambda_l$	≤-20 dB	1.87 dB	Elliptical monopole antenna	Electrical: Varactor diode

Thèse de Mhamad Hassanein Rabah, Lille 1, 2015

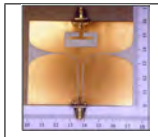 [35]	2012	2.6–11	74 × 59	6	$(0.64 \times 0.51)\lambda_l$	≤-10 dB	80%	Coplanar Vivaldi monopole	Electrical: Printed dipole with lumped elements
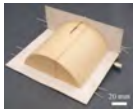 [42]	2013	0.615 – 0.836	80 × 84	18	$(0.16 \times 0.17)\lambda_l$	≤ -14.4 dB	47.1 %	Perturbed half-cylindrical Dielectric resonator antenna	Electrical: Switches controlling the electrical length of the slots
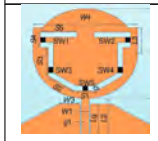 [43]	2014	2.4–8.7	25 × 25	4.4	$(0.2 \times 0.2)\lambda_l$	NA	NA	A coplanar waveguide fed U-shaped monopole patch with a tapered ground	Optical: Photoconductive silicon switches.
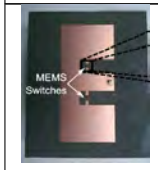 [44]	2014	2–3.2	120 × 100	2.2	$(0.8 \times 0.66)\lambda_l$	NA	7.79 dB	E-shaped patch antenna	Electro-mechanical: RF MEMS switches between the E-shape arms.
[45]	2015	0.72–3.44	120 × 65	4.4	$(0.28 \times 0.15)\lambda_l$	≤ -11.5 dB	40 %	Planar monopole with two meander-line reconfigurable antennas	Electrical: slots in the ground plane controlled by varactor diodes.

NA: Not available.

Thèse de Mhamad Hassanein Rabah, Lille 1, 2015

TABLE 2.2: **Overview on proposed antennas for spectrum underlay and wideband sensing operation in the past years**

Ref. capture	Year	Antenna operating frequency in [GHz]	Antenna Dimensions in [mm^2]	ϵ_r	Electrical size	Design configuration	Efficiency/ Min gain
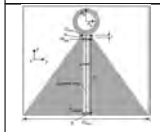 [46]	2006	0.69–10	140×140	3.48	$(0.59 \times 0.59)\lambda_l$	Monopole patch of an annular shape with a trapizoform ground	4.2 dB
[47]	2007	2.5–10.6 / [5.15–5.825]	30×35	4.4	$(0.44 \times 0.52)\lambda_l$	Planar modified rectangular monopole with U shaped slot	6 dB
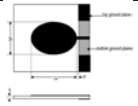 [37]	2007	1.1–13.61	26×24	4.4	$(0.09 \times 0.08)\lambda_l$	Elliptical printed monopole with modified excitation position	7.3 dB
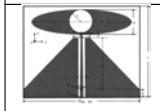 [48]	2007	0.44–10.6	140×93	3.48	$(0.2 \times 0.13)\lambda_l$	Hallowed microstrip monopole	6 dB

Thèse de Mhamad Hassanein Rabah, Lille 1, 2015

[49]	2008	1–10	110×30	1	$(0.36 \times 0.1)\lambda_l$	Circular disk monopole mounted on a slant ground plane for power pattern stabilisation	NA
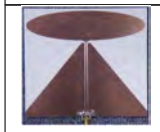 [38]	2011	1.08–27.4	124×120	3.48	$(0.44 \times 0.43)\lambda_l$	Printed monopole with trapezoid ground plane and semi-ring feed	6.2 dB
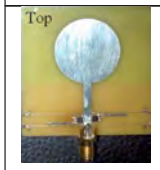 [50]	2012	2.4–10.6	50×50	4.3	$(0.4 \times 0.4)\lambda_l$	Circular printed monopole (Switches OFF for UWB mode)	70 %
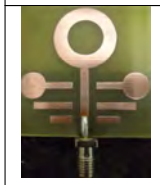 [51]	2014	3.1–10.6	40×40	4.4	$(0.41 \times 0.41)\lambda_l$	Circular ring patch antenna	NA

NA: Not available.

Thèse de Mhamad Hassanein Rabah, Lille 1, 2015

2.3.3 Summary

It can be deduced from both tables (2.1 and 2.2) that when the electrical size of the antenna system decreases, a sacrifice in terms of bandwidth, gain or efficiency is imposed. In fact, when the least matched frequency decrease, the electrical size decrease and this affects the other antenna parameters. This trade-off is due to the physical limitations governing these antennas. This comparison will help to highlight two main objectives of this thesis. The first one is to show what metamaterials can do for antennas beyond physical limitations. Secondly, it shows how the theory of characteristic modes can prove to be a powerful analysis tool for antenna design, instead of "trial and error" approaches.

2.4 Physical limitations of Antennas

The electrical size of an antenna is defined with respect to the length of the wave it radiates. For example Fig. 2.6 shows a half-wave dipole ($L = \lambda/2$).

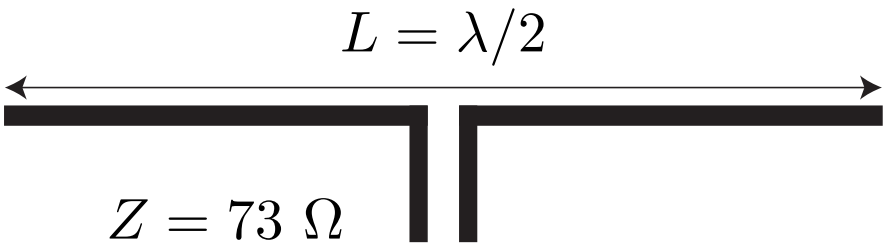

FIGURE 2.6: **Half-wave dipole antenna.**

Antenna physical limitations depend on the electrical size. Electrically small antennas (ESA's) occupy a volume of the sphere whose radius a is a small fraction of the free-space wavelength of the radiated electromagnetic field (Fig. 2.7).

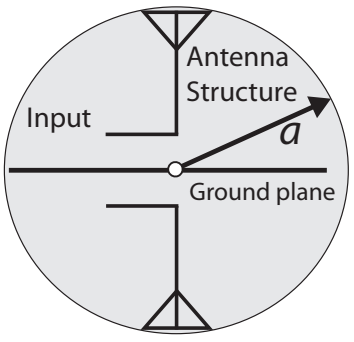

FIGURE 2.7: **Illustration of the smallest sphere a containing an antenna.**

The $k \times a$ product is commonly used to describe this relation, where k is the wave vector defined as $k = 2\pi/\lambda$. An antenna is electrically small if:

© 2015 Tous droits réservés. doc.univ-lille1.fr

Thèse de Mhamad Hassanein Rabah, Lille 1, 2015

- $k \times a < 1$ (without a ground-plane)
- $k \times a < 0.5$ (with a ground-plane)

Fundamental limitations of small antennas are still an active research area [11, 32, 52–54]. Physical bounds of ESAs can be estimated with the quality factor Q:

$$Q = \frac{2.\omega.W_{\{\text{elec,mag}\}}}{P_{\text{rad}}} \tag{2.1}$$

where ω is the angular frequency, $W_{\{\text{elec,mag}\}}$ is the time-average, non propagating stored energy by the antenna and P_{rad} is the radiated power. Q is inversely proportional to a , i.e. antenna dimensions. The smaller the quality factor is, the higher the radiated power by the antenna. For example the first compact expression for the quality factor has been proposed by Chu [11].

$$Q = \frac{1 + 2k^2a^2}{k^3a^3[1 + k^2a^2]} \tag{2.2}$$

Moreover, the bandwidth is inversely proportional to the quality factor. The general form for this relation is given by [55].

$$\Delta f = \frac{f_0}{Q} \tag{2.3}$$

For mono-band antennas the bandwidth at -3dB and -7dB is expressed as follows.

$$BW_{-3\text{dB}} = \frac{2}{\sqrt{2} \times Q_{lb}} \tag{2.4}$$

$$BW_{-7\text{dB}} \approx \frac{f}{Q \times RE} \tag{2.5}$$

where Q_{lb} is the lower bound quality factor corrected by Hansen [22]. $Q_{lb} = Q \times RE$ whereas RE is the radiation efficiency. The tradeoff between dimensions and other antenna parameters can be shown for example in equation (2.5). When the dimensions are diminished, the quality factor increases. Also, if a radiation efficiency RE close to unity is needed, the bandwidth of the antenna will decrease automatically. A trade-off between the RE and the Q factor is imposed: if we want to keep the bandwidth ($BW_{-7\text{dB}}$ = constant), the radiation efficiency RE will decrease proportionally to the dimensions.

For wide-band antennas (bandwidth > 500 MHz), it is reported in the literature that a Q factor could not be defined. Instead, a formulation of the relative bandwidth at

© 2015 Tous droits réservés. doc.univ-lille1.fr

Thèse de Mhamad Hassanein Rabah, Lille 1, 2015

-10 dB is proposed [55]:

$$BW_{-10\text{dB}} = \frac{f_{\max} - f_{\min}}{f_0}. \tag{2.6}$$

In order to push up the limits on the bandwidth, researchers like Veselago [56], Pendry [57] and Smith [58] have paved the way to artificially fabricated materials such as metamaterials. Since metamaterials can propose an equivalent medium with electric and magnetic characteristics beyond the properties of readily available materials, their capacity to enhance the performances of antennas namely in term of miniaturization, bandwidth, efficiency and directivity is sought for. As a matter of that, many metamaterial antennas can be found in the literature for applications with radiation efficiency and bandwidth enhancement [6, 21].

2.5 Metamaterial Based Antennas

The advent of metamaterials raised the hope that physical limitations presented in the previous section might be overcome [59]. It has been demonstrated using the forward dispersion relation for the extinction cross section that electrically small antennas consisting of metamaterial media are of limited use to overcome radiation fundamental limitations [60, 61]. However, Ziolkowski et al. [23] show from both analytical and numerical results that the presence of homogeneous and isotropic metamaterials around an electrically small antenna such as an infinitesimal dipole presenting either a negative refractive index [62] or a negative permittivity [2] can improve the radiation efficiency beyond the limitation described in section 2.4. For example, he has considered an electric dipole enclosed in a metamaterial shell (Fig. 2.8(a)) of inner radius, $r_1 = 10\ mm$ of real permittivity, $\epsilon_r = -3$ and realistic values of loss tangent. The radiated power ratio, $\mathrm{P_{rad}}$ (2.7) is calculated for this metamaterial shell dipole for an input current of 1A and shown in Fig. 2.8(a).

$$\mathrm{P_{rad}} = 10\log_{10}\left(\frac{P_{\text{with metamaterial}}}{P_{\text{without metamaterial}}}\right) \quad \text{in dB} \tag{2.7}$$

A peak value of $\mathrm{P_{rad}}$ is obtained for an outer shell radius of 18.79 mm . The high values of $\mathrm{P_{rad}}$ even when a loss tangent is considered show the potential of metamaterials to improve radiated power of small dipoles.

Hansen et al. [22] consider the potential of metamaterials for the miniaturization of patch antennas with improved radiating performance. Let us consider a square metallic patch antenna printed on a magneto-dielectric substrate with electromagnetic characteristics (ϵ_r, μ_r). If the values of the permittivity ϵ_r or the permeability μ_r are increased, the patch dimensions get smaller for identical operating frequencies. For

© 2015 Tous droits réservés. doc.univ-lille1.fr

Thèse de Mhamad Hassanein Rabah, Lille 1, 2015

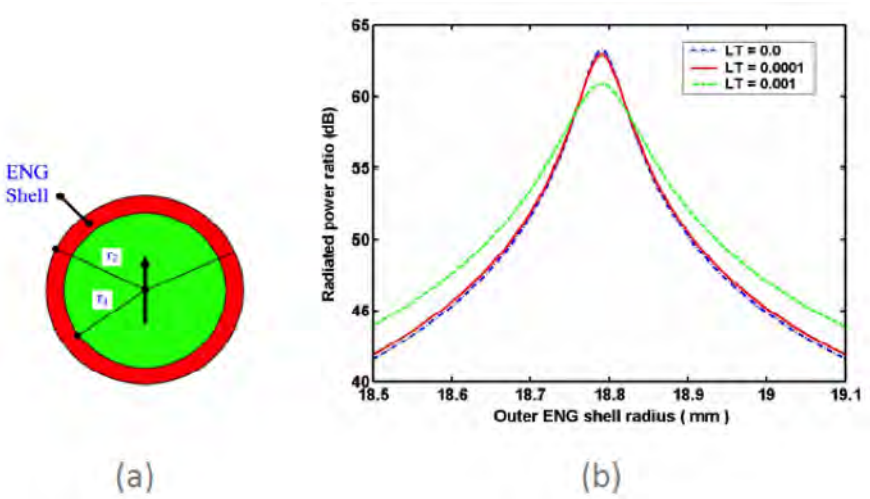

FIGURE 2.8: **(a) Electric dipole enclosed in a shell ($r_1 = 10\ mm$) made up of metamaterial of frequency independent negative permittivity ($\epsilon_r = -3$), (b) Associated radiated power ratio for different values of loss tangent of the permittivity of the metamaterial shell [2].**

instance, Hansen predicted from the zeroth-order transmission line model of a resonant patch antenna that magneto-dielectric ($\mu_r > \epsilon_r$) substrates should present higher performances in terms of bandwidth without affecting the radiation efficiency when miniaturized. It has been proposed in [3] an antenna with a metamaterial substrate made up of a stack of magnetic and dielectric materials as shown in Fig. 2.9 (a) and (b). The metamaterial antenna was then studied by a numerical model based on finite-difference-time-domain (FDTD) technique. The resulting reflection coefficient of the metamaterial antenna is shown Fig. 2.9 (c). It is compared to a reference patch antenna of identical size on a dielectric substrate of permittivity adjusted to yield the same resonance frequency. The bandwidth enhancement is shown to be relatively high. The radiation pattern shown in Fig. 2.9 (d) confirms that no distortion is induced by the metamaterial substrate.

Unfortunately, natural magnetic material are unusable for antennas in microwave frequency range because they are very lossy. At higher frequencies when low-loss magnetic materials are not readily available, artificial magnetic metamaterial can be useful. The effect of artificial magneto-dielectric substrates on the impedance bandwidth properties of patch antennas has been evaluated [4, 63] both numerically and experimentally. The effective permittivity and permeability of the metamaterial are shown in Fig. 2.10 (a). The artificial magnetic metamaterial is described in Fig. 2.10 (b). The real part of the permeability shows a resonance (2.3 GHz) as expected for a metamaterial consisting of split-ring resonators. This metamaterial is then used as the substrate of a patch antenna as depicted in the inset of figure Fig. 2.10 (a). The measured reflection coefficient of the patch antenna with metamaterial substrate is shown in Fig. 2.10 (c).

© 2015 Tous droits réservés. doc.univ-lille1.fr

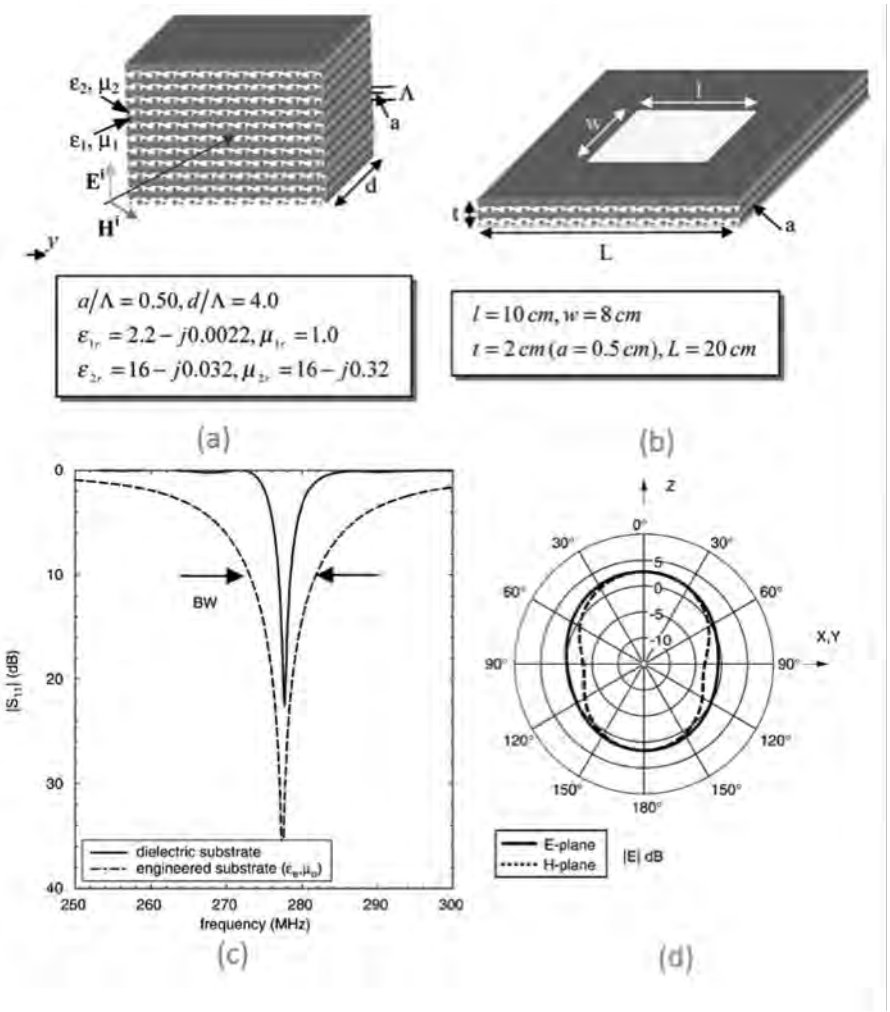

FIGURE 2.9: **(a) Bulk periodic metamaterial, (b) Patch antenna with metamaterial substrate, (c) Reflection coefficient of the metamaterial antenna and the reference antenna with respect to frequency, (d) Radiation pattern of the metamaterial antenna for the E and H planes [3].**

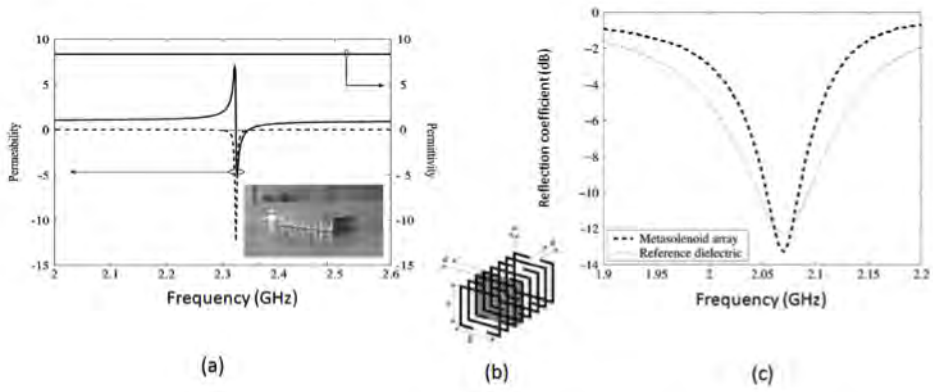

FIGURE 2.10: **(a) Permittivity and permeability of the metamaterial with respect to frequency. The dashed lines represent the imaginary part and solid lines real parts. The inset show a picture of the antenna with the metamaterial substrate (b) Schematic of the metasolenoid metamaterial, (c) Reflection coefficient of the metamaterial and reference antenna with respect to frequency [4].**

© 2015 Tous droits réservés.

Thèse de Mhamad Hassanein Rabah, Lille 1, 2015

The bandwidth of the metamaterial is shown to be smaller than the reference dielectric antenna. The authors demonstrate that this is due to the dispersive behavior of the permeability. These results demonstrate the limits of this approach to miniaturize patch antennas. Frequency dispersion, high value of losses and fabrication issues make bulk metamaterials less appealing for antenna miniaturization applications. Surfaces made of metamaterials have been proposed for patch antenna miniaturization. For instance, reactive impedance metamaterial substrates have been studied [5]. The metamaterial is shown in Fig. 2.11 (a) and the corresponding surface impedance on Fig. 2.11 (b). This metamaterial is termed reactive impedance metamaterial since the real part of the effective impedance is zero such that the magnitude of the reflection coefficient is equal to one and its phase is different from π as for metallic surfaces. Fig. 2.11 (c) depicts the metamaterial antenna designed and fabricated and its reflection coefficient is shown in Fig. 2.11 (d). Compared to a conventional antenna of same surface

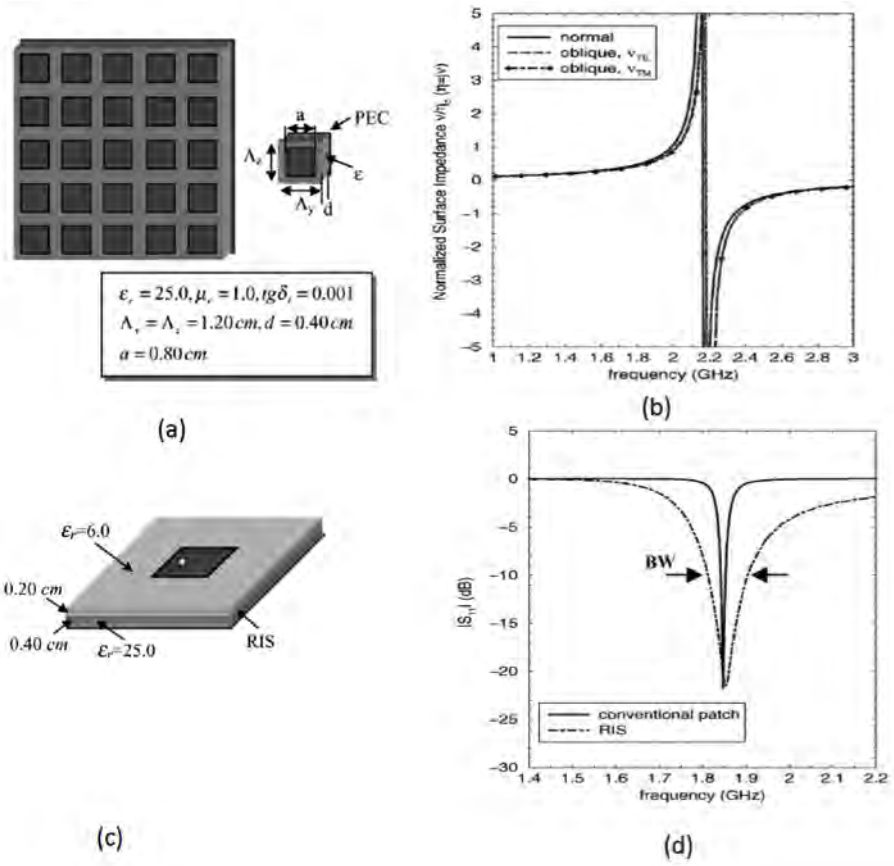

FIGURE 2.11: **(a) Metamaterial reactive impedance substrate, (b) Normalized surface impedance with respect to frequency, (c) Patch antenna on a reactive impedance substrate, (d) Reflection coefficient with respect to frequency for a conventional patch antenna and the reactive impedance metamaterial antenna [5].**

and resonating at the same frequency, the bandwidth is much higher. The antenna

© 2015 Tous droits réservés. doc.univ-lille1.fr

Thèse de Mhamad Hassanein Rabah, Lille 1, 2015

is miniature (almost $\lambda/10$). The measured bandwidth is 6.7% and the radiation efficiency is 90%. These results are very promising for antennas based on metamaterial surfaces. In this work, a modal study of this design is presented in Chapter 4. It will be shown that this RIS presents artificial magnetic response such as metasolenoids, for a particular excitation.

Furthermore, another class of metamaterial-based wideband antennas is overviewed in [64]. These antennas are mainly frequency independent. They are based on spiral configurations and use Band Gap material (a class of FSS) for the ground plane. Unfortunately, this type of antennas is directive and not suitable for cognitive radio systems since the latter require omnidirectional power patterns.

2.6 Metamaterial Inspired Antennas

Based on the studies of metamaterial based antennas, and to ensure practical realizations, a novel approach has been proposed by Erentok [6]. The authors propose to insert a single tailored metamaterial inclusion as a parasitic element in the extreme near-field of an ESA to enhance the input impedance matching and radiation efficiency. The term "metamaterial-inspired antennas" has been coined for this approach to differentiate it from "metamaterial-based antennas" where bulk homogenous metamaterials are considered.

Metamaterial-inspired antennas are constructed as a driven element and a resonant parasitic element in the very near field of the driven element. These ESAs are nearly completely matched to a real source and have a very high overall efficiency [6]. These properties are achieved through the parasitic element, which replaces the need for an external matching network and which works with the driven element to enhance the radiation process. Fig. 2.12 illustrates the coupling and radiation behavior of a small-loaded antenna. In fact, electrically small antennas suffer from the high reactive energy in their near field. This energy could be electric, then modelled by a capacitor (Fig. 2.12) or magnetic and modelled by an inductor. However, each case needs a specific parasitic element in the near field to act like and ENG and MNG medium, respectively. This is the main idea of metamaterial-inspired antennas.

Authors of [6] present two categories of MTM inspired antennas: magnetic based and electric based antennas. They are available in 3D and 2D configurations. In the next sections, 3D magnetic based and 2D electric based antennas are studied. The other 2D and 3D structures are not presented because they possess the same behaviour as the presented designs.

© 2015 Tous droits réservés. doc.univ-lille1.fr

Thèse de Mhamad Hassanein Rabah, Lille 1, 2015

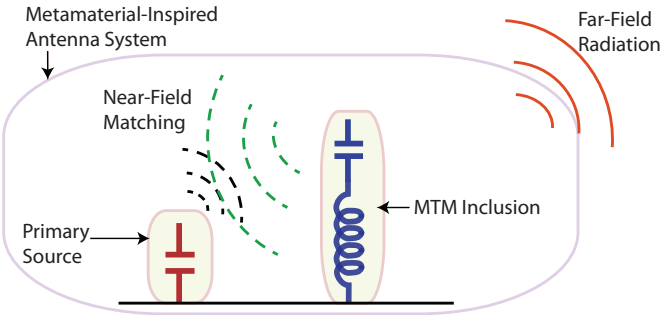

FIGURE 2.12: **Illustration of the coupling and radiation behavior of the near-field metamaterial-inspired small antenna. The driven element (capacitor) represents a monopole/dipole antenna which stores electric energy in his near-field. The parasitic element, replaces the need for an external matching network.**

2.6.1 Magnetic-Based MTM Inspired Antenna

3D magnetic-based antenna design was implemented with an MNG metamaterial inspired structure which consists of an extruded 3D capacitively-loaded loop (CLL) element. The CLL is driven by an electrically-small circular antenna which is coaxially-fed through a finite PEC ground plane. The design configuration is shown in Fig. 2.13.

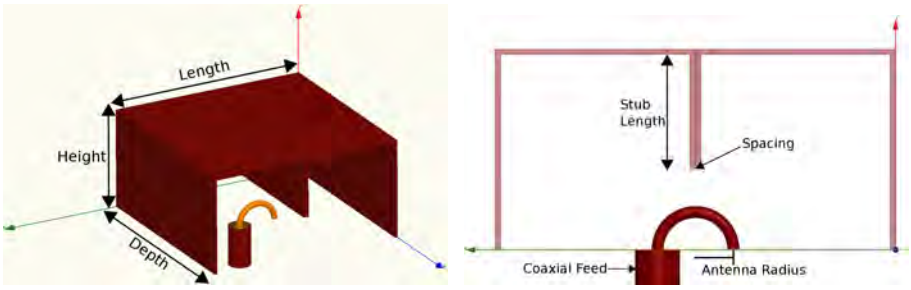

(a) (b)

FIGURE 2.13: **3D magnetic based antenna presented in [6]: (a) 3D view and (b) 2D cross-sectional view. The driven element is an electrically small loop antenna and the resonant parasitic element is the capacitively coupled loop [7].**

The time varying magnetic flux generated by the loop antenna induces currents on the extruded CLL structure and produces correspondingly large electric fields between two stub arms which stores electric energy. This energy is sufficiently large to match both the magnetic energy stored by the current path formed by the extruded CLL structure and the ground plane, and that of the electrically-small semi-circular loop antenna. Thus, the self-resonant nature of the CLL is mutually transmitted to the electrically-small semi-loop circular antenna via the near-field coupling and hence, make a resonating (antenna + inclusion) system. The complex input impedance behavior for the considered 3D magnetic based antenna is shown in Fig. 2.14. The antenna is matched at 300 MHz and presents a narrow bandwidth. This is due to the

© 2015 Tous droits réservés. doc.univ-lille1.fr

Thèse de Mhamad Hassanein Rabah, Lille 1, 2015

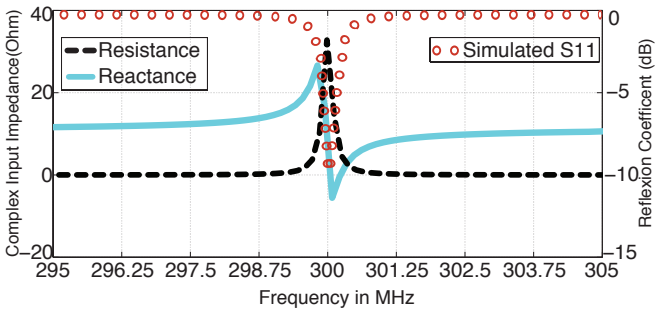

FIGURE 2.14: **S_{11} (right) and complex input impedance (left) of the 3D magnetic-based antenna presented in [6]. The input reactance behave like magnetic dipole resonant antenna. The anti-resonance occurs when the reactance crosses zero from positive to negative.**

narrow bandwidth of the resonant CLL element alone. The anti-resonant nature of the input impedance is apparent: the resistance and reactance curves exhibit characteristics analogous to the anti-resonant behavior of an electrically-small circular loop (i.e. a magnetic dipole) antenna [55].

2.6.2 Electric-based MTM Inspired Antenna

The proposed 3D electric based antenna in [6] was reduced to a planar design by integrating an electrically small printed monopole antenna with a 2D meander-line structure over a finite ground plane. The bottom of the 2D meander line is connected directly to the finite ground plane. The design configuration of the proposed 2D electric-based antenna achieved with a planar 2D meander line matching element is illustrated in Fig. 2.15. The transmission line is naturally inductive. Hence, the mean-

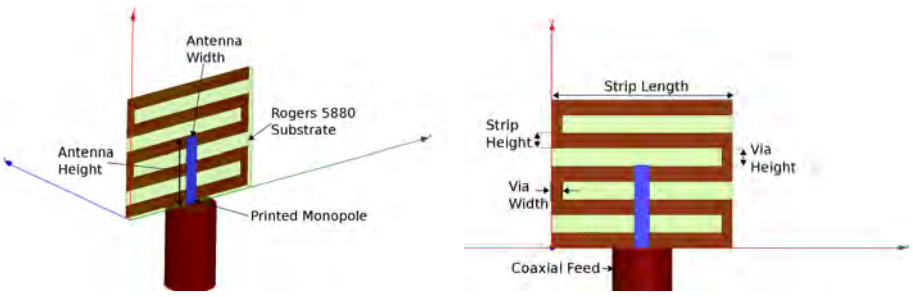

(a) (b)

FIGURE 2.15: **2D Electric based antenna presented in [6]: (a) 3D view and (b) 2D cross-sectional view. The driven element is an electrically small monopole antenna and the resonant parasitic element is a meander line.**

der line here could be considered as a series of inductors which store a large amount of magnetic energy. This stored energy is enough to conjugate the electric energy stored by the electrically small monopole antenna. Therefore, the self-resonant nature of the

© 2015 Tous droits réservés. doc.univ-lille1.fr

Thèse de Mhamad Hassanein Rabah, Lille 1, 2015

meander line is mutually transmitted to the electrically small monopole antenna via the near-field coupling and hence, make a resonating (antenna + inclusion) system. The complex input impedance behavior for the considered 2D electric based antenna is shown in Fig. 2.16.

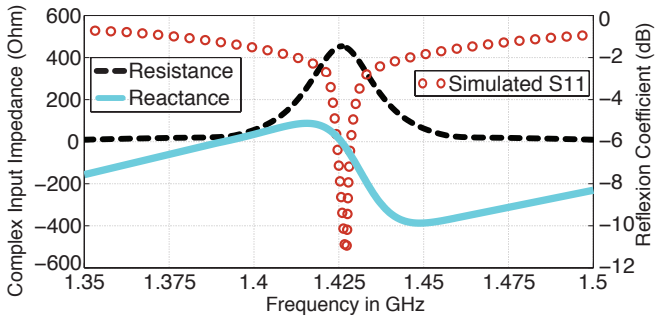

FIGURE 2.16: **S_{11} (right) and complex input impedance (left) of the 2D electric-based antenna presented in [6]. The input reactance presents a monopole like resonance behaviour. The resonance occurs when the reactance cross zero from negative to positive.**

The antenna is matched at 1.425 GHz and presents a wider bandwidth that the 3D magnetic based because of the losses into the substrate. The resonant nature of the input impedance is apparent: the resistance and reactance curves exhibit characteristics of a typical resonant behavior of an electrically-small monopole (i.e. an electric dipole) antenna [55].

The MTM inspired antenna is a very promising concept for narrow band antenna design. However, the design of such antennas is still intuitive and not systematic, since it is based on classical elementary antennas such as dipoles and loops. In this work a systematic methodology serving as an antenna synthesis technique will be proposed in chapters 5 and 6, through the use of the theory of characteristic modes.

2.7 Existing Antenna Solutions Using the Theory of Characteristic Modes

The application of the theory of characteristic modes to antennas has been attracting a lot of researchers since TCM has been revisited by Cabedo *et al.* [19] in 2007. The main concerned designs in [19] were wire and patch antennas. The modal study helps designers to identify the best type and placement of the excitation for a specific structure (for example see Fig. 2.17).

© 2015 Tous droits réservés. doc.univ-lille1.fr

Thèse de Mhamad Hassanein Rabah, Lille 1, 2015

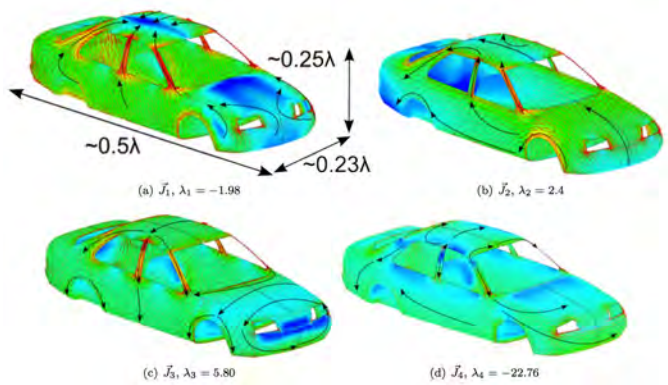

FIGURE 2.17: **The first four eigencurrents and eigenvalues for a vehicle modelled with FEKO in order to find the optimum antenna placement [8, 9].**

Moreover, the TCM has been extended and used by many research groups to design antennas. In [65], the bandwidth of a TM_{10} electrically small antenna has been enhanced and tuned using the characteristic input admittance analysis. Furthermore, the modal concept has been used to formulate an expression for antenna Q factor and then many groups developed their own algorithms to optimise the antenna size in order to reduce the antenna Q [66–68]. More details about the TCM metrics used in antenna application are provided in Chapter 3. Also, TCM has been applied to antenna isolation in the context of MIMO systems [69–71] (for example see Fig. 2.18).

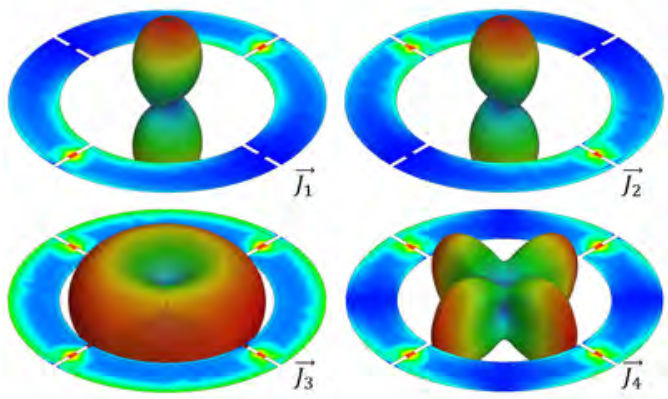

FIGURE 2.18: **The first four eigencurrents and eigenfields for ring antenna used for 2×2 MIMO system [10].**

Meanwhile, to date, no work on the application of TCM to metamaterial is found in the literature. This topic will be heavily discussed in next chapters. Next, the mathematical formulation and characteristic modes computation are reported.

© 2015 Tous droits réservés. doc.univ-lille1.fr

Thèse de Mhamad Hassanein Rabah, Lille 1, 2015

2.8 Conclusion

In this chapter, a brief state of the art on CR configurations and required antennas are presented. The design challenges and associated physical limitations were reported. Antennas using metamaterials to overcome these limitations are also presented. They exist into two versions: metamaterial-based and metamaterial-inspired antennas. Furthermore, it has been emphasised that a systematic design tool, namely, the theory of characteristic modes, has not been yet applied to metamaterial based/inspired antennas, and will be involved in the present work to design MTM Inspired structures.

© 2015 Tous droits réservés.

doc.univ-lille1.fr

Chapter 3

Introducing TCM for Metamaterial Inclusions

3.1 Introduction

The Theory of Characteristic Modes (TCM) had its humble beginnings in the early 1970's. The beauty of TCM lies in its ability to fully characterise the radiation and scattering properties of an object of arbitrary shape, and material properties. This ability provides valuable insight into an antenna physical behavior without the need of a feeding arrangement as well as providing information about how desirable radiation modes can be excited. This feature has led to its use to antenna design in the High Frequency (HF) band when integrated in land vehicles, ships and aircraft. In particular, TCM provides a powerful tool to understand and exploit excitation in the near field of an antenna (or inclusion), unlike conventional approaches which consider only plane wave excitation. However, TCM remained narrowly used until it was rediscovered a decade ago for aiding to the design of mobile handset antennas. Even so, TCM had not been addressed yet to study antennas with metamaterials or metamaterial inclusions. We believe that TCM features provide a very interesting tool for the study of metamaterials.

In this chapter, the mathematical formulation of TCM is presented. A relationship between the first eigenmode and an expression of the polarizability is proposed for a split ring resonator. It thus allows us to describe a link between the artificial magnetic response of a split ring resonator and modal characteristics. Using the new metrics proposed, a reactive impedance substrate based on metal-dielectric metamaterial excited by a parallel magnetic field is shown to exhibit artificial magnetism. These

© 2015 Tous droits réservés. doc.univ-lille1.fr

Thèse de Mhamad Hassanein Rabah, Lille 1, 2015

metrics are shown to propose good agreement with other analytical and numerical methods.

3.2 Formulations of The Theory of Characteristic modes and Computation Assumptions

The theory of characteristic modes was first developed by Garbacz [72] and was later refined by Harrington and Mautz [73] in the seventies. Initially it was given for perfectly conducting (PEC) objects [73], then expanded for penetrable objects [74]. It was originally applied to antenna-shape synthesis [75], and to control the obstacle scattering by reactive loading [76]. However, this theory practically fell into disuse later, in spite of the fact that it leads to modal solutions even for arbitrary shapes. This is particularly useful in problems involving analysis, synthesis, and optimization of antennas and scatterers. Nowadays, this analysis is brought to action again [19, 65, 67, 70, 77, 78] and therefore it became constructive to re-explain in this section what TCM is. For more details about TCM formulations and applications, reader is invited to see the book in [79] since it compiles and organises the advanced research achievements made in the area of CM studies.

In 1971 Garbacz [72] approached the problem of scattering of conducting bodies by diagonalizing the corresponding scattering matrix. On the other side, Harrington approached the same problem by diagonalizing the operator relating the current to the tangential electric field on the body. In this work, the Harrington approach is adopted when the characteristic modes are computed.

Consider the problem of one or more conducting bodies, defined by the surface S. Any applied electric field $\underline{E}^{\mathrm{i}}$ will produce a surface current $\underline{J}$ over S as illustrated in Fig. 3.1.

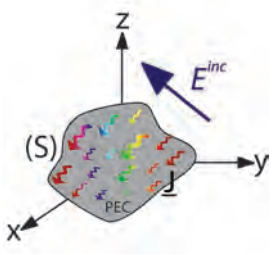

FIGURE 3.1: **Arbitrary PEC object S in an impressed field E and the induced surface current $\underline{J}$.**

From Maxwell equations and the boundary conditions derived therein, the total tangential electric field must be zero on the surface of the conductor. Thus, these surface

© 2015 Tous droits réservés. doc.univ-lille1.fr

Thèse de Mhamad Hassanein Rabah, Lille 1, 2015

currents on the conductor must produce a scattered field that enforces this boundary condition. The surface currents generated in this way are defined using the operator L with impedance dimensions:

$$[L(\underline{J}) - \underline{E}^{\mathrm{i}}]_{\tan} = 0 \tag{3.1}$$

while

$$[L(\underline{J})]_{tan} = Z(\underline{J}) = R(\underline{J}) + jX(\underline{J}), \tag{3.2}$$

where R and X are the real and imaginary part of the impedance operator Z which is real and symmetric [73], also known as a Hermitian operator. Satisfying physical interpretations can be made for these operators if we consider the complex power associated with an arbitrary complex current density $\underline{J}$ as:

$$P_{\mathrm{comp}} = \left\langle \underline{J}^*, Z(\underline{J}) \right\rangle = \left\langle \underline{J}^*, R(\underline{J}) \right\rangle + j\left\langle \underline{J}^*, X(\underline{J}) \right\rangle, \tag{3.3}$$

where $\left\langle *, * \right\rangle$ is defined as the inner product for all square integrable functions in the Hilbert space on the surface S, such that $\left\langle a, b \right\rangle = \oiint_S a^* \cdot b \, dS$. R and X are associated to the real power and net stored energy (reactive power) of the current $\underline{J}$, respectively, since the relationships $P_{\mathrm{rad}} = \left\langle \underline{J}^*, R(\underline{J}) \right\rangle$ and $P_{\mathrm{reac}} = \left\langle \underline{J}^*, X(\underline{J}) \right\rangle$ hold true [73]. Since real power must be greater than or equal to zero, it implies that the operator R must be positive definite in addition to being Hermitian. By making a change of variables in the most general form of the eigen-value problem involving the operator Z, we can re-write the eigen-value problem in the alternative form $Z(\underline{J}_n) = (1 + j\lambda_n)R(\underline{J}_n)$ which can be further simplified, leading to the final generalized eigen-value problem:

$$X(\underline{J}_n) = \lambda_n R(\underline{J}_n). \tag{3.4}$$

The operators R and X are both real symmetric, making the eigenvalues λ_n and eigen-vectors $\underline{J}_n$ real and equiphase, respectively.

3.2.1 Characteristic fields Orthogonality

The electric fields $\underline{E}_n$ and the magnetic fields $\underline{H}_n$ produced by an eigencurrent $\underline{J}_n$ on S are called the characteristic fields or eigen-fields associated to $\underline{J}_n$. The orthogonality relationships for the characteristic fields corresponding to the characteristic currents are obtained by means of the complex Poynting theorem [73]. In fact, the orthogonality properties of the characteristic modes is inherited from the currents to the fields.

© 2015 Tous droits réservés. doc.univ-lille1.fr

Thèse de Mhamad Hassanein Rabah, Lille 1, 2015

Explicitly, the complex power balance for currents J on S is given by:

$$P_{\text{comp}} = \oiint_{S'} \underline{E} \times \underline{H}^* \, dS + j\omega \iiint_{V'} (\mu \underline{H} \cdot \underline{H}^* - \epsilon \underline{E} \cdot \underline{E}^*) \, dV' \tag{3.5}$$

where S' is any surface enclosing the object S and V' is the volume enclosed by S'. When considering the modal currents, we derive a similar expression for the complex power associated with the mth and nth characteristic mode as:

$$P_{\text{comp,n}} = \left\langle \underline{J}_m^*, R(\underline{J}_n) \right\rangle + j \left\langle \underline{J}_m^*, X(\underline{J}_n) \right\rangle = (1 + j\lambda_n)\delta_{mn}, \tag{3.6}$$

which further implies that

$$\oiint_{S'} \underline{E}_m \times \underline{H}_n^* \, dS = \delta_{mn} \tag{3.7}$$

and

$$\omega \iiint_{V'} (\mu \underline{H}_m \cdot \underline{H}_n^* - \epsilon \underline{E}_m \cdot \underline{E}_n^*) \, dV' = \lambda_n \delta_{mn} \tag{3.8}$$

which can be interpreted as the orthogonality of active power and orthogonality of net stored energy between characteristic modes [80].
In order to prove this orthogonality in the far field region, we consider the eigen electric field of purely outward traveling waves, with the form:

$$\underline{E}_n = \eta_0 \underline{H}_n \times \hat{n} = \frac{-j\omega\mu}{4\pi} \frac{e^{-jkr}}{r} \underline{F}_n(\theta, \phi), \tag{3.9}$$

where η_0 is the free-space intrinsic impedance, r the radial distance from the origin, $\hat{n}$ the unit normal to the sphere at infinity, and $\underline{F}_n(\theta, \phi)$ the characteristic pattern or eigen-pattern associated with the eigen-current $\underline{J}_n$.
By adding equation (3.6) to its conjugate, and interchanging m and n, we obtain the orthogonality properties of the characteristic fields $\underline{E}_n$ and $\underline{H}_n$

$$\frac{1}{\eta_0} \oiint_{S'} \underline{E}_m \cdot \underline{E}_n^* \, dS = \delta_{mn} \tag{3.10}$$

and

$$\eta_0 \oiint_{S'} \underline{H}_m \cdot \underline{H}_n^* \, dS = \delta_{mn} \tag{3.11}$$

Therefore, equations (3.11) and (3.10) show that the far fields associated with each characteristic mode are mutually orthogonal, which is a very important condition for the study of the modes. This issue will be further discussed in chapter 6.

© 2015 Tous droits réservés. doc.univ-lille1.fr

Thèse de Mhamad Hassanein Rabah, Lille 1, 2015

3.2.2 Surface Current Decomposition and Associated Metrics

The scattered field from an arbitrary PEC scatterer can be expressed in terms of the characteristic modes of that structure [73]. In other words, the surface currents can be written as a linear summation of the eigen-currents, and consequently the scattered field can be written as a linear summation of the eigen-fields. Given some arbitrary excitation, it is possible to determine which characteristic modes is excited. The excitation can be in the form of a feeding mechanism (voltage gap, coaxial feed, aperture coupling) or arbitrary incident electromagnetic waves. Any excitation will produce a surface current over the conducting surface S. Since the modal currents are weighted and orthogonal over the surface S, thus, any arbitrary current can be expanded as follows:

$$\underline{J} = \sum_{n=0}^{\infty} w_{c,n} \underline{J}_n \qquad \text{with} \qquad \mathrm{n} = 0, 1, 2, 3, ... \tag{3.12}$$

where $w_{c,n}$ are the modal weighting coefficients. These modal currents are the eigen-modes of the structure and they are calculated by solving the eigenvalue problem in equation (3.4). For each eigenvalue λ_n a reactive energy $P_{\mathrm{reac},n}$ and a radiated energy $P_{\mathrm{rad},n}$ are associated:

$$\lambda_n = \frac{P_{\mathrm{reac,n}}}{P_{\mathrm{rad,n}}} = \frac{\left\langle \underline{J}_n^*, X(\underline{J}_n) \right\rangle}{\left\langle \underline{J}_n^*, R(\underline{J}_n) \right\rangle} = \frac{2\pi f W_{\mathrm{net,n}}}{P_{\mathrm{rad,n}}}, \tag{3.13}$$

where $W_{\mathrm{net},n}$ is the net stored energy of a specific mode n and f is the frequency.

The physical sense behind the calculated quantities could be exploited using many metrics derived from the eigenvalue λ_n. The characteristic angles ϕ_n are given by [19]:

$$\phi_n = 180^\circ - \tan^{-1}(\lambda_n). \tag{3.14}$$

Indeed, modes having a ϕ_n close to 270° and 90° are considered storing electric and magnetic energy, respectively. Radiating modes have characteristic angles near to 180°. The modal significance (MS) which reflects the mode radiation intensity is defined at each frequency as:

$$\mathrm{MS}_n = \left| \frac{1}{1 + j\lambda_n} \right|. \tag{3.15}$$

To take into consideration both the effects of an excitation and the mode resonance condition, an expression for the modal weighting coefficient $w_{c,n}$ is defined by substituting equation (3.12) into equation (3.4) and taking the inner product of (3.4) with

© 2015 Tous droits réservés. doc.univ-lille1.fr

Thèse de Mhamad Hassanein Rabah, Lille 1, 2015

respect to $\underline{J}_m$

$$\sum_{n=0}^{\infty} \omega_{c,n} \left\langle \underline{J}_m^*,\ Z(\underline{J}_n) \right\rangle - \left\langle \underline{J}_m^*,\ \underline{E}_{\tan}^{\text{inc}} \right\rangle = 0 \qquad \text{with } m \neq n. \tag{3.16}$$

Modal currents being orthogonal [73],

$$w_{c,n}(1 + j\lambda_n) = \left\langle \underline{J}_n,\ \underline{E}_{\tan}^{\text{inc}} \right\rangle. \tag{3.17}$$

The expression of the modal weighting coefficient then becomes

$$w_{c,n} = \left| \frac{\left\langle \underline{J}_n,\ \underline{E}_{\tan}^{\text{inc}} \right\rangle}{1 + j\lambda_n} \right|, \tag{3.18}$$

where

$$\left\langle \underline{J}_n,\ \underline{E}_{\tan}^{\text{inc}} \right\rangle = \oiint_S \underline{J}_n \cdot \underline{E}_{\tan}^{\text{inc}} dS = V_n^i. \tag{3.19}$$

V_n^i is the modal excitation coefficient and it shows how much an eigencurrent is affected by the type and position of the excitation. The main advantage of such a metric, is that it can be defined for an arbitrary excitation and for a plane wave. It could be, for example, a voltage gap, an electric or magnetic dipole in the near field of the structure.

3.2.3 Active and Reactive Modal Powers

When all the modes in a structure are involved, the total active and reactive powers can be calculated theoretically with TCM. The contribution to the overall net stored energy of the arbitrary PEC surface can be expressed in terms of CMs as follows [80]:

$$\begin{aligned} P_{\text{reac}} = \omega W_{\text{net}} &= \left\langle \underline{J}^*, X(\underline{J}) \right\rangle \\ &= \left\langle \sum_{n=0}^{\infty} w_{c,n}^* \underline{J}_n^*, X\left(\sum_{n=0}^{\infty} w_{c,n} \underline{J}_n \right) \right\rangle \\ &= \sum_{n=0}^{\infty} w_{c,n}^* w_{c,n} \left\langle \underline{J}_n^*, X(\underline{J}_n) \right\rangle \\ &= \sum_{n=0}^{\infty} \left| w_{c,n} \right|^2 \lambda_n. \end{aligned} \tag{3.20}$$

Thus, the reactive power per mode could be expressed as:

$$P_{\text{reac,n}} = \left| w_{c,n} \right|^2 \lambda_n. \tag{3.21}$$

© 2015 Tous droits réservés. doc.univ-lille1.fr

Thèse de Mhamad Hassanein Rabah, Lille 1, 2015

The sign of the eigenvalue λ_n decides wether the reactive power $P_{\text{reac,n}}$ is capacitive or inductive.
In a similar manner we can also expand the radiated power as:

$$\begin{aligned} P_{\text{rad}} &= \left\langle \underline{J}^*, R(\underline{J}) \right\rangle \\ &= \left\langle \sum_{n=0}^{\infty} w_{c,n}^* \underline{J}_n^*, R\left(\sum_{n=0}^{\infty} w_{c,n} \underline{J}_n \right) \right\rangle \\ &= \sum_{n=0}^{\infty} w_{c,n}^* w_{c,n} \left\langle \underline{J}_n^*, R(\underline{J}_n) \right\rangle \\ &= \frac{1}{2} \sum_{n=0}^{\infty} \left| w_{c,n} \right|^2 \quad \text{since} \quad \left\langle \underline{J}_n^*, R(\underline{J}_n) \right\rangle = \frac{1}{2}, \end{aligned} \tag{3.22}$$

with the individual contribution of each mode expressed as:

$$P_{\text{rad,n}} = \frac{1}{2} \left| w_{c,n} \right|^2. \tag{3.23}$$

In equation (3.22), the inner product $\left\langle \underline{J}_n^*, R(\underline{J}_n) \right\rangle$ is equal to 0.5 in order to normalize the radiated power per mode to a half Watt. This value is with respect to the considered normalization in the code used to calculate the eigencurrents in this work [8].

So far, it will be shown that in the electrically small regime, the first modes capture the most of the power in the structure. In other words, electrically small antennas could be considered single-mode antennas. Therefore, it can be said that the summation of the powers of predominant modes is close to the total power injected.

3.2.4 Characteristic Modes Computations and Assumptions

When Harrington and Mautz introduced their approach to the theory of characteristic modes [73], they immediately followed by a description of how to obtain the characteristic modes numerically using a moment method formulation [81]. Rather than diagonalizing the scattering matrix directly, Harrington and Mautz instead diagonalized the impedance operator. A straightforward algorithm to diagonalize the impedance matrix [Z], and then, calculate the characteristic modes is detailed in [82]. They obtained a set of currents, and their respective far-field patterns, that were orthogonal and could be used in general as expansion functions for the currents and scattered field. What sets this formulation apart from the previous attempt by Garbacz is that it allowed a universal technique [the method of moments (MoM)] to obtain the characteristic modes. The detailed knowledge of the impedance operator allowed

© 2015 Tous droits réservés. doc.univ-lille1.fr

Thèse de Mhamad Hassanein Rabah, Lille 1, 2015

a slew of properties to be derived that would have been otherwise difficult to obtain using Garbacz's original formulation [72].

CMs for PEC objects: Surface integral equation (SIE), together with the MoM, is used for solving CMs time harmonic electromagnetic radiation and scattering problems from PEC objects. There are two basic SIEs for PEC structures: the electric field integral equation (EFIE) and the magnetic field integral equation (MFIE). In the EFIE, the boundary condition is enforced on the tangential electric field and is suitable for open objects, whereas in the MFIE, the boundary condition is enforced on the tangential magnetic field [82] and is suitable for closed objects. Furthermore, a new formulation based on EFIE and MFIE is suggested in [83] when PEC sheets are considered. It proves to be more efficient while computing a complete solution for the current densities.

CMs for composite (dielectric+metallic) objects: The formulation proposed by Harringtone in [74] to calculate CMs in penetrable bodies, is suitable only for pure dielectric (or magnetic) objects. When a metal is included, this method becomes invalid. Several approaches can be found in the literature for the simulation of combined metallic and dielectric objects. For instance, an approach based on the MoM and the PMCHWT [84–86] is used in [87] to simulate infinite PEC and dielectric sheets. Furthermore, when periodic structures are considered (*i.e.* metamaterials), a modified version of the PMCHWT formulation based on doubly periodic Green's function is proposed in [88] to solve the problem. Meanwhile, it is well acknowledged in the computational electromagnetic community that the correctness of the CM formulation derived from this PMCHWT integral equation has not been validated for obtaining correct natural resonant frequencies and their corresponding modal fields yet [79]. To the best of our knowledge, the only work using the PMCHWT formulation to calculate eigenmodes of a periodic metamaterial is found in [89].
Otherwise, volume integral equation (VIE) formulations are reliable but computationally burdensome [90].

In this work, in order to calculate CMs in composite planar structures we refer to the generalized eigenvalue equation developed from the mixed-potential integral equation (MPIE) with the spatial domain Green's functions of multi-layered medium as it is described in [79, Chapter 4]. The Green's function takes into account the multi-layered medium environment of the metallic object. Therefore, the CM theory based on this Green's function can accurately characterize the resonant frequencies, modal currents,

© 2015 Tous droits réservés. doc.univ-lille1.fr

Thèse de Mhamad Hassanein Rabah, Lille 1, 2015

and modal far fields of both fundamental and high-order radiating modes. It also avoids confusing non-radiating modes as computed from the conventional TCM [73].

Another approach based on layered medium Green's function has been proposed recently in [91] in order to simulate spherical nanoparticles. However, this approach is not adopted here since it is not implemented in the code we are using. In fact, the TCM has been implemented in the commercial integral equation solver FEKO [9], as well as many in-house codes based on Makarov code [92], [19, 77, 78, 80].

In this work, we use FEKO to solve the eigenvalue problem and calculate the eigencurrents which is a MoM solver using Rao-Wilton-Glisson (RWG) basis functions [93] and has a multi-layered medium tool.

On the other hand, the structures that we need to calculate their characteristic modes are mainly planar patch antennas, metamaterial inclusions and metamaterial inspired antennas as described in [5, 6, 94], respectively. Hence, considering the types of the studied structures we emphasise many assumptions in the simulations:

1. For MTM Inspired antennas the substrate is used as a mechanical support [6] and it could be neglected when calculating characteristic modes. This will not affect the physical behaviour analysis since modes on the metal in presence of the dielectric material hold the same when $\epsilon_r = 1$ [95]. A slight shifting of the resonance proportional to $\sqrt{\epsilon_r}$ can be produced when $\epsilon_r > 1$. However, this will simplify the problem solving and prevent the calculation of the equivalent surface currents on the dielectric faces. In doing so, the computation time will be drastically reduced. Furthermore, when the substrate needs to be considered in modal analysis (especially for high ϵ_r values used in Chapter 4), an infinite substrate based on a Green's functions of multi-layered medium is used [79].

2. It has been demonstrated using a Sub-Structure-Modes approach based on a modified Green's function that eigencurrents with an infinite ground plane approches those on a finite ground plane [96]. In this work, an infinite ground plane is considered when performing characteristic mode analysis of planar antennas with ground planes. This will prevent the calculation of non-physical current modes on the ground plane −which do not affect the analysis− and reduces the computation complexity.
   It should be noticed that when calculating scattering parameters (*i.e.* the reflection coefficient) of the antenna, a finite ground plane is considered.

Characteristic modes tracking: CMs are theoretically continuous with respect to frequency. Numerically, the impedance operator Z is discretized by the MoM to an

© 2015 Tous droits réservés. doc.univ-lille1.fr

Thèse de Mhamad Hassanein Rabah, Lille 1, 2015

impedance matrix [Z]. This discretization is done with respect to the structure subdomaines. Thus, the surface currents and fields are also discretized into vectors [82]. Unfortunately, due to the numerical solution limitations (only a finite number of modes is found at each frequency [19]), both eigencurrents and eigenvalues are disordered. This means that the resulting characteristic basis should be sorted (tracked) throughout the spectrum [97, 98].

Finally, it must be noted that it is still possible for other time domain methods, such as the Finite Difference Time Domain (FDTD) method, to compute characteristic modes [99].

3.3 New metrics validation for metamaterial inclusions

In order to use the previously proposed metrics for the analysis of metamaterials, we present a comparison with other existing approaches. For instance, the polarizability, an intrinsic parameter of the inclusions, is investigated and linked to the proposed metrics, namely the eigenvalues of the structure.

The inclusion chosen here is the broadside-coupled split-ring-resonator (BC-SRR, described in Fig. 3.2) commonly used for artificial magnetism in bulk metamaterials [57]. It is selected for its independence from E-field polarisation for axial magnetic field and absence of bi-anisotropic effects [94, 100]. Thus, the polarizability can be easily calculated.

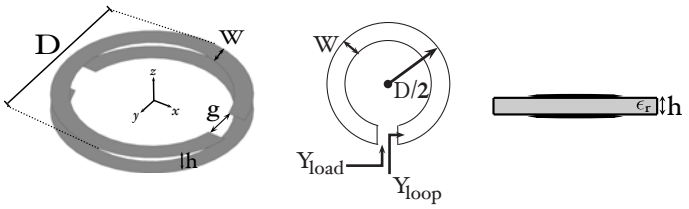

(a) 3D view (b) Top view (c) Side view

FIGURE 3.2: **Schematic of the considered BC-SRR structure. The dimensions are:** $D = 11.25$ mm, $W = 1$ mm, $g = 1.95$ mm, **the substrate height** $h = 1.08$ mm **with relative permittivity** $\epsilon_r = 2.2$. **The load admittance** Y_{load} **represents the gap admittance and** Y_{loop} **is the loop input admittance.**

The magnetic dipole moment m of this structure is defined as [101]

$$m = \bar{\bar{a}}_{mm} \cdot H + \bar{\bar{a}}_{me} \cdot E, \tag{3.24}$$

where $\bar{\bar{a}}_{mm}$ and $\bar{\bar{a}}_{me}$ are the dyadic magnetic and electric polarizabilities, respectively. For an axial magnetic field $\overrightarrow{H} = H.\hat{z}$, the electric polarizability $\bar{\bar{a}}_{me}$ vanishes and the

© 2015 Tous droits réservés. doc.univ-lille1.fr

Thèse de Mhamad Hassanein Rabah, Lille 1, 2015

dyadic magnetic polarizability becomes a scalar

$$\bar{\bar{a}}_{mm} = a_{mm} = \frac{m}{H_z} \,. \tag{3.25}$$

It is shown that m depends exclusively on the first current mode I_0, where $m = \mu.A.I_0$ and A is the area of the loop [101]. The first current mode I_0 is uniform while the second mode I_1 is not. This agrees with other proposed models [102]. The expression of I_0 is given by [101]

$$I_0 = -2r\frac{J_{\text{Bessel},1}(kr)}{A_0}\left(1 + \frac{j}{Y_{loop} + Y_{load}}\frac{1}{\pi\eta A_0}\right)H_z \tag{3.26}$$

where

$$\begin{aligned} A_0 &= \frac{kr}{\pi}\left[log(\frac{8r}{W}) - 2\right] + \frac{1}{\pi}\left[0.667(kr)^3 - 0.267(kr)^5\right] \\ &- j\left[0.167(kr)^4 - 0.033(kr)^6\right]. \end{aligned} \tag{3.27}$$

$J_{\text{Bessel},1}(kr)$ is the Bessel function of the first order, $r = D/2$ is the loop radius, η is the free space wave intrinsic impedance, and $k = \omega\sqrt{\mu\epsilon}$. The load in this case is the gap (*i.e.* open circuit) thus $\text{Y}_{\text{load}} = 0$. Y_{loop} contains the information about the eigenvalues of the characteristic modes. These modes are equivalent to characteristic port modes [75]. In the theory of characteristic modes, the impedance matrix elements are calculated from the interaction of fictitious small dipoles between two consecutive Rao, Wilton and Glisson basis functions triangles, and relate the surface current density to the electric field [93]. On the other hand, the theory of characteristic port modes is based on an identical principle relating the network impedance matrix elements to the voltages and currents at each defined port. Using both formulations, an expression of the modal input loop admittance $Y^{(n)}_{\text{loop, in}}$ is derived as follows [80]:

$$Y^{(n)}_{\text{loop, in}} = \frac{\left|\underline{J}_{n,\text{in}} \cdot \ell_{\text{edge}}\right|^2}{1 + j\lambda_n}. \tag{3.28}$$

$\underline{J}_{n,\text{in}}$ is the value of the surface current density of the nth mode at the edge where the input admittance of the loop is determined (see Fig. 3.2(b)). ℓ_{edge} is the edge length of the RWG mesh elements, it is considered to be equal to $\lambda_{\text{free}}/40$ for an ultra fine mesh, where λ_{free} is the free space wavelength. Combining (3.26) and (3.28), and substituting the first eigen current (I_0) into the magnetic dipole moment expression, lead to a relation between the polarizability and the first eigenmode λ_0

$$a_{mm} = -2\mu_0\pi r^3\frac{J_{\text{Bessel},1}(kr)}{A_0}\left(1 + \frac{j(1 + j\lambda_0)}{\left|\underline{J}_{0,\text{in}}\right|^2}\frac{1}{\pi\eta A_0}\right). \tag{3.29}$$

© 2015 Tous droits réservés. doc.univ-lille1.fr

Thèse de Mhamad Hassanein Rabah, Lille 1, 2015

Fig. 3.3 shows the eigenvalues with respect to the frequency of the considered BC-SRR. The first mode resonates at 2.4 GHz since its eigenvalue equals zero at this

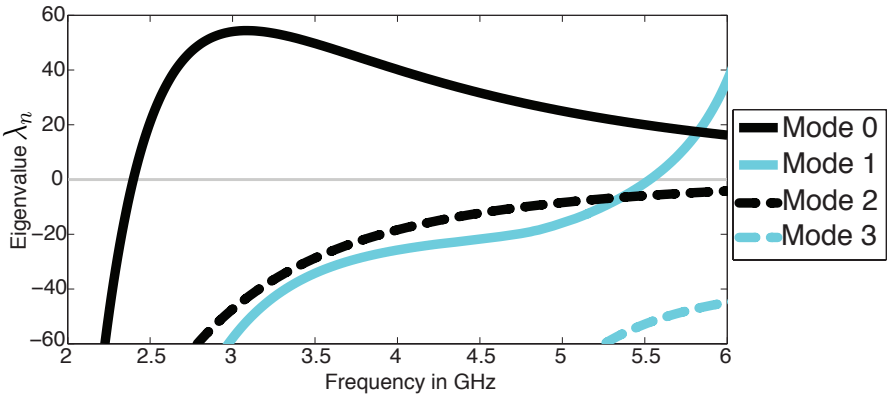

FIGURE 3.3: **First four eigenvalues of the considered BCSRR printed over both substrate faces.**

frequency. To better explain the behaviour of the modes Fig. 3.4 shows the calculated characteristic angles of the first three eigenmodes of the BC-SRR. In order to validate the new proposed metrics, the normalized polarizability $a_{mm} \cdot 3/(4\pi\epsilon_0 r^3)$ with respect to the frequency is shown on Fig. 3.4(b). The normalization is done with respect to the volume [103]. Furthermore, the transmission coefficient calculated from a plane wave excitation of a BC-SRR unit-cell [24, 104] is also plotted.

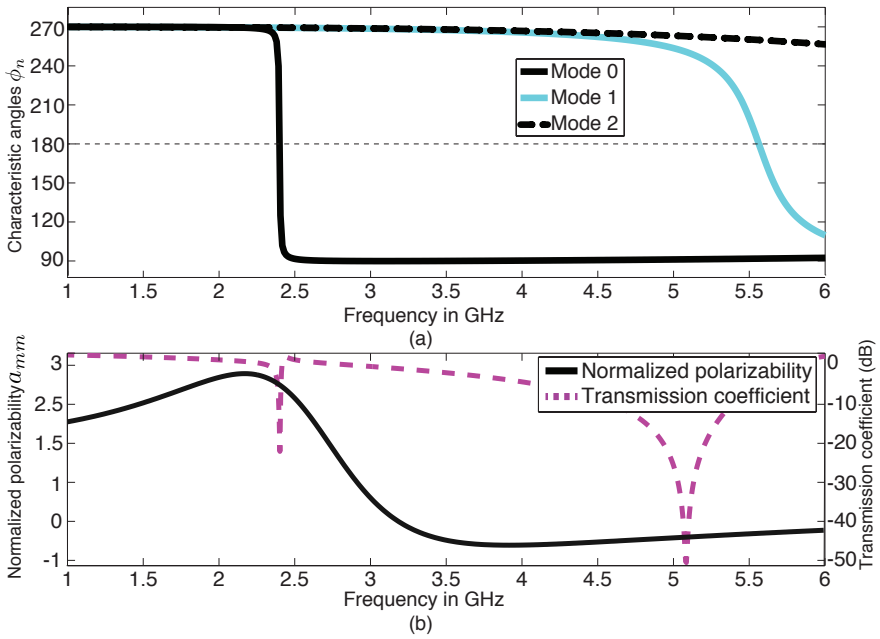

FIGURE 3.4: **(a) Characteristic angles for the first three eigenmodes ϕ_0, ϕ_1 and ϕ_2. (b) Normalized polarizability $a_{mm} \cdot 3/(4\pi\epsilon_0 r^3)$ from equation (3.29) and the transmission coefficient from conventional unit-cell analysis.**

© 2015 Tous droits réservés.

doc.univ-lille1.fr

Thèse de Mhamad Hassanein Rabah, Lille 1, 2015

The polarizability reaches a maximal value at f_0 =2.4 GHz which also corresponds to the first resonance in the transmission coefficient (Fig. 3.4(b)). At f_0, the characteristic angle, ϕ_0 is equal to 180° (eigenvalue, $\lambda_0 = 0$), indicating a first resonant mode. The inductive nature of the energy stored by the first mode J_0 is demonstrated in Fig. 3.4(a). Indeed ϕ_0 is equal to 90° ($\lambda_0 > 0$) after the resonance indicating from equation (3.13) that $P_{\text{reac},0} > 0$ since $P_{\text{rad},0}$ is always positive.

The second mode J_1 stores capacitive energy at 2.4 GHz with $\phi_1 = 270°$ (Fig. 3.4(a)). Modes 0 and 1 present the same eigenvalue behaviour except for the mode profile as shown in Fig. 3.5.

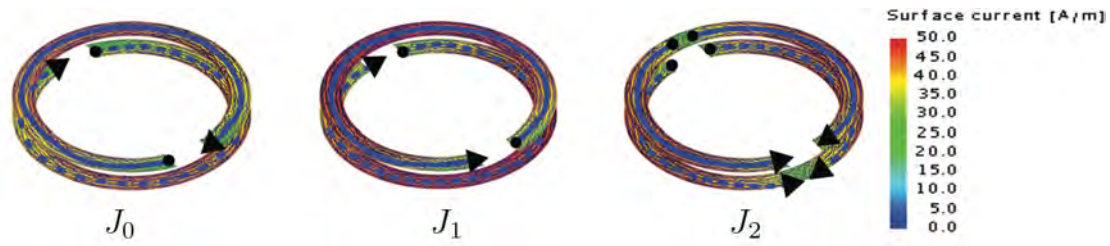

FIGURE 3.5: **First three eigencurrents profiles of the considered BC-SRR.**

Indeed, modal surface currents on BC-SRR rings are in phase for J_0 and out of phase for J_1. This explains why the second eigencurrent J_1 resonates at a higher frequency (5.6 GHz) then expected by the transmission coefficient unit-cell analysis. Only the first eigenmode is responsible of the structure resonance at 2.4 GHz while the second resonance at 5.1 GHz (Fig. 3.4(b)) is a contribution of both the first and second modes. The third mode J_2 is a purely capacitive one storing electrical energy over all the frequency band. J_2 presents an in-phase dipole-like current distribution on the BC-SRR rings (Fig. 3.5).

The TCM modal weighting coefficients are calculated for two configurations: parallel and perpendicular magnetic field $\overrightarrow{H}$ are shown in Fig. 3.6. Each mode presents a coefficient peak at the eigenmode resonance for both configurations, expect for the third mode since it is a pure reactive mode between 1−6 GHz. This can be predicted from equation (3.18). For two identical excitations, the coefficient values for a perpendicular excitation are greater than those of the parallel one by a factor of 10^2. Therefore, for J_0 the modal weighting coefficient $w_{c,0}$ is greater when $\overrightarrow{H}$ is perpendicular, whereas for J_1, $w_{c,1}$ is greater when $\overrightarrow{H}$ is parallel (*i.e.* when the electric field $\overrightarrow{E}$ is perpendicular). Nevertheless, $w_{c,1} >> w_{c,2}$ when $\overrightarrow{H}$ is perpendicular. This demonstrates that J_0 is a magnetic mode which presents the dominant magnetic response of the loop when the magnetic field is perpendicular to the loop.

© 2015 Tous droits réservés. doc.univ-lille1.fr

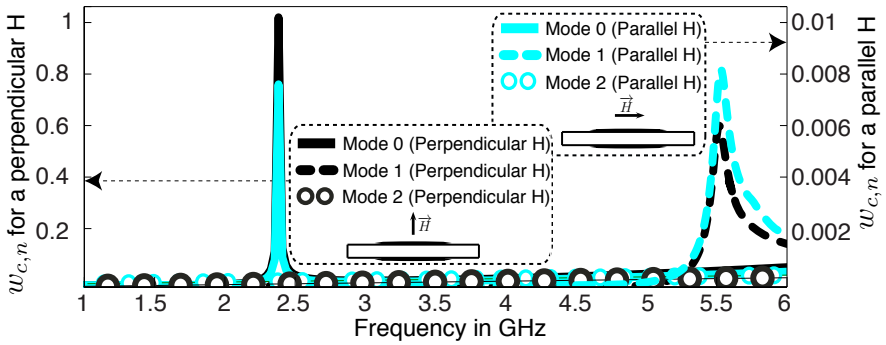

FIGURE 3.6: **Modal weighting coefficients (from equation 3.18) of the 1st, 2nd and 3rd modes of the considered broadside-coupled split-ring-resonator in presence of a perpendicular (left) and parallel (right) magnetic excitation. J_0 and J_1 have higher weighting coefficients at their resonances, when the magnetic field is perpendicular to the ring. The third mode J_2 has a weighting coefficient close to zero for both configurations since its is not a resonant mode. When the magnetic field is parallel to the plane of the ring, J_1 (electric) is more reactive than J_0. Nonetheless, J_0 (magnetic) is the most reactive when the magnetic field is perpendicular to the ring.**

This analysis agrees with the polarizability interpretation presented in this work and with other results obtained from analytical and numerical approaches [24, 101, 102].

3.3.1 Application of new metrics to demonstrate an equivalence between magnetic artificial media

After validation of the approach for a broadside-coupled split-ring-resonator, an identical analysis was performed for the reactive impedance surface shown in the inset of Fig. 3.7, together with the first five calculated characteristic angles. The reactive impedance substrate consists of small patches distributed periodically into two directions and printed on a high permittivity grounded substrate.

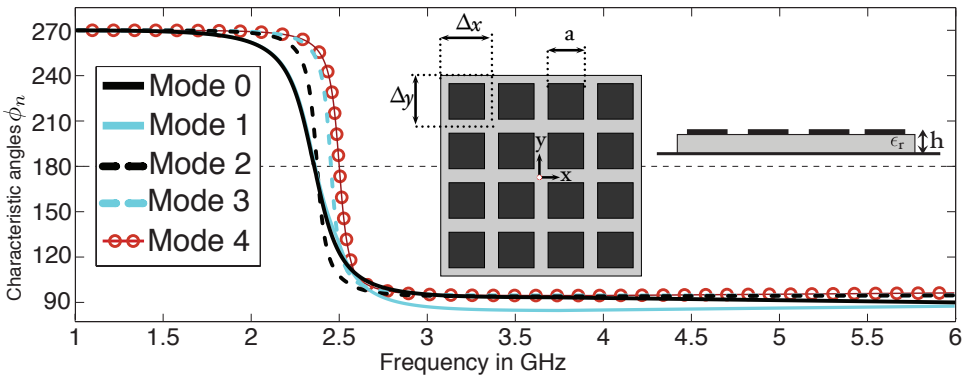

FIGURE 3.7: **Characteristic angles of the first five modes of a 4×4 reactive impedance substrate as depicted. The dimensions are $a = 12$ mm, $\Delta_x = \Delta_y = 18$ mm, $h = 4$ mm and $\epsilon_r = 25$ (Ref.[5]).**

© 2015 Tous droits réservés.

Thèse de Mhamad Hassanein Rabah, Lille 1, 2015

The first five modes resonate at very close frequencies. The first two modes J_0 and J_1 resonate at 2.4 GHz which is exactly the operational frequency of the reactive impedance substrate considered [5]. Fig. 3.7 shows that the eigenmodes can be considered magnetic after their resonances since they keep $\phi_{n=0,1,2,3,4} < 180°$. All these modes present the same behavior as the magnetic dominant mode of a broadside-coupled split-ring-resonator: all modes store electric energy up to resonance, then stored energy is transformed to a magnetic energy. In order to identify the modes reaction to different excitation configurations we follow the same analysis performed for the BC-SRR. The modal weighting coefficients are calculated for an excitation by a magnetic field $\overrightarrow{H}$ of identical magnitude for two polarizations: $\overrightarrow{H}$ parallel and perpendicular.

Fig. 3.8 shows the modal weighting coefficients of the first two modes in both configurations. The modes $J_{2,3,4}$ are omitted since they behave exactly like the first two modes. Values for a parallel excitation are greater than those for the perpendicular

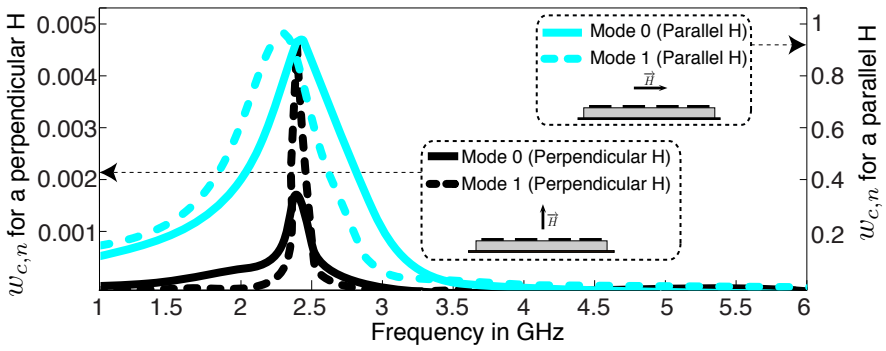

FIGURE 3.8: **Modal weighting coefficients of the $1^{st}$and 2nd modes of the considered 4×4 reactive impedance substrate in presence of a perpendicular (left) and parallel (right) magnetic excitation. Modes 1 and 2 are more reactive when the magnetic field is parallel to the substrate.**

one by a factor of 2×10^2. It is shown that the values of the coefficients of both modes are close to each other in each configuration. This confirms that both modes have the same nature which is magnetic dominant after the resonance.

3.3.1.1 Discussion

It is shown that the reactive impedance substrate current modes are very sensitive to a parallel magnetic field (*i.e.* perpendicular electric field). This means that this metamaterial behaves as an artificial magnetic material for a magnetic field parallel to the periodicity plane. The key difference between both cases is that artificial magnetism is achieved with a reactive impedance substrate for a perpendicular electric field while

© 2015 Tous droits réservés. doc.univ-lille1.fr

Thèse de Mhamad Hassanein Rabah, Lille 1, 2015

for a broadside-coupled split-ring-resonator, it is achieved with a perpendicular magnetic field. It means, for instance, that patch antennas can be easily realised without the use of bulk structures but through structures like RIS while achieving the same performances as those predicted by Hansen and Burke [22].
This analysis is suitable to study the potential metamaterials with particular magnetic response when associated to radiating objects such as antennas or cloaking applications. At much higher frequencies where the design of metamaterial can be challenging from the technological point of view, this analysis can be used to synthesise the magnetic response in the convenient polarization without going through bulky structures.

3.4 Conclusion

In this chapter, the formulation and computation of characteristic modes have been reported. New metrics for artificial magnetism has been defined. We have demonstrated the validity of these new metrics to analyze metamaterials and provide physical insight into their synthesis applications by means of characteristic modes. An agreement is shown between the analysis of the polarizability of a BC-SRR based on modal quantities and other results obtained from analytical and numerical approaches. An analogy has been made between artificial magnetic medium based on broadside-coupled split-ring-resonators used for bulk metamaterials and reactive impedance substrates used as planar metamaterials when the magnetic field is parallel to the substrate plane.

© 2015 Tous droits réservés. doc.univ-lille1.fr

Chapter 4

Quality Factor Computation for ESAs using the TCM: Application to Metamaterial-Based and Arbitrary-Shaped Antennas

4.1 Introduction

The need for miniaturized CR terminal and cohabitation of growing number of systems require antennas with small sizes and good performances. This has opened large interest in research and development of small antennas and antenna miniaturization techniques. Electrically small antennas occupy a volume of the sphere whose radius is a small fraction of the free-space wavelength of the radiated electromagnetic field [11]. Fundamental limitations of small antennas are still an active research area. Antenna size and performances are linked; for instance the bandwidth is inversely proportional to the dimensions.

Among the general techniques used to design electrically small antennas, the optimization of the antenna topology [105, 106] and the use of magneto-dielectric materials [3, 107–109] are common.

However, to approach the physical limits while keeping an acceptable radiating performance, new sophisticated techniques such as the use of artificial materials [2, 5] are more and more considered. In addition, in mobile terminals, antennas must take arbitrary shapes in order to fit the chassis geometry. This adds an extra difficulty to

© 2015 Tous droits réservés. doc.univ-lille1.fr

Thèse de Mhamad Hassanein Rabah, Lille 1, 2015

the analysis as well as to the estimation of the figure of merit of an antenna. For ESAs the figure of merit often considered is the quality factor (Q).

Metamaterial and magneto-dielectric patch antennas are attractive solutions for miniaturization [59] since it has been predicted from the zeroth-order transmission line model of a resonant patch antenna that magneto-dielectric substrates should present higher performances in terms of radiation efficiency and bandwidth when miniaturized [22]. They demonstrated, for instance, that a high effective permeability substrate is more interesting than one with a high permittivity. However at microwave frequencies, magnetic materials tend to be lossy and metamaterials should be considered to achieve a high effective permeability. Then, these metamaterial substrates have to be analyzed numerically; homogenisation techniques are generally applied for effective parameters retrieval to provide physical insight. However these techniques are invalid if the metamaterial consisting of metallic inclusions embedded in a dielectric medium is to be used in the near field of a source or close to resonance [24], as it is the case with a patch antenna. A new approach based on a numerical technique allowing for physical insight is essential.

In this context, characteristic modes (CMs) analysis can prove to be a powerful approach particularly when planar or patch antennas are involved. It can indeed address all the complexities such as metamaterial substrate, complex, arbitrary and non-canonical shapes while providing physical insight to guide antenna design and synthesis [110]. Moreover, it allows for antenna structure analysis independent from the excitation; hence enabling better design optimisation.

In this chapter, we will use the theory of characteristic modes (TCM) to address the challenge of the analysis of metamaterial-based antennas, and arbitrary-shaped antennas. The potential of such an approach for evaluating small antennas when surrounded by conventional and metamaterial substrates will be discussed. Since CMs depend only on the geometry and surrounding materials, then, the Q factor is defined as a function of the eigenvalues. This offers a huge advantage for antenna shape optimisation without any *a priori* knowledge of the excitation [67]. Indeed, TCM can be useful when appropriate metrics are defined [110] where homogenisation techniques fails for the physical understanding of metamaterial substrate antennas due to the near field analysis .
The present chapter has three main goals:

1. To present a new approach for analysing metamaterial based antennas using modal concept, and to propose a new expression for the Q factor based exclusively on eigenvalues.

© 2015 Tous droits réservés. doc.univ-lille1.fr

Thèse de Mhamad Hassanein Rabah, Lille 1, 2015

2. To validate the new proposed expression of the Q factor and to show the potential of TCM for the synthesis and evaluation of electrically small arbitrary-shaped antennas.

3. To demonstrate from a modal point of view that a magnetic substrate enhances the antenna bandwidth while a dielectric substrate reduces it. Furthermore, we will show that a metamaterial reactive impedance substrate acts similarly to a magneto-dielectric substrate in a specific frequency range, when associated to a miniaturized patch antenna with greatest dimension of $\lambda_0/10$. Indeed, this has been predicted from the zeroth-order transmission line model of a resonant patch antenna that magneto-dielectric ($\mu_r > \epsilon_r$) substrates should present higher performances in terms of bandwidth without affecting the radiation efficiency when miniaturized [22].

This is done by focusing on the first contributing modes in the small antenna regime.

4.2 State of the art on Electrically Small Antennas Quality Factor Calculation

An antenna doesn't radiate a wave whose wavelength is much greater than its size; therefore it doesn't resonate at that corresponding frequency. This so-called Electrically small antenna occupies a volume of the sphere whose radius a is a small fraction of the freespace wavelength of the radiated electromagnetic field (Fig. 2.7). In fact, it seems to be choking by the non-propagating reactive energy surrounding it, as it has high input reactance and low input resistance. Several approaches to describe the problem have been proposed in which Wheeler [111] and Chu [11] who were the first to consider the physical limitations of small antennas and to evaluate their performance concerning radiation efficiency, bandwidth and gain. Although Wheeler's work was important, Chu's formulation is the most common in antenna communities. The early studies (1947) on minimum Q bounds by Chu [11] were based on spherical mode circuits. For example, Fig. 4.1 shows the equivalent circuit of a TM_n spherical wave. Chu has defined the quality factor Q as:

$$Q = \frac{2.\omega_0.\max\{W_{\text{elec}}, W_{\text{mag}}\}}{P_{\text{rad}}} \tag{4.1}$$

where ω_0 is the angular frequency, $W_{\{\text{elec,mag}\}}$ is the time-average, non propagating stored energy by the antenna and P_{rad} is the radiated power. This expression represents the Q factor of a tuned antenna where the total input reactance equal to zero at

© 2015 Tous droits réservés. doc.univ-lille1.fr

Thèse de Mhamad Hassanein Rabah, Lille 1, 2015

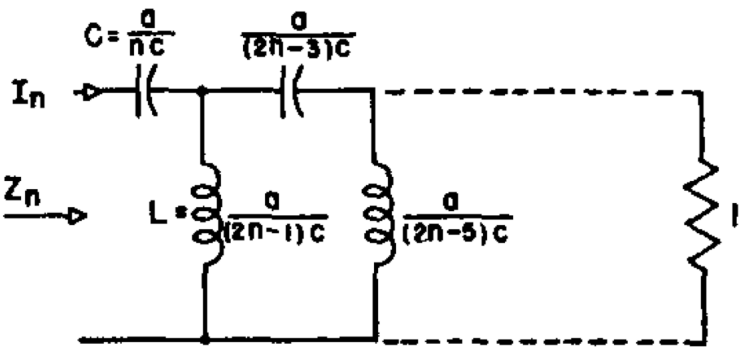

FIGURE 4.1: **Equivalent circuit of TM_n spherical wave, proposed by Chu [11].**

the resonance ω_0. Q is inversely proportional to a, i.e. antenna dimensions (Fig. 2.7). The smaller the quality factor is, the higher the radiated power by the antenna (see Section 2.4). For example the first compact expression for the quality factor proposed by Chu [11] was:

$$Q = \frac{1 + 2k^2a^2}{k^3a^3[1 + k^2a^2]}, \tag{4.2}$$

where k is the wave vector defined as $k = 2\pi/\lambda$. Chu's expression has been then refined to take into account the polarization by Mc-Lean [32]:

$$Q = \frac{1}{k^3a^3} + \frac{1}{ka}, \tag{4.3}$$

and the radiation efficiency by Hansen et al. [22]:

$$Q_{lb} = RE \times \left(\frac{1}{k^3a^3} + \frac{1}{ka}\right) \quad , \tag{4.4}$$

where RE is the radiation efficiency of the antenna.

In his formulation, Chu neglected all internal energy in the fictitious sphere which resulted into a very low bound of Q. This problem has been solved later by Hansen and Collin on the field level [112], and by Thal [113] on the circuit level, which led to the new Chu bounds. However, equations based on Chu's expression are not the most suitable for planar structures (*e.g.* patch antenna), since the antenna does not effectively use all the volume containing it. Yaghjian and Best [53] defined an efficient and accurate quality factor of antennas through a relation between the stored/radiated energies and the input impedance of the antenna; it is given by:

$$Q_z = \frac{\omega}{2R_{in}} \left| \frac{\partial Z_{in}}{\partial \omega} + j\frac{|X_{in}|}{\omega} \right|, \tag{4.5}$$

where $Z_{in} = R_{in} + jX_{in}$ is the complex input impedance of the antenna. A huge

© 2015 Tous droits réservés. doc.univ-lille1.fr

Thèse de Mhamad Hassanein Rabah, Lille 1, 2015

advantage of Yaghjian-Best expression is its suitability for the modal concepts as it will be shown later. However, it has been shown recently in [114] that the Q_Z factor is limited to first order systems and can fail when multiple resonances occur in high-order systems.

A different approach has been proposed by Gustafsson [115, 116]; it is based on searching for the minimum bound of Q with respect to the static polarizabilities γ and the antenna directivity D :

$$Q_{min} = \eta \frac{D(ka)^3}{2\pi} \gamma, \tag{4.6}$$

where η the absorption efficiency. The main advantage of this approach is that limitations can be found for antennas with arbitrary shapes while studying the impact of the polarization on the antenna performances. An arbitrary shape can be enclosed into any circumscribing metal necessary have a higher polarizability, and hence calculate the quality factor [117].

If the different features of the previous approaches are compared, one can deduce that there is no perfect formula, and especially for planar structures, such as patch antennas. Indeed, formulas based on Chu's expression are not accurate for 2D problems. Gustafsson approach is interesting in case of antennas with metamaterials, since it deals with non-canonical shapes. Furthermore, in their recent work [**?**], the authors include magnetic currents in their model to calculate the lower bounds of D/Q through the computation of the stored energies. Yaghjian-Best formula depends on a specific excitation.

Table 4.1 summarises the presented quality factor expressions emphasising on their features for comparison purposes.

© 2015 Tous droits réservés. doc.univ-lille1.fr

Thèse de Mhamad Hassanein Rabah, Lille 1, 2018

TABLE 4.1: **Summary of quality factor expressions proposed in literature.**

Reference	Expression	Notes
Chu [11]	$Q = \frac{1+2k^2a^2}{k^3a^3[1+k^2a^2]}$	• Approximate expression. • Available only in the electrically small regime. • Limited to linear polarizations.
Mc-Lean [32]	$Q = \frac{1}{k^3a^3} + \frac{1}{ka}$	• Exact expression derived from Chu's formula. • Linear and circular polarizations. • Inaccurate for planar structures.
Hansen [22]	$Q_{lb} = RE \times (\frac{1}{k^3a^3} + \frac{1}{ka})$	• Gives the lower bound of Q. • Limited to linear polarizations. • Inaccurate for planar structures.
Yaghjian [53]	$Q_z = \frac{\omega}{2R_{in}} \left\lvert \frac{\partial Z_{in}}{\partial \omega} + \jmath \frac{\lvert X_{in} \rvert}{\omega} \right\rvert$	• Proportional to the variation of the input impedance. • Accurate for planar structures. • Linear and circular polarizations. • A specific excitation needs to be defined.
Gustafsson [115]	$Q_{min} = \eta \frac{D(ka)^3}{2\pi} \gamma$	• Gives the minimum Q. • A prior knowledge of the the directivity D, the polarisability γ, the absorption efficiency η and radiation efficiency are needed. • Limited to linear polarizations. • Accurate for planar structures. • Can be calculated for canonical and non-necessarily spherical geometries. • Don't need a particular excitation.

Thèse de Mhamad Hassanein Rabah, Lille 1, 2015

When comparing the different features of equations in Table 4.1, one can deduce that there is no perfect formula, and especially for planar structures, including patch antennas. Indeed, formulas based on Chu's expression are not accurate for 2D problems, while Yaghjian-Best formula depends on a specific excitation which could not be the case when only evaluating the performances of a given structure. The Gustafsson approach is interesting in case of antennas with metamaterials, since it deals with arbitrary shapes. Nonetheless, to calculate the minimal bound of the quality factor, this still require knowledge of further antenna parameters such as the directivity, polarisability and absorption efficiency. The advantage of using the theory of characteristic modes (TCM) consists in the fact that characteristic modes can be calculated for random shapes surrounded by complex media and independent of excitations since CMs depends only on the geometry and surrounding materials. In fact, characteristic modes can be computed from a modal decomposition of the impedance MoM matrix [Z], which can be calculated for arbitrary shaped objects and separately from an external excitation. Also, the recently implemented TCM in the commercial software FEKO [8] providing access to several modal quantities has been used here. Defining a quality factor only in terms of characteristic modes, will allow us to evaluate the performances without the need to consider a specific excitation or further antenna parameters..

4.3 State of the Art (Continued): Q Factor Based on TCM

The recent advances of characteristic modes (2006–2015), and the increasing number of published papers on this topic, have made from the TCM a novel systematic tool for antenna designers, especially since that TCM deals with arbitrary-shaped antennas. Defining a quality factor based on CMs has been the subject of many recent works [19, 66, 67, 118, 119] and conferences discussions[1]. It can be found in the literature three categories of modal Q including expressions based on EM fields, those based on the eigenvalues and those based on the modal input impedance of the antenna. This paragraph will summarise these expressions.

The starting point for the definition of modal input impedance, is defining characteristic modes for generalized ports network [75]. It has been referred to as equivalent characteristic port modes [75]. In fact, in the theory of characteristic modes, the impedance matrix elements are calculated from the interaction of fictitious small dipoles between two consecutive Rao, Wilton and Glisson basis functions triangles, and relate the surface current density to the electric field [93].

[1]Private communications with R. Martens (University of Kiel), and Y. Hao (Queen Mary University of London)

© 2015 Tous droits réservés. doc.univ-lille1.fr

On the other hand, the theory of characteristic port modes is based on an identical principle relating the network impedance matrix elements to the voltages and currents at each defined port. Then, the input impedance at each port can be defined as [67]:

$$Z_{in,n} = \frac{V_n^{in}}{I_{n,in}}, \tag{4.7}$$

where

$$V_n^i = \left\langle \underline{J}_n, \underline{E}_{\text{tan}}^{\text{inc}} \right\rangle = \oiint_S \underline{J}_n \cdot \underline{E}_{\text{tan}}^{\text{inc}} \, dS \tag{4.8}$$

and

$$I_{n,in} = \int_{\text{C}_{\text{port contour}}} \underline{J}_n(\bar{r}) \cdot \hat{n}_{\text{port}} \, dC. \tag{4.9}$$

V_n^i is the modal excitation coefficient and it shows how much an eigencurrent is affected by the type and position of the excitation. $I_{n,in}$ is the modal current calculated from the surface eigencurrent densities at the considered port. For instance, if a feed-gap port is used (typical in MoM), the current is calculated using a simple integration at the port contour as shown in Fig. 4.2.

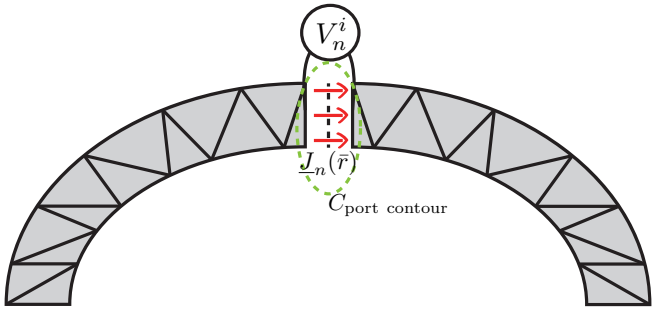

FIGURE 4.2: **Portion of an antenna in the vicinity of a feeding gap. The modal impedance is calculated using the computed $I_{n,in}$ and V_n^i.**

For a particular excitation, the input modal complex impedance $Z_{in,n} = R_{in,n} + \jmath X_{in,n}$, where $R_{in,n}$ is input modal resistance and $X_{in,n}$ is the input modal reactance of the n-th characteristic mode. The expression of the modal Q factor depending on the input impedance has been proposed in [71]; given by $Q_{z,n}$:

$$Q_{z,n} = \frac{\omega}{2R_{in,n}} \left| \frac{\partial Z_{in,n}}{\partial \omega} + \jmath \frac{|X_{in,n}|}{\omega} \right|. \tag{4.10}$$

© 2015 Tous droits réservés.

Thèse de Mhamad Hassanein Rabah, Lille 1, 2015

Furthermore, a modal fractional bandwidth can be defined including the VSWR of the antenna:

$$b_n Q_{z,n} = \frac{s-1}{\sqrt{s}} \tag{4.11}$$

where b_n is the fractional bandwidth and s =VSWR.

Eq. (4.10) has been successfully tested and compared in [71, 120]. $Q_{z,n}$ shows good accuracy for a large bandwidth and not only at the resonance. However, the total quality factor issued from Eq. (4.10) had to be derived when multiple modes contribute at the considered frequency. To do so, modal admittances at the excitation port are considered parallel, then, the total quality factor is derived as follows:

$$Q_{Z,\text{tot}}(\omega) = \frac{\omega}{2Re\left(Z_{in}\right)} \times \sqrt{\left[Re\left(\frac{\partial Z_{in}}{\partial \omega}\right)\right]^2 + \left[Im\left(\frac{\partial Z_{in}}{\partial \omega}\right) + \frac{\left|Im\left(\frac{1}{Z_{in}}\right)\right|}{\omega}\right]^2}, \tag{4.12}$$

where

$$\frac{1}{Z_{in}} = \sum_{n=1}^{N} \frac{1}{Z_n(\omega)}. \tag{4.13}$$

The values obtained from Eq. (4.12) approach those of Eq. (4.5) when the number of contributing modes is limited. When only one mode is predominant, Eq. (4.11) gives the antenna overall fractional bandwidth. According to [53] this relation between the Q factor and fractional bandwidth b remains a good approximation for $Q > 4$.

Furthermore, the original modal Q is believed to be a weighted summation of modal Qs. Then, the relation between the input impedance and the modal weighting coefficient has been used to derive a such expression. It depends on the modal Q_n based on the eigen value [e.g. Eq. (4.24)] and the modal weighting coefficients [(Eq. 3.18)]:

$$Q_{z,\text{tot}} = \frac{\sum_{n=1}^{N} Q_n |w_{c,n}|^2}{\sum_{n=1}^{N} |w_{c,n}|^2} \tag{4.14}$$

Details about the derivation can be found in [121, p. 160].

Expressions based on EM fields to derive the modal quality factor have been proposed in [66, 119, 120]. Authors in [66] derive the modal energies from current charges and densities, while in [119] the Poynting theorem has been used.
For a total radiated power P_0, they defined the radiation quality factor for the n-th

© 2015 Tous droits réservés. doc.univ-lille1.fr

Thèse de Mhamad Hassanein Rabah, Lille 1, 2015

characteristic mode over some frequency range as [119]:

$$Q_{\text{rad,n}} = \frac{2\omega \max(\langle W_{\text{mag},n}\rangle, \langle W_{\text{elec},n}\rangle)}{P_0} = \max\left(\frac{\omega}{4P_0}\left\langle \mathbf{J}_{s,n} \middle| \frac{\delta \hat{X}}{\delta \omega} \mathbf{J}_{s,n}\right\rangle_{S_0} \pm \frac{\lambda_n}{2}\right), \quad (4.15)$$

where,

$$2\langle W_{\text{mag},n}\rangle = \frac{\lambda_n P_0}{2\omega} + \frac{1}{4}\left\langle \mathbf{J}_{s,n} \middle| \frac{\delta \hat{X}}{\delta \omega} \mathbf{J}_{s,n}\right\rangle_{S_0} \quad (4.16)$$

is the time averaged magnetic stored energy and

$$2\langle W_{\text{elec},n}\rangle = -\frac{\lambda_n P_0}{2\omega} + \frac{1}{4}\left\langle \mathbf{J}_{s,n} \middle| \frac{\delta \hat{X}}{\delta \omega} \mathbf{J}_{s,n}\right\rangle_{S_0} \quad (4.17)$$

is the time averaged electric stored energy.
The expression of $Q_{\text{rad,n}}$ in (4.15) was compared with Gustafsson's analytical expression [116] for the modes TM_{10} and TE_{10}. It shows an excellent agreement for $ka < 0.65$, [119]. Note that practically all methods agree well if we are in electrically small regime, since the antenna energy behaviour can sufficiently be modeled by first order models.

The total modal Q is believed to be a weighted summation of modal Qs [121, p. 160]. However authors in [66] claim that the total Q factor can only be calculated from the modal stored energies and powers. In fact they show that a direct superposition of modal Q factor is impossible since characteristic modes are orthogonal only with respect to the far-field, not the near-field. A modal Q_N factor was proposed in[66]; it was based on stored modal energies including cross-energies between modes. For example, consider the calculation of total Q for N characteristic modes:

$$Q_N = 2\omega_0 \frac{\max\left\{\sum_n^N \sum_m^N \beta_{n,m} W_{elec}^{n,m}, \sum_n^N \sum_m^N \beta_{n,m} W_{mag}^{n,m}\right\}}{\sum_n^N \sum_m^N \beta_{n,m} P_r^{n,m}}, \quad (4.18)$$

where for the n-th and m-th characteristic modes $W_{elec}^{n,m}$, $W_{mag}^{n,m}$ and $P_r^{n,m}$ are the electric power density, the magnetic power density and the radiated power, respectively. $\beta_{n,m}$ is the coupling matrix and expressed as follows:

$$\beta_{n,m} = \frac{\langle \mathbf{J_n}, \mathbf{E^i}\rangle \langle \mathbf{J_m}, \mathbf{E^i}\rangle (1 + \lambda_n \lambda_m)}{(1+\lambda_n^2)(1+\lambda_m^2)}. \quad (4.19)$$

$\beta_{n,m}$ takes into account the feeding effect when an excitation is considered. More details about the derivation of Eq. (4.18) and Eq. (4.19) can be found in [66]. Eq. (4.18) has shown very good agreement with classical approaches over a large frequency band, and not only in the electrically small regime [66].

© 2015 Tous droits réservés. doc.univ-lille1.fr

Thèse de Mhamad Hassanein Rabah, Lille 1, 2015

In [66, Table 2] a comparative study of modal approaches for the calculation of Q is presented. It is shown that expressions based on the input impedance variation and modal energies have the fastest performances. Meanwhile, expressions based on modal energies provide more information. Table 4.2 summarises modal Q factor expressions emphasising their features; all the formulas in Table 4.2 are accurate for planar structures. However, to compute them, reactive energies must be computed or a specific excitation needs to be defined. However, for equations (4.15), (4.18) and (4.19), accessing to eigencurrent vectors and modal energies to calculate the quality factor is not possible for every antenna designer and requires to possess an in-house code. This limits the access to the calculation of these formulas only to the designers possessing their own TCM solver. Hence, to offer the advantage of using characteristic modes by a broader number of users, a simpler Q Factor expression based only on eigenvalues need to be defined.

© 2015 Tous droits réservés.

doc.univ-lille1.fr

Thèse de Mhamad Hassanein Rabah, Lille 1, 2015

TABLE 4.2: **Summary of quality factor expressions based on characteristic modes.**

Reference	Expression providing the modal Q_n	Notes
Bouezzeddine [71]	$Q_{z,n} = \frac{\omega}{2R_{in,n}} \left\| \frac{\partial Z_{in,n}}{\partial \omega} + j\frac{\|X_{in,n}\|}{\omega} \right\|$	• Modal form of Yaghjian-Best expression. • Linear and circular polarizations. • A specific excitation needs to be defined. • Accurate for planar structures. • The total Q is calculated from the superposition of parallel input admittances (Eq. 4.12).
Krewski [119]	$Q_{\text{rad,n}} = \max\left(\frac{\omega}{4P_0} \left\langle \mathbf{J}_{s,n} \middle\| \frac{\delta \hat{X}}{\delta \omega} \mathbf{J}_{s,n} \right\rangle_{S_0} \pm \frac{\lambda_n}{2} \right)$	• Require the manipulation of modal currents and energies (open-source code unavailable*). • Highly accurate in the electrically small regime. • Linear and circular polarizations. • Don't need a particular excitation • Accurate for planar structures..
Reference	Expression providing the total Q	Notes
Strojny [121]	$Q_{z,\text{tot}} = \frac{\sum_{n=1}^{N} Q_n \|w_{c,n}\|^2}{\sum_{1}^{N} \|w_{c,n}\|^2}$	• Calculated from the superposition of parallel input admittances (Eq. 4.12). • Linear and circular polarizations. • A specific excitation needs to be defined. • Accurate for planar structures. • Provides the total Q.
Capek [66]	$Q_N = 2\omega_0 \frac{\max\left\{ \sum_n^N \sum_m^N \beta_{n,m} W_{elec}^{n,m}, \sum_n^N \sum_m^N \beta_{n,m} W_{mag}^{n,m} \right\}}{\sum_n^N \sum_m^N \beta_{n,m} P_r^{n,m}}$	• Require the manipulation of modal currents and energies (open-source code unavailable*). • Linear and circular polarizations. • Accurate over a wide frequency band. • Accurate for planar structures. • The calculation of the coupling matrix $\beta_{n,m}$ requires a particular feed.

* Actual commercial softwares using MoM such as FEKO [8] and EMCoS [122], provide only the impedance matrix [Z]. To obtain eigencurrents and modal energies, a post processing need to be done. It should be noticed that FEKO has CMA feature. Meanwhile, exporting eigencurrents still not supported yet.

Thèse de Mhamad Hassanein Rabah, Lille 1, 2015

4.4 Beyond State of The art: New Q Factor expression based -only- on Eigenvalues

We propose an expression based on the frequency derivative of the Rayleigh quotient for the eigenvalue λ_n proposed earlier by Harrington [76]. His motivation was to find the current with the lowest Q to obtain a broadband scatterer. In other words, finding the currents which change slowly with frequency. Thus, contrarily to Chu's Q expression in (4.1), Harringtone defined the quality factor as:

$$Q = \omega \frac{[\tilde{\mathrm{I}}^*]\left[\frac{\delta X}{\delta \omega}\right][I]}{[\tilde{\mathrm{I}}^*][R][I]} \tag{4.20}$$

where [I] is an eigencurrent and the $'*'$ denotes the complex conjugate operation. From Rayleigh quotient of Eq. (4.20) the lowest Q currents for a given surface can be found and the resulting eigenvalue equation becomes:

$$[\omega X'][I] = Q[R][I], \tag{4.21}$$

where Q is the eigenvalue. Thus, the first eigenvalue (smallest in absolute value) is the minimum Q for all possible currents [I]. This makes Eq. (4.21) suitable for ESA since in general, in the electrically small regime the first fundamental mode presents the smallest eigenvalue.

Furthermore, if one assumes that the dominant frequency variation is due to the reactance [X], and considering the Rayleigh quotient formula for λ, the Q factor in Eq. (4.20) can be approximated as follows:

$$Q \approx \omega \frac{\delta \lambda}{\delta \omega} \tag{4.22}$$

The main advantage of this expression is that Q depends only on the eigenvalues and the frequency, and don't need further calculation of energies. Nevertheless, (4.22) cannot be used for every type of antennas since the condition on [X] is not always guaranteed, especially when the derivative is calculated numerically. In fact, the frequency step of the derivative can make a big difference between calculated Q factors. Meanwhile, we can enforce the condition $[X] >> [R]$ by controlling the derivation step of λ. Then, a new expression to calculate the total Q factor from those calculated with (4.22) by involving the modal significances (MS $= |\frac{1}{1+j\lambda_n}|$) is proposed. One should ensure that the chosen derivation window provides a reactance matrix [X] which is higher than the resistance matrix [R]. Fortunately, this is the typical case of an electrically small antenna, which makes this approximation suitable and sufficient for the

© 2015 Tous droits réservés. doc.univ-lille1.fr

problem. A modal derivative is defined as follows:

$$\frac{\partial \lambda_n}{\partial f_n} = \frac{\lambda_n^+ - \lambda_n^-}{f_n^+ - f_n^-}, \tag{4.23}$$

where λ_n^- and λ_n^+ are the eigenvalues for which the variation of λ_n between f_n^+ and f_n^- is linear. It represents the conversion rate of the stored electric energy to magnetic energy and vice versa, near the modal resonance. Analytically, the linearity condition is trivial but it must be ensured numerically by controlling the frequency step. The idea behind this condition is to find the shortest path for which, the eigenvalue crosses the zero line (resonance), and then finding the best interval of the eigenvalues ($\partial\lambda_n$) and associated frequencies in which the largest difference between [X] and [R] is obtained, as illustrated in Fig. 4.3.

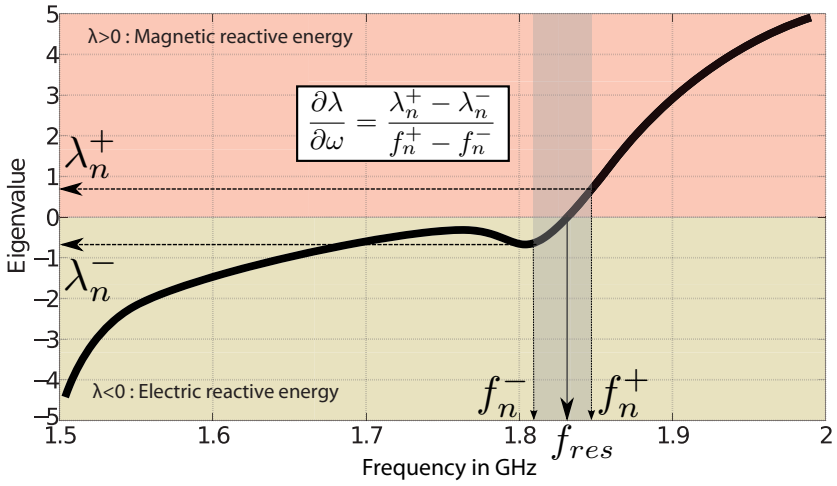

FIGURE 4.3: **Illustration of an eigenvalue curve with respect to the frequency crossing zero line. The modal derivative $\frac{\partial \lambda_n}{\partial f_n}$ is defined at the mode resonance using particular eigenvalues. The choice of these eigenvalues depends on the linearity region near to the resonance in order to ensure that $[X] >> [R]$ condition.**

By multiplying the modal derivative by the resonance frequency $f_{n,\text{res}}$ of the n-th mode (where $\lambda_n = 0$) we retrieve the modal quality factor:

$$Q_{n,\text{f}_\text{res}} = f_{n,\text{f}_\text{res}} \cdot \frac{\lambda_n^+ - \lambda_n^-}{f_n^+ - f_n^-}. \tag{4.24}$$

The total quality factor can be deduced from modal quality factors. However, a linear superposition of modal quality factor is impossible, since characteristic modes are orthogonal between each others. This explains why authors in [66] believe that the total Q can be calculated only from the modal stored energies and powers. However, it is shown using other Q factor definitions that when the antenna is electrically small, the quality factor of the first fundamental mode becomes the total quality factor

© 2015 Tous droits réservés.

Thèse de Mhamad Hassanein Rabah, Lille 1, 2015

[67], [121, A].

To find the total Q factor in terms of $Q_{n,\mathrm{f_{res}}}$, the interaction between characteristic modes must be taken into account. Usually, such a relation can be found using the mutual modal admittances when an excitation is defined [123], [121, A.30]. Since in the present work a Q factor depending only on eigenvalues is required. The product of the modal Q factor with the modal significance ($Q_{n,\mathrm{f_{res}}}\mathrm{MS}_n$) is considered to identify the contribution of each mode in the total Q factor at a specific frequency. In fact, this product includes the mode intensity along with the quality factor. We assume that at a specific frequency ($f_{n,\mathrm{res}}$), the n-th mode is the active contributor and the rest of the modes m ($m \in [1:N]$, $m \neq n$, where N is the number of considered modes) are contributing to the reactive behaviour. Then, the ($Q_{m,\mathrm{f_{res}}}\mathrm{MS}_m$) product must be subtracted M times from ($Q_{n,\mathrm{f_{res}}}\mathrm{MS}_n$) at each frequency. Thus, the Q_{tot} factor is defined as:

$$Q_{\mathrm{tot}} = \frac{3}{N^2}\sum_{n=1}^{N}\sqrt{\left|\mathrm{MS}_n^2 Q_{n,\mathrm{f_{res}}}^2 - M\sum_{m\neq n}^{M}\mathrm{MS}_m^2 Q_{m,\mathrm{f_{res}}}^2\right|} \tag{4.25}$$

M is the number of modes contributing to the reactive behaviour. In general, for ESAs $M = N - 1$. The purpose of calculating the weighted least square is the high sensitivity of Q_{tot} to the small modal significance values, and in doing so the Q_{tot} variation becomes smoother with respect to the number of considered modes. The absolute value is used to prevent negative values when N modes are mainly reactive. The $3/N^2$ parameter is a correction factor which has been obtained by performing many iterations on a set of different classical small antennas (i.e. dipole and loop). For instance, this factor depends on the number of considered modes N, and found to be more suitable for planar electrically small antennas. Furthermore, numerical investigations have shown that for these type of antennas $N = 5$ is sufficient to obtain an accurate Q_{tot}. If only one mode is considered ($N = 1$, $M = 0$) the total factor equals the corresponding modal quality factor. However, the proposed Q_{tot} is based on the assumption that the antenna has only one active mode (mono-mode) at a particular frequency.

4.5 Validation Of The Proposed Q Factor Expression For Arbitrary-Shaped Antenna

One of the interesting features of TCM is that it deals with arbitrary-shaped structures. Furthermore, we have demonstrated that we can evaluate the total quality factor of

© 2015 Tous droits réservés. doc.univ-lille1.fr

Thèse de Mhamad Hassanein Rabah, Lille 1, 2015

the antenna using characteristic modes (Section 4.4). In order to validate the new proposed expression, we study the Q factor of a totally arbitrary-shaped antenna using characteristic modes.

The candidate antenna chosen has the shape of the acronym of 'Institut français des sciences et technologies des transports, de l'aménagement et des réseaux' (IFSTTAR), where the symbol of a star replaces the word 'STTAR'. The antenna is planar, printed over a grounded dielectric substrate. The configuration of the proposed antenna is shown in Fig. 4.4.

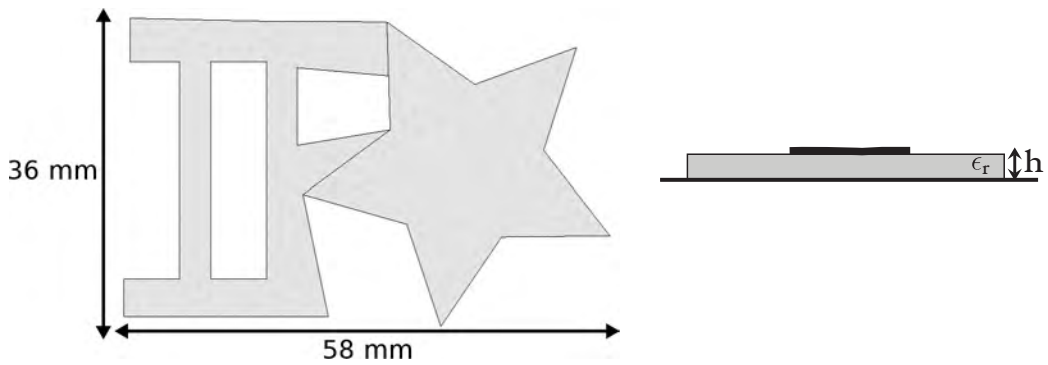

(a) Top view (b) Side view

FIGURE 4.4: **Schematic of the optimised arbitrary star-like shaped antenna. The antenna is printed over an Arlon substrate with $\epsilon_r = 10.7$ and the height $h = 1.5\ mm$.**

The targeted frequency band extends from 0.4 to 1.2 GHz, then, with respect to the dimensions it is obvious that the antenna can operate in the electrically small regime. The theory of characteristic modes is used here for two main purposes: 1) first, the eigenvalue problem is solved with modal quality factors from Eq. (4.25). Then, the total Q_{tot} is calculated independently from the excitation. 2) Secondly, ones chooses the adequate excitation point on the antenna to ensure matching, thus, calculating the classical Q_Z factor from Eq. (4.5).

4.5.1 Modal Q Calculation for the IFSTTAR Antenna

The first five modal significances with respect to the frequency are shown in Fig. (4.5). Mode 1 resonates at 0.7 GHz, with a corresponding MS_1=0.42, while modes 2−5 resonate at 1.17 GHz, 1.42 GHz, 1.75 GHz and 1.96 GHz, respectively. The mode with the higher radiation intensity is mode 4, since it presents the higher modal significance (MS_4=0.82 at 1.75 GHz). However, mode 1 is the only resonating mode in the electrically small regime of the antenna, and we focus on this mode for calculating the Q

© 2015 Tous droits réservés. doc.univ-lille1.fr

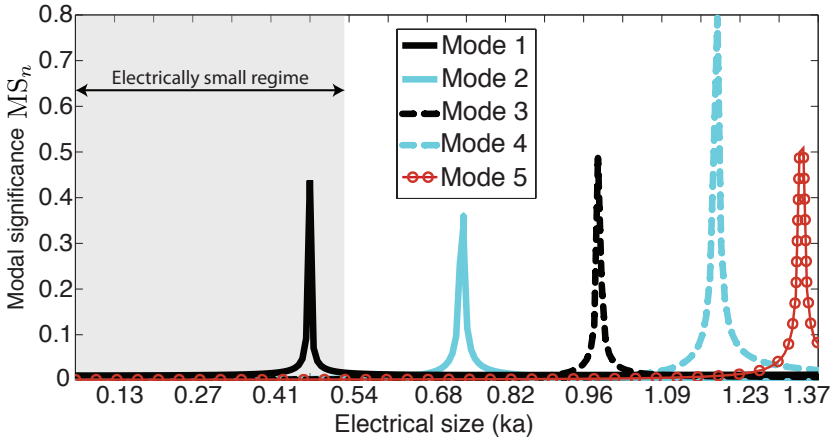

FIGURE 4.5: **Modal significance with respect to the frequency of the first five modes on the arbitrary-shaped antenna.**

factor since it is the dominant mode at 0.7 GHz. Fig. 4.6 shows the first eigenvalue with respect to the frequency.

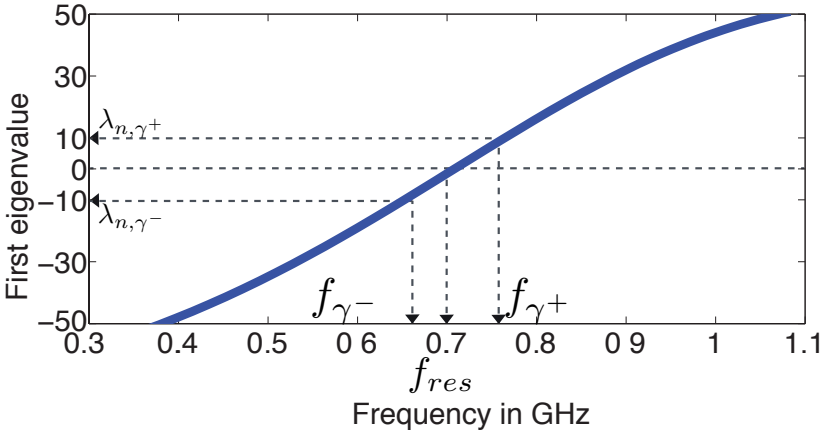

FIGURE 4.6: **Eigenvalue with respect to the frequency of mode 1 with indication of the used values to calculate the first modal slope** $\text{Slope}_{1,f_{\text{res}}}$**. In this case** $\gamma = 10$**.**

On Fig. 4.6, we added some indications for the calculation of the first modal slope [using Eq. (4.23)]. Mode 1 is the dominant mode in the electrically small regime, thus the total Q factor should approach $Q_{1,f_{\text{res}}}$. The behaviour of its eigenvalue is found to be linear between -10 and 10. Thus, using Fig. 4.6, the $\text{Slope}_{1,f_{\text{res}}}$ is calculated as follows:

$$Slope_{\ 1,f_{\text{res}}} = \left| \frac{\lambda_{1,\gamma^+} - \lambda_{1,\gamma^-}}{f_{\gamma^+} - f_{\gamma^-}} \right| = \frac{20}{0.785 - 0.679} = 188.67,$$

$$\text{where } \gamma = 10.$$

Then, the first modal quality factor becomes:

$$Q_{1,f_{\text{res}}} = f_{1,\text{res}} \times Slope_{\ 1,f_{\text{res}}} = 0.7 \times 188.67 = 132.07.$$

© 2015 Tous droits réservés.

Thèse de Mhamad Hassanein Rabah, Lille 1, 2015

In general, the first modal quality factor provides the lowest bound of Q_{tot} of a mono-band mono-mode antenna [67]. However, this quantity will be used in Eq. (4.25) to calculate the Q_{tot} and compare it to the classical one [53].

4.5.2 Excitation of the IFSTTAR Antenna

Generally, to match such an arbitrary-shaped antenna, an antenna engineer would use a trial & error technique. Here, we show how modal configuration of eigencurrents can help. The first two eigencurrents are shown in Fig. 4.7.

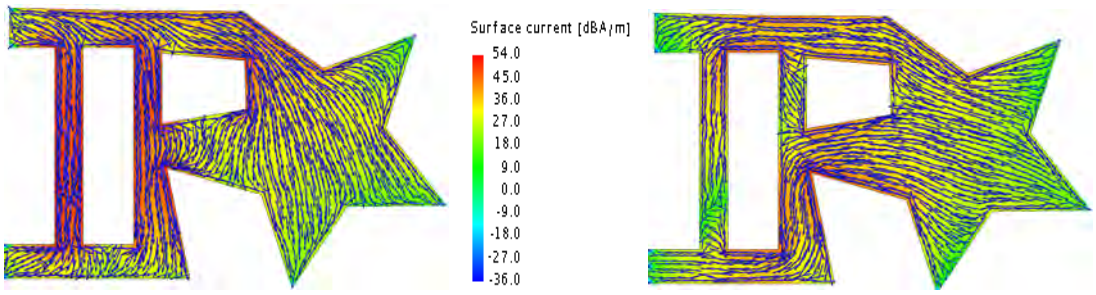

(a) Mode 1 (b) Scale (c) Mode 2

FIGURE 4.7: **Profiles of the first two eigencurrents of the proposed IFSTTAR antenna.**

Modes 1 and 2 presents completely different current profiles. However, those profiles inform us on the location of the maxima of each mode. A simple analysis of the surface currents provides us a clear idea about how to feed the antenna in the correct position. The eigencurrents in both arms of the shape "IF" are in-phase for the first mode and out of phase for mode 2. Furthermore, the maxima of mode 1 are localised at the upper middle of both arms of the shape "IF". Thus, the best configuration to feed mode 1 is shown in Fig. 4.8.

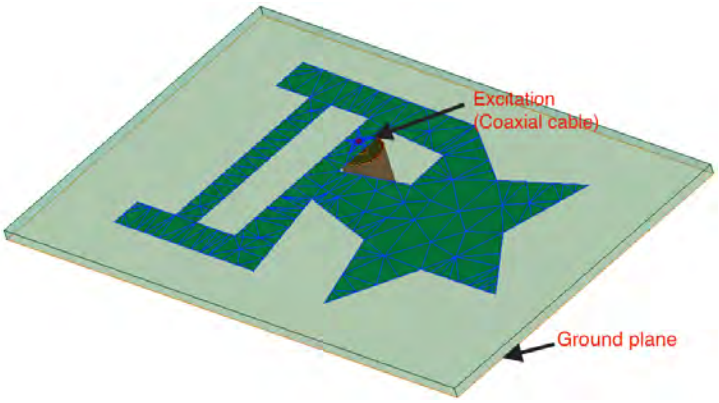

FIGURE 4.8: **Position of the optimum feeding in order to excite mode 1 at 0.7 GHz.**

© 2015 Tous droits réservés. doc.univ-lille1.fr

Thèse de Mhamad Hassanein Rabah, Lille 1, 2015

Feeding the structure following the configuration in Fig. 4.8 excites mainly the first mode. A prototype has been fabricated in order to measure the reflection coefficient as shown in Fig. 4.9

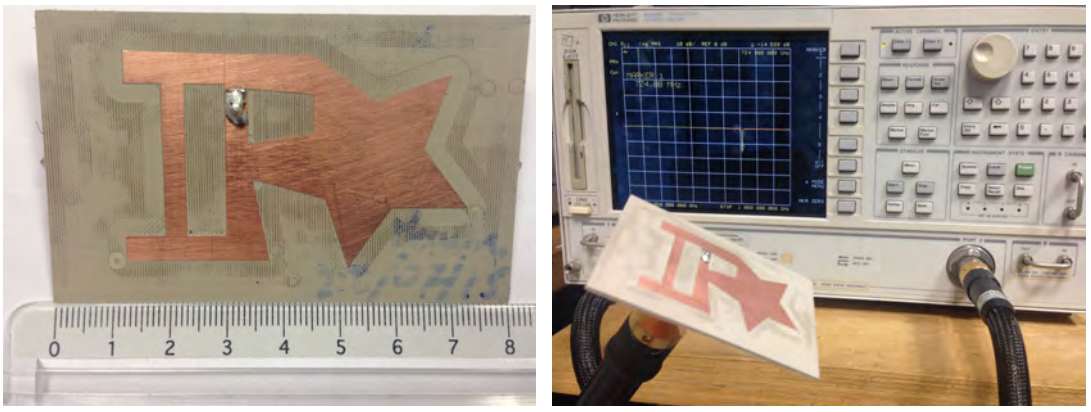

(a) (b)

FIGURE 4.9: **(a) Photo of the fabricated prototype of the arbitrary-shaped IFSTTAR antenna. (b) Measurements setup of the reflexion coefficient using an HP8720D vector network analyser.**

The simulated and measured reflection coefficients are shown in Fig. 4.10 (a), together with the complex input impedance in Fig. 4.10 (b). A very good matching is achieved at 0.7 GHz.

A good agreement is observed between simulated and measured S_{11}. The slight shifting around 0.7 GHz is due to the coaxial cable impact. The bandwidth is narrow since the used substrate presents a high permittivity. Fig. 4.10 (b) presents the complex input impedance of the antenna. The anti-resonant nature at 0.7 GHz justify that only one mode (mode 1) is the main contributor into the behaviour of the input impedance [124], while the resonance at 0.32 GHz is due the coaxial cable which has not been included in the characteristic mode analysis.

The Q factor based on Yaghjian-Best and Gustafsson [115] formula are then calculated at 0.7 GHz and compared to the Q_{tot} factor based on eigenmodes as summarised in Table 4.3.

Table 4.3 demonstrates a good agreement between the calculated total Q factors. However Q_{tot} is lower than Q_Z since only five modes are considered. If a higher number of modes (higher Q values) are considered the total Q_{tot} can be increased and then approach to Q_Z. On the other hand, $Q_{Gustafsson}$ is higher since the directivity of the antenna is supposed to be $D = 1.5$ at 0.7 GHz. If the the directivity is calculated from full wave simulation it approaches 1.4 which results in a more accurate Q factor.

© 2015 Tous droits réservés. doc.univ-lille1.fr

Thèse de Mhamad Hassanein Rabah, Lille 1, 2015

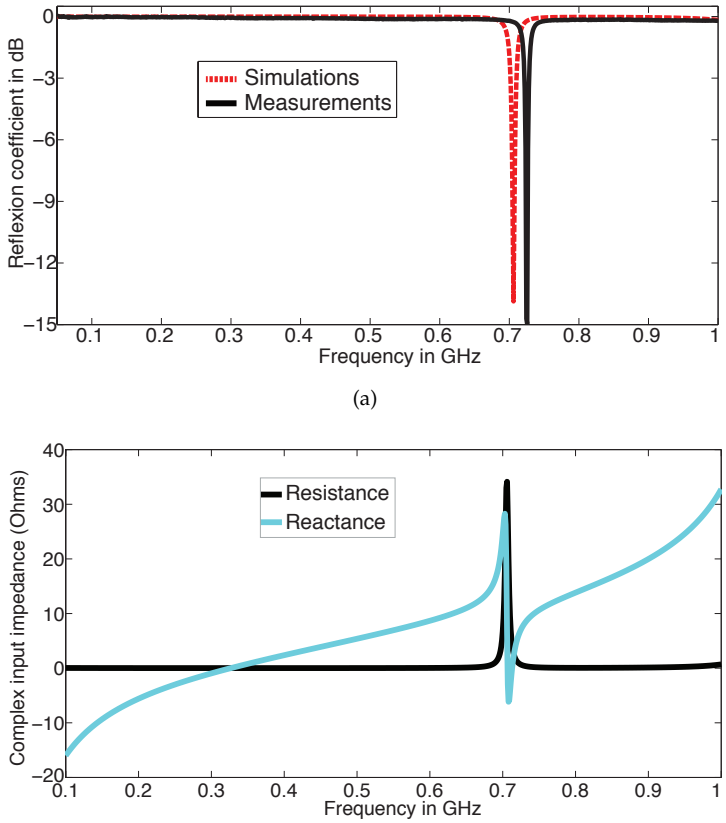

FIGURE 4.10: **(a) Reflection coefficient of the arbitrary-shaped IFSTTAR antenna fed by a coaxial cable as in Fig. 4.8. (b) Simulated complex input impedance used for the calculation of the Yaghjian-Best original Q_Z.**

TABLE 4.3: Comparison between modal based, and conventional input impedance based total Q factor of the arbitrary-shaped antenna at 0.7 GHz.

Design name	Used expression			
Arbitrary-shaped IFSTTAR antenna	*ka*	Modal based Q^*_{tot} (4.25)	Classical Q_Z (4.5)	$Q_{Gustafsson}$[115, 116]
	0.48	**162**	**158**	**167.4**

*Each modal quality factor $Q_{n,f_{res}}$ is calculated at its own resonance, and multiplied by the modal significance MS_n value at the 0.7 GHz. The number of considered modes $N = M = 5$.

© 2015 Tous droits réservés.

doc.univ-lille1.fr

Thèse de Mhamad Hassanein Rabah, Lille 1, 2015

4.6 Characteristic Modes Analysis of Patch Antennas over Metamaterial and Magneto-Dielectric Substrates

Patch antenna modal analysis has taken the attention of many researchers in the past years [19, 125]. Existing works aim to study the resonance behaviour of lower and higher modes, and to find good mode excitation, in order to obtain the desired polarization. To the best of our knowledge no work has yet (date of writing this thesis) investigated the use of high permittivity dielectric, magneto-dielectric, or metamaterial substrates with patch antennas from a modal point of view, except the work in [126] where the losses in the substrates are not included. In this section we aim to apply the modal analysis in order to evaluate the Q factor of small patch antennas over classical, magneto-dielectric and metamaterial substrates.

In this section we fix two main goals:

1. Evaluation of metamaterial-based patch antennas in terms of miniaturization using the proposed metrics based on modal approach.
2. Application of metrics from Chapter 3 and Section 4.4 to compare metamaterial substrate to a magneto-dielectric substrate.

4.6.1 Considered Patch Antennas

The typical design configuration is shown in Fig. 4.11, together with the profiles of the first three eigencurrents. Fig. 4.11 illustrates how the first two eigencurrents maxima are respectively separated by the length and the width of the patch. These maxima coincide with the virtual apertures of the fundamental TE and TM modes described in the cavity model [55]. These are two radiating modes, whereas the third one stores energy. This can be seen from characteristic angles in Fig. 4.12. Mode 1 resonates at 1.85 GHz ($\phi_1 = 180°$) and mode 2 at 2.12 GHz. Mode 3 stores magnetic energy since ϕ_3 is equal to 90° over the frequency band of interest.

We studied the miniaturized patch antenna as proposed in [5]. It resonates at 1.85 GHz with total dimensions of Length $\times$ Width $= 20 \times 16$ mm ($\approx \lambda_0/10$), printed over two layers as shown in Fig. 4.13 (a). The upper layer is a classical dielectric layer of thickness of 2 mm with relative permittivity $\epsilon_r = 6$. The lower layer is a 4×4 reactive impedance substrate as shown in Fig. 4.13 (b,c).

The reactive impedance substrate consists of small square metallic patches distributed periodically in two directions and printed on a high permittivity grounded

© 2015 Tous droits réservés. doc.univ-lille1.fr

Thèse de Mhamad Hassanein Rabah, Lille 1, 2015

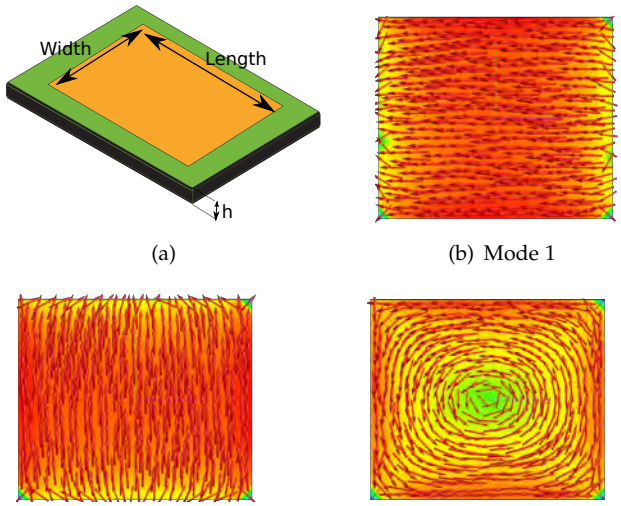

(a) (b) Mode 1

(c) Mode 2 (d) Mode 3

FIGURE 4.11: **(a) Schematic a patch antenna over a substrate representing classical, magneto-dielectric or metamaterial substrate. (b, c, d) Profiles of the first three calculated eigencurrents, respectively. Modes profiles are frequency independent. The eigencurrents are calculated only on the metallic patch, since an infinite substrate (multi-layered green function) is considered. The same current profiles have been found in all considered cases.**

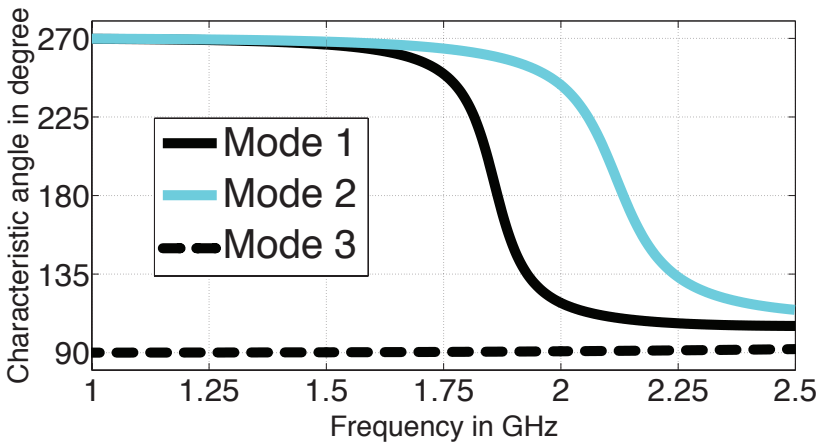

FIGURE 4.12: **Characteristic angles with respect to the frequency of the first three eigenmodes for a patch antenna resonating at 1.85 GHz.**

dielectric substrate. It has been demonstrated in [5], that the miniaturized patch is four times smaller than a patch over a substrate made of vacuum ($\mu_r = 1, \epsilon_r = 1$) operating at the same frequency. This patch over vacuum will be considered as the reference design. Both designs are analyzed and compared with other patches designed over conventional dielectric, magnetic and magneto-dielectric substrates. Table 4.4 summarises the specifications of all considered cases described in Fig. 4.14.

Simulations have been done using a MoM solver. An infinite ground plane based on Green's function for multilayered medium is used in order to prevent the calculation of equivalent surface currents over the substrate faces, hence simplifying the

© 2015 Tous droits réservés. doc.univ-lille1.fr

Thèse de Mhamad Hassanein Rabah, Lille 1, 2015

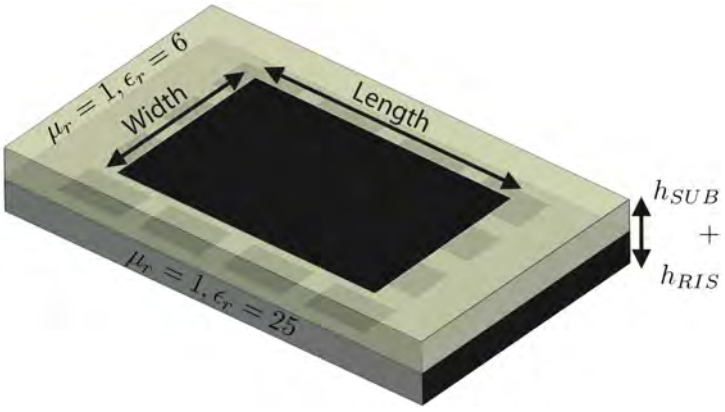

(a) 3D view of a miniaturized patch over RIS

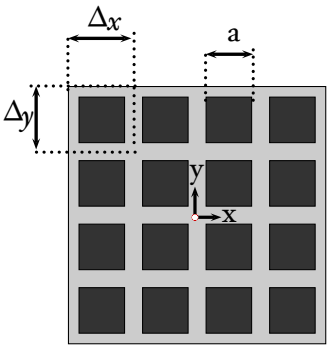

(b) Top view of an Isolated RIS

(c) Side view of an Isolated RIS

FIGURE 4.13: **(a) Schematic of a miniaturized patch antenna over two substrates: classical substrate ($\epsilon_r = 6$) and RIS. (b,c) Schematic of a 4×4 reactive impedance substrate. The dimensions are $a = 12$ mm, $\Delta_x = \Delta_y = 18$ mm, $h = 4$ mm and $\epsilon_r = 25$, [5].**

TABLE 4.4: **Specifications of the considered patch designs**

	Design name	Size (mm)	Substrate type*	Theoretical f_{res} (MHz)
A	Reference design	$77 \times 67 \times 2$	$(\mu_r = 1, \epsilon_r = 1)$	1850
B	Electric	$20 \times 16 \times 2$	$(\mu_r = 1, \epsilon_r = 21)$	1850
C	Magnetic	$20 \times 16 \times 2$	$(\mu_r = 21, \epsilon_r = 1)$	1850
D	Magnetic +Electric	$20 \times 16 \times 2$	$(\mu_r = 4.55, \epsilon_r = 4.45)$	1850
E	RIS [5]	$20 \times 16 \times (\underbrace{2}_{SUB} + \underbrace{4}_{RIS})$	Metamaterial	1850

* Losses included: electric loss tangent $tan\ \delta_e = 0.001$, and magnetic loss tangent $tan\ \delta_m = 0.1$.

© 2015 Tous droits réservés.

doc.univ-lille1.fr

Thèse de Mhamad Hassanein Rabah, Lille 1, 2015

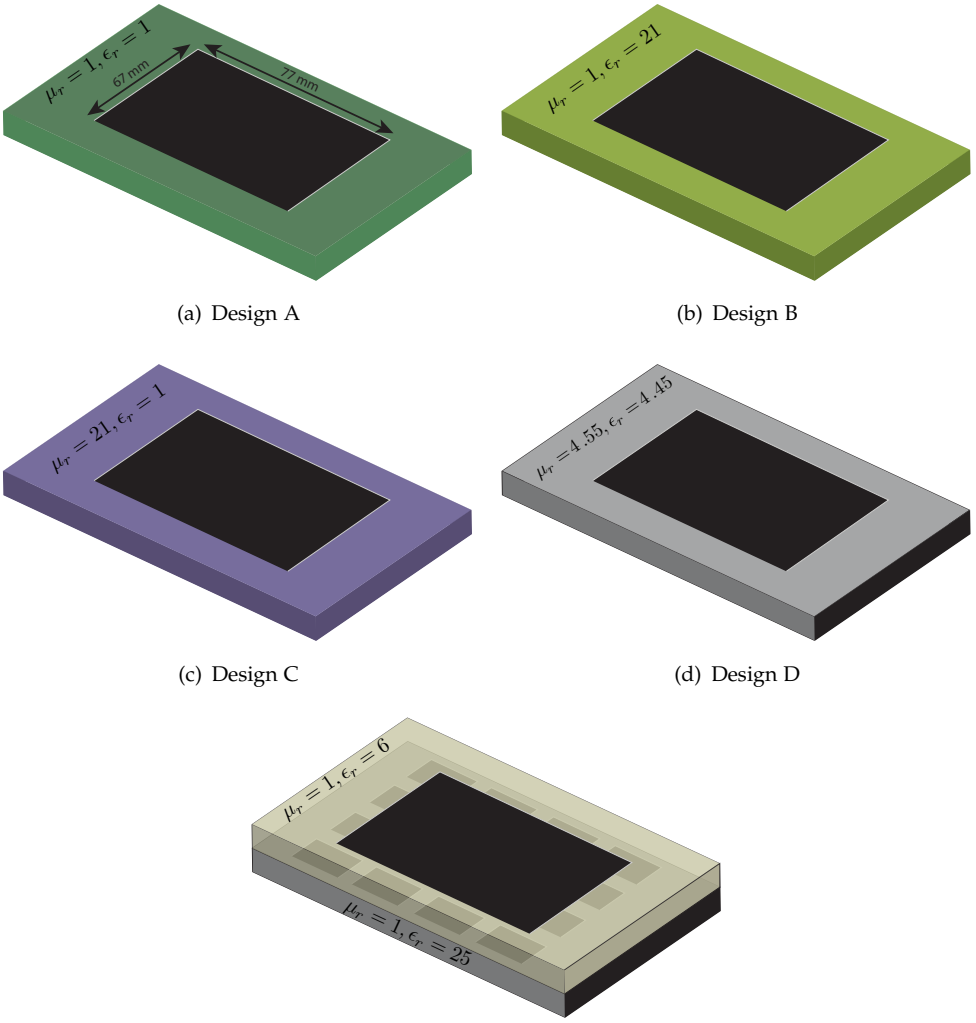

(a) Design A (b) Design B

(c) Design C (d) Design D

(e) Design E

FIGURE 4.14: **Configuration of studied designs over different substrates. Except for design A, patch dimensions are 20×16 mm. These dimensions are identical to the considered patch antenna in [5].**

problem. Furthermore, unlike the assumption done in [126], in this study, losses are included, where electric loss tangent $tan\ \delta_e = 0.001$, and magnetic loss tangent $tan\ \delta_m = 0.1$.

4.6.2 Modal Significances Evaluation and Comparaison

Fig. 4.15 shows the modal significance of mode 1. MS_1 is close to unity in all cases at the first resonance frequency which is ≈ 1.85 GHz, because mode 1 is purely radiative at this frequency. Reference Design A ($\mu_r = 1, \epsilon_r = 1$) resonates at this frequency because it is four times bigger than the other miniaturized patches.

The contrast with other cases is the width of the curve near to the resonance,

© 2015 Tous droits réservés. doc.univ-lille1.fr

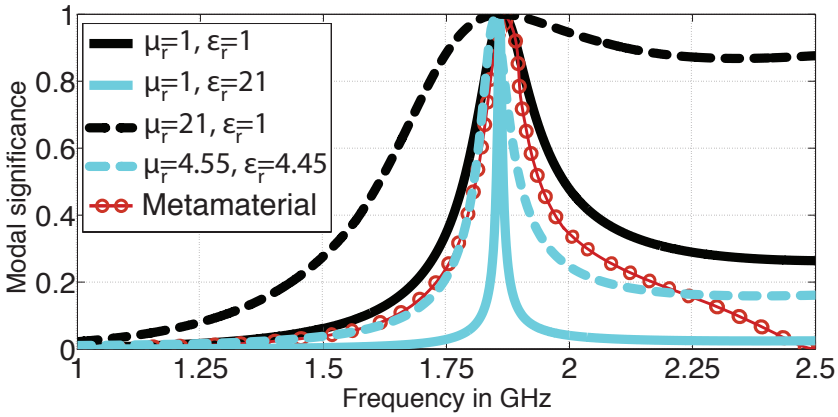

FIGURE 4.15: **Modal significance with respect to the frequency of the first mode for the studied cases: the MS_1 is close to unity at the resonance frequency (1.85 GHz) for all cases because it is a radiating mode. The width of the curve varies between cases because it is proportional to the mode bandwidth in each case.**

which is proportional to the mode relative bandwidth [19]: the electric substrate $(\mu_r = 1, \epsilon_r = 21)$ presents the narrower bandwidth while the magnetic substrate $(\mu_r = 21, \epsilon_r = 1)$ possesses the larger. The modal significance MS_1 of the magneto-dielectric substrate
$(\mu_r = 4.55, \epsilon_r = 4.45)$ is a combination of both substrate types. It is closer to that of the magnetic substrate near to the resonance and decreases when getting far from the resonance like the electric substrate. The patch over a the metamaterial (RIS) substrate presents a similar behaviour to the magneto-dielectric substrate in term of MS_1. This similarity can be predicted since the considered metamaterial has shown to provide artificial magnetic response when polarised by a patch antenna [110]. This also agrees with the conclusion conducted by Hansen and Burke about how magneto-dielectric substrates ensure antenna miniaturization without scarifying in bandwidth [22].

Fig. 4.16 shows the modal significance of mode 2 for the studied cases. The second mode presents the same behaviour of mode 1 for all cases at 2.12 GHz because it is resonating (radiating) at this frequency. Nonetheless, mode 2 presents a larger curve with the RIS compared to the magneto-dielectric substrate.

The third mode over the patch is an energy storer regardless of the used substrate. The corresponding MS_3 is close to zero for all cases, hence, not shown in this chapter. This could be also predicted from the third characteristic angle in Fig. 4.12.

Figures 4.15 and 4.16 show that the relative bandwidths of modes 1 and 2 are qualitatively better for the Design C compared to Design B. This could also be due to the losses in both substrates because losses broaden the bandwidth [55], since $\tan \delta_m >> \tan \delta_e$. The RIS and the magneto-dielectric substrates correspond to the

© 2015 Tous droits réservés.

Thèse de Mhamad Hassanein Rabah, Lille 1, 2015

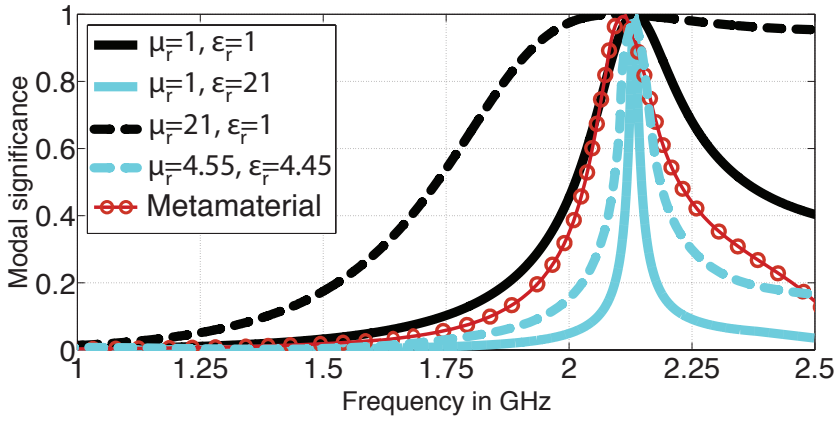

FIGURE 4.16: **Modal significance with respect to the frequency of the second mode for the studied cases: Similarly to the first active mode, MS_2 is close to unity at the resonance frequency (2.12 GHz) for all cases because it is a radiating mode. The width of the curve varies from case to another because it is proportional to the mode bandwidth in each case.**

intermediate cases between the electric and magnetic one. In order to approve these observations quantitatively, we refer to the modal Q factor introduced in Section 4.4.

4.6.3 Modal Q Factors Evaluation and Comparaison

Table 4.5 shows the modal slope and modal quality factor of the first mode (radiating mode) for all considered cases.

TABLE 4.5: **Summary of the eigen slopes and modal quality factor -at the resonance- for mode 1 ($\gamma = 0.1, \tan\delta_e = 0.001$ and $\tan\delta_m = 0.1$)**

Design name	$f_{1,res}$ (MHz)	$Slope_{1,f_{1,res}}$	$Q_{1,f_{1,res}}$
Reference design ($\mu_r = 1, \epsilon_r = 1$)	1864.89	17.6	32.82
Electric ($\mu_r = 1, \epsilon_r = 21$)	1858.21	199.6	370.89
Magnetic ($\mu_r = 21, \epsilon_r = 1$)	1877.89	1.91	3.6
Magnetic+Electric ($\mu_r = 4.55, \epsilon_r = 4.45$)	1788.31	9.676	17.3
Metamaterial RIS ($\mu_r = 1, \epsilon_r = 25$)	1875.44	26.59	49.8

The modal slope in Design B ($\epsilon_r = 21$) is greater than Design A (vacuum). The magnetic substrate gives the smaller value. This fact is reflected on the modal quality factor since it is proportional to the modal slope. Physically, this means that the dielectric substrate enhances the phenomena of energy storing, while the magnetic substrate promotes the radiation phenomena by decreasing the amount of stored energy. This explains the relative bandwidths achieved in each case. This interpretation agrees with other studies based on the spherical eigen modes approach [107], equivalent transmission line model [4], and cavity model [127]. For

© 2015 Tous droits réservés. doc.univ-lille1.fr

Thèse de Mhamad Hassanein Rabah, Lille 1, 2015

the metamaterial-based RIS (Design E), the value of the modal slope is closer to the magneto-dielectric substrate (Design D) near to the resonance. The energy storage exists in the artificial substrate but it is minimal within the studied frequency range, regarding the high value of the permittivity ($\epsilon_r = 25$).

4.6.3.1 Impact of the losses on $Q_{1,f_{1,res}}$

In this paragraph we compare the first modal quality factor $Q_{1,f_{1,res}}$ with and without the presence of losses. Table 4.6 details the $Q_{1,f_{1,res}}$ of the studied patch antenna over all the considered substrates. Table 4.6 shows that for all cases (except the vacuum

TABLE 4.6: Impact of the losses on $Q_{1,f_{1,res}}$

Design name	Without losses	With losses ($\tan\delta_e = 0.001$ and $\tan\delta_m = 0.1$)
Reference design ($\mu_r = 1, \epsilon_r = 1$)	32.82	32.82
Electric ($\mu_r = 1, \epsilon_r = 21$)	378.1	370.89
Magnetic ($\mu_r = 21, \epsilon_r = 1$)	19.3	3.6
Magnetic+Electric ($\mu_r = 4.55, \epsilon_r = 4.45$)	32.5	17.3
Metamaterial RIS ($\mu_r = 1, \epsilon_r = 25$)	54.3	49.8

substrate) the losses have decreased the modal quality factor. Furthermore, since $\tan\delta_m >> \tan\delta_e$, we can see that the impact of the losses in the magnetic and the magneto-dielectric substrates is bigger than the one of the pure dielectric substrate. This conclusions are valid for the total Q factor and agree with another analytical study based on cavity model of patch antennas [127].

It has been shown from the modal significance, that mode 2 presents the same behaviour as mode 1 at a higher frequency (2.12 GHz). This is approved quantitatively in Table 4.7 which shows the modal slope and modal quality factor of the second mode for all considered cases.

© 2015 Tous droits réservés. doc.univ-lille1.fr

Thèse de Mhamad Hassanein Rabah, Lille 1, 2015

TABLE 4.7: **Summary of the eigen slopes and modal quality factor -at the resonance- for mode 2 (**$\gamma = 0.1, \tan\delta_e = 0.001$ and $\tan\delta_m = 0.1$)

Design name	$f_{2,res}$ (MHz)	$Slope_{2,f_{2,res}}$	$Q_{2,f_{2,res}}$
Reference design ($\mu_r = 1, \epsilon_r = 1$)	2133.358	11.3	24.26
Electric ($\mu_r = 1, \epsilon_r = 21$)	2241.35	103.51	232.01
Magnetic ($\mu_r = 21, \epsilon_r = 1$)	2260.36	0.812	1.83
Magnetic+Electric ($\mu_r = 4.55, \epsilon_r = 4.45$)	2091.75	7.03	14.7
Metamaterial RIS ($\mu_r = 1, \epsilon_r = 25$)	2124.44	19.24	40.86

Comparing Design A to other designs by calculating the modal quality factors, gives the same conclusion as for the first mode: the impact of the substrate type is similar for both modes. Furthermore, mode 2 presents a wider relative bandwidth since the corresponding quality factor values are lower compared to mode 1. Indeed, the difference between $Q_{1,f_{1,res}}$ and $Q_{2,f_{2,res}}$ increases between 2 and 9, for Designs C, E, D, respectively. In contrast, the difference with the dielectric substrate is much higher ($\approx$ 138). This is because modes 1 and 2 are electric modes, and are more sensitive to dielectric substrates. Nonetheless, Table 4.8 shows how the modal slope and quality factor varies with respect to the permeability and permittivity of the two extreme cases: the electric and the magnetic substrates. By varying ϵ_r from 21 to 31 the modal

TABLE 4.8: **Summary of the eigen slopes and modal quality factor -at the resonance- for mode 1 for different values of** μ_r **and** ϵ_r**, (**$\gamma = 0.1, \tan\delta_e = 0.001$ and $\tan\delta_m = 0.1$)

Design name	$f_{1,res}$ (MHz)	$Slope_{1,f_{1,res}}$	$Q_{1,f_{1,res}}$
Electric ($\mu_r = 1, \epsilon_r = 21$)	1858.21	199.6	370.89
Electric ($\mu_r = 1, \epsilon_r = 26$)	1627.42	340.22	553.68
Electric ($\mu_r = 1, \epsilon_r = 31$)	1465.62	502	735.74
Magnetic ($\mu_r = 21, \epsilon_r = 1$)	1877.89	1.91	3.6
Magnetic ($\mu_r = 26, \epsilon_r = 1$)	1634.93	1.7	2.76
Magnetic ($\mu_r = 31, \epsilon_r = 1$)	1509.24	1.62	2.44

slope increases from 199.6 to 502 (and $Q_{1,f_{1,res}}$ from 370.89 to 735.74). The higher the permittivity, the greater the modal slope (*i.e.* energy storage). On the other hand, the modal slope is inversely proportional to the permeability. When μ_r changes from 21 to 31 the modal slope decreases from 1.91 to 1.62 (and $Q_{2,f_{2,res}}$ from 3.6 to 2.44). This demonstrates -again- how much the first active mode over the patch is sensitive to the permittivity while it is not the case for the permeability. The same description applies to mode 2 at 2.12 GHz, because it is also an active electric mode at this frequency.

© 2015 Tous droits réservés. doc.univ-lille1.fr

Thèse de Mhamad Hassanein Rabah, Lille 1, 2015

Mode 3 is a pure reactive mode within the studied frequency band and then, it only contributes in the calculation of the total Q_{tot} factor. However, in mono-modal antennas, only the consideration of the first mode is sufficient when the patch is operating within the electrically small regime, since in this region the first mode is dominant and its quality factor approaches the total quality factor.

Yet, we consider in our calculation for the first fives modes. Eq. (4.25) based on eigenvalues is used to calculate the total quality factor. Table 4.9 shows an overview over the classical Q factor calculated using the Yaghjian-Best formula (Eq. 4.5) compared to the total Q_{tot} factor based on modal quantities at the first resonance (patch resonance 1850 MHz).

TABLE 4.9: **Comparison Between The Classical Q Factor and The Proposed Q Factor Based on Eigenvalues, at 1850 MHz**

Design name	Used Expression							
Reference design patch over vacuum	*ka*	Modal Based $Q_{tot,f_{res}}$ (Eq. 4.25)						Classical Q_Z^* (Eq. 4.5)
	1.97	MS_1	MS_2	MS_3	MS_4	MS_5	**49.2**	**55.62**
		0.98	0.17	3.28×10^{-3}	1.8×10^{-3}	5.9×10^{-4}		
Patch over magneto-dielectric substrate	0.49	0.99	0.09	3.35×10^{-2}	4.12×10^{-2}	3.42×10^{-2}	**7.06**	**7.99**
Patch over metamaterial substrate (RIS)	0.49	0.99	0.18	1.79×10^{-2}	10.8×10^{-3}	10.5×10^{-3}	**32.4**	**35.62**

* The defined excitation is a coaxial cable feeding the patch at ($x_0 = Length/3$, $y_0 = Width/2$). Q_Z is calculated at the resonance frequency where the matching is greater that 10 dB.

The electrical size of the considered antenna is mentioned. This is to inform us wether the antenna is in electrically small regime or not. Here, since we consider an infinite ground plane, the electrical size of an electrically small antenna should be $ka \leq 0.5$ instead of 1. The patch over vacuum is not electrically small, but it is kept in Table 4.9 as the reference case. The first five modal significances have been included since they are involved by Eq. (4.25) to calculate Q_{tot}. At 1850 MHz the calculated total Q_{tot} factor is in good agreement with Q_Z for the case of the magneto-dielectric and metamaterial substrates, while a slight difference occurs with respect to the reference case (vacuum). In fact, this agreement is guaranteed when the antenna is electrically small ($ka = 0.49$), namely in the case of a patch over the metamaterial substrate and

© 2015 Tous droits réservés. doc.univ-lille1.fr

Thèse de Mhamad Hassanein Rabah, Lille 1, 2015

the magneto-dielectric substrate. When $ka = 1.97$, the number of considered modes ($N = 5$) is not sufficient to collect the overall reactive energy, and this results into a such inaccuracy (see Section 4.4).

When moving towards higher frequencies (ka increases), the disagreement increases between the values from both expressions. Table 4.10 presents the same comparaison in Table 4.9 but at 2120 MHz.

TABLE 4.10: **Comparison Between The Classical Q Factor and The Proposed Q Factor Based on Eigenvalues, at 2120 MHz**

Design name	Used Expression							
Reference design patch over vacuum	ka	Modal Based Q_{tot} (Eq. 4.25)						Classical Q_Z^* (Eq. 4.5)
	2.26	MS_1	MS_2	MS_3	MS_4	MS_5	**45.5**	**56.26**
		0.35	0.99	5.82×10^{-3}	5.4×10^{-3}	1.5×10^{-3}		
Patch over magneto-dielectric substrate	0.57	0.19	0.98	6.45×10^{-2}	5.18×10^{-2}	3.4×10^{-2}	**6.28**	**8.37**
Patch over metamaterial substrate (RIS)	0.57	0.25	0.98	3.8×10^{-2}	2.1×10^{-2}	2×10^{-2}	**30.1**	**25.8**

* The defined excitation is a coaxial cable feeding the patch at ($x_0 = Length/3$, $y_0 = Width/2$). Q_Z is calculated at the resonance frequency where the matching is greater that 10 dB.

Table 4.10 shows that when the patch becomes electrically larger, the error between Q_{tot} and Q_Z increases. This error reaches 23.6% for the reference case, while for the metamaterial substrate this error equals to 14.2% . This difference is smaller compared to reference case because ka still equals to 0.57 compared to 2.26 for the vacuum substrate. The main reason for this is that reactive energies of higher order modes are not taken into account in (4.25). Thus, the expression becomes less accurate with bigger electrical sizes.

Designs B and C are not shown in Tables 4.9 and 4.10 since it is difficult to calculate an accurate Q_Z at -10 dB, because of poor matching. Indeed, with such 'theoretical' substrates, an external matching network is strongly needed and this is not the concern of this study.

© 2015 Tous droits réservés. doc.univ-lille1.fr

Thèse de Mhamad Hassanein Rabah, Lille 1, 2015

4.7 Discussion

The modal study of patch antenna over different substrates achieved the goals announced at the beginning of this chapter. In fact, beside the qualitative analysis that the theory of characteristic modes has provided, the quantification of a modal quality factor has proven to provide very useful information about the performances with a prior knowledge -only- on the geometry and materials surrounding the patch. Furthermore, the expression of the total Q factor has been validated in Section 4.5 in order to be used with other designs. Compared to a previous study [126], the present work has included losses in the substrate. Table 4.8 demonstrates that the higher the permeability, the lower the quality factor. For the permittivity, this relation is inverted. This conclusion agrees with another analytical approach based on transmission line model [128], or the cavity model of a patch antenna [127]. Nevertheless, this agreement applies for magneto-dielectric substrates which proved to present good performances in terms of antenna bandwidth (*i.e.* low quality factor) as shown in Tables 4.9 and 4.10. Theses conclusions have been found earlier by Hansen et al. [22].
Moreover, the reactive impedance substrate which is a composite metal dielectric metamaterial, has proven to present performances closer to a magneto-dielectric substrate than the classical dielectric substrate. In other words, this metamaterial substrate acts like an artificial magnetic medium when it surrounds the patch. In fact, this response is achieved in a particular configuration when the electric field is parallel to the periodicity plane which is naturally the case of patch antenna. These findings are further detailed in [110]. Nevertheless, it should be emphasized that the analysis made for the patch with the RIS can be done for any other type of substrate containing metamaterials with complex conductor patterns, when associated to antennas. This adds more generality to the modal analysis of metamaterial when associated to antennas.

4.8 Conclusion

In this chapter, a modal approach has been used to evaluate the performance of patch antennas over conventional and artificial metamaterial substrates in terms of miniaturization. The good accordance between this approach and others from the literature proves its validity for the analysis of such problems. The main advantage of this analysis is that eigencurrents are calculated numerically and thus could be computed for arbitrary and non canonical shapes such as metamaterial inclusions. This was demonstrated through the analysis of an arbitrary-shaped antenna based on the shape of the acronym of 'Institut français des sciences et technologies des transports,

© 2015 Tous droits réservés. doc.univ-lille1.fr

Thèse de Mhamad Hassanein Rabah, Lille 1, 2015

de l'aménagement et des résaux' (IFSTTAR). An experimental validation for a fabricated prototype has been presented, and it demonstrates good agreements between Q values from Yaghjian-Best expression and the proposed one.
This work has highlighted that a magneto-dielectric substrate presents a significant bandwidth enlargement for the first active mode while an electric substrate shows the opposite effect. Calculated modal quality factors demonstrate that a reactive impedance substrate presents a similar response to a magneto-dielectric one when associated to a patch antenna within a specific frequency band. Excellent agreement is achieved between quality factors calculated using the proposed approach and the conventional approach based on the variation of the input impedance. This accordance is valid when the antenna is operating in the electrically small regime where the total quality factor is close to the modal quality factor of the first radiating mode.

The usefulness of this approach is that quality factors can be calculated without defining a specific excitation, therefore the performances of electrically small antennas can be evaluated from the eigenvalue problem solutions. This offers a huge advantage for the antenna shape optimisation techniques. In addition to this, it is possible to perform the same analysis on different kinds of structures, with arbitrary shapes, such as metamaterials with complex conductor patterns because the modal currents can be purely computed using numerical methods.

© 2015 Tous droits réservés. doc.univ-lille1.fr

Chapter 5

Metamaterial Inspired Antennas: Systematic Design Based on Characteristic Modes

5.1 Introduction

Nowadays, an antenna occupies more than 20% of the overall size of a mobile terminal. Therefore, miniature antennas are in high demand, since the antenna size often imposes a significant limitation on the overall size of a portable wireless system. Metamaterial inspired concept is a very promising technique to miniaturise antennas suffering from their small electrical sizes while keeping a good radiation efficiency. In Section 2.6, the first proposed metamaterial inspired antennas proposed by Erentok et al. [6] are presented. The technique proposed in [6] relies on classical antennas such as monopoles and loops to which a metamaterial inclusion is coupled.

However, antenna systems become progressively electrically smaller and arbitrary shaped when they are integrated into the chassis of the terminal. Hence, Erentok's technique cannot be used. More precisely, it is not easy to identify whether the inclusion must be capacitive or inductive at a specific frequency. This problem is illustrated in Fig. 5.1.

In this chapter, we introduce a new methodology to be used by antenna designers to address this problem. It will be able to find the adequate inclusion in order to match an arbitrary shaped antenna in its electrically small regime and keep high overall efficiency. This will require the solving of the eigenvalue problem with further post-processing of the quantities provided by TCM.

© 2015 Tous droits réservés. doc.univ-lille1.fr

Thèse de Mhamad Hassanein Rabah, Lille 1, 2015

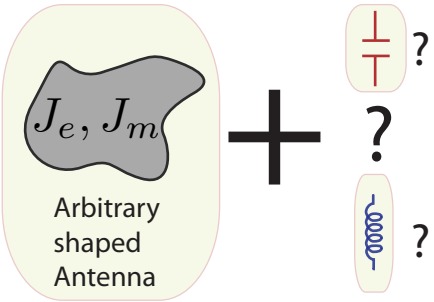

FIGURE 5.1: **Illustration of the problem of associating metamaterial inclusion to non-classical arbitrary shaped antennas.**

Section 5.2 details step by step the process of looking for the right inclusion to be associated with the antenna. We will further apply the proposed methodology to the previously published metamaterial inspired antennas [6] in order to validate the methodology. A comparison between the quality factors issued from [6] and the presented approach will be done and discussed.

5.2 Methodology Proposed for the Design and Analysis of Metamaterial Inspired Antennas

The proposed methodology consists of analyzing the antenna (driven element) and the inclusion separately using TCM. The aim is to define the type of the dominant (scattered) power in their near field.

First, we compute the characteristic modes of the antenna using a CM solver. Then, a mode selection must be done in order to keep only the efficient dominant modes within the targeted frequency band f_{target}. The total reactive power of the considered modes in then calculated. This informs us about the nature of the dominant energy in the near field of the antenna at the same frequency.

The same analysis is then performed on a set of MTM inclusions in order to select an inclusion which stores the opposite type of the energy stored by the driven element. The selected inclusion is then associated to the driven element in order to conjugate it (matching it) at the targeted frequency f_{target}.

5.2.1 Modes Selection

Modes selection is based on two criteria. The first one consists in retaining modes with the lowest eigenvalues (in absolute value) since these modes are capable to resonate

© 2015 Tous droits réservés. doc.univ-lille1.fr

($|\lambda_n| \to 0$), and can be used for antenna radiation. A threshold for the eigenvalues is applied as shown in Fig. 5.2.

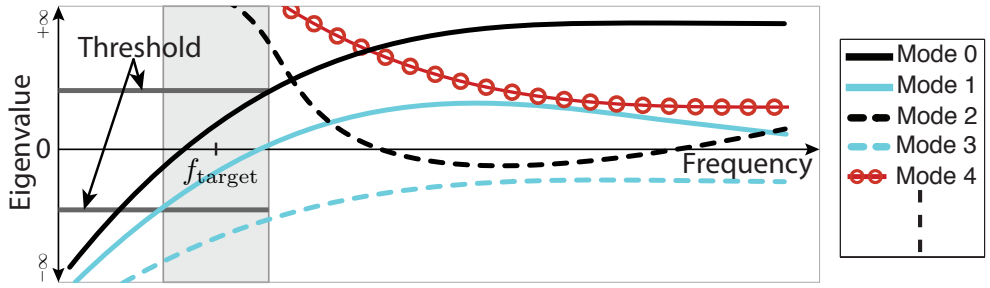

FIGURE 5.2: **Illustration of the threshold applied on the eigenvalues within a targeted frequency band in order to identify the dominant modes.**

Fig. 5.2 shows an illustration of eigenvalues of 4 modes with respect to the frequency with a zoom on dominant modes. This window is limited horizontally by the frequency band of interest and vertically by the thresholds fixed for the eigenvalues. There are two thresholds positive and negative in order to consider both magnetic and electric modes, respectively. The choice of the threshold value depends on the studied cases. It can be 10 as it can be 100 or other values. This is controlled by the studied frequency. Moreover, another type of thresholding can be used [121]. Authors in [121] calculate the eigenvalue of the n-th mode in dB scale:

$$\lambda_{n,\text{dB}} = 20\log(\lambda_n). \tag{5.1}$$

Only modes with $\lambda_{n,\text{dB}} \leq 30$ dB are considered in order to reduce the eigenvalue spectrum. In this work, a threshold on eigenvalues in linear scale is considered.

The second criterion for dominant modes selection considers the effect of the external excitation. We use the modal weighting coefficients from Eq. (3.18) to compare the influence of the specific external excitation on each mode. This coefficient takes into accounts the resonance condition of the mode. Modes with the highest modal weighting coefficients are kept. Typically, in electrically small antennas, one or two modes have high values for these coefficients, and thus, arex considered dominant.

5.2.2 Near Field Dominant Energy Identification

Once dominant modes are identified, their total reactive power is calculated:

$$P_{\text{reac,tot}} = \sum_{n}^{N} |w_{c,n}|^2 \lambda_n. \tag{5.2}$$

© 2015 Tous droits réservés.

Thèse de Mhamad Hassanein Rabah, Lille 1, 2015

The sign of $P_{\text{reac,tot}}$ informs us about the type of the dominant energy in the near field of the antenna. It tells us whether the antenna stores electric or magnetic energy in its near field.

5.2.3 Inclusion Analysis and Selection

An analysis similar to the one performed on the antenna is done on the metamaterial inclusions. The difference is that inclusions are not excited by an external feeding, but they couple to the antennas.

After calculating the CMs of an inclusion, resonant modes are identified ($\lambda_n = 0$). In general, at the resonance frequency the inclusion is single moded. This mode specifies the response of the inclusion. The sign of the eigenvalue after the resonance must then be investigated. In fact, in this region the inclusion presents the strongest response, and its behaviour is determined with respect to the sign of the eigenvalue after the resonance:

- If the eigenvalue is positive, the inclusion is considered storing magnetic energy, and then can be associated to an antenna storing electric energy in its near field.
- If the eigenvalue is negative, the inclusion is considered storing electric energy, and then can be associated to an antenna storing magnetic energy in its near field.

Several metamaterial inclusions are analysed and a database is built. This look up table (LUT) is useful to the antenna designers to check for an adequate inclusion to associate with a given antenna.

To sum up all the mentioned steps, Fig. 5.3 shows a workflow chart that summarises the methodology to enhance the efficiency of ESA using TCM. Fig. 5.3 also shows how to build the LUT of metamaterial inclusions. It should be mentioned that sometimes only interpreting the eigenvalues is not sufficient since they depend exclusively on the geometry of the inclusion. Hence, further steps can be added to include the polarization of the inclusion itself. Some cases require an extra study for the modal weighting coefficient in order to know the influence of the fields generated by the antenna on the inclusion. These steps are not included in Fig. 5.3 since they are not needed systematically.

For instance, one can place in the near field of the inclusion an external field source issued form the driven element in order to know how much each of the dominant modes reacts to these fields.

© 2015 Tous droits réservés. doc.univ-lille1.fr

Thèse de Mhamad Hassanein Rabah, Lille 1, 2015

Another solution consists of studying all possible polarizations and calculate in each case the weighting coefficients. This permits to identify the dominant modes in the case of a particular polarization.

© 2015 Tous droits réservés.

doc.univ-lille1.fr

Thèse de Mhamad Hassan Raad, Lille, 2015

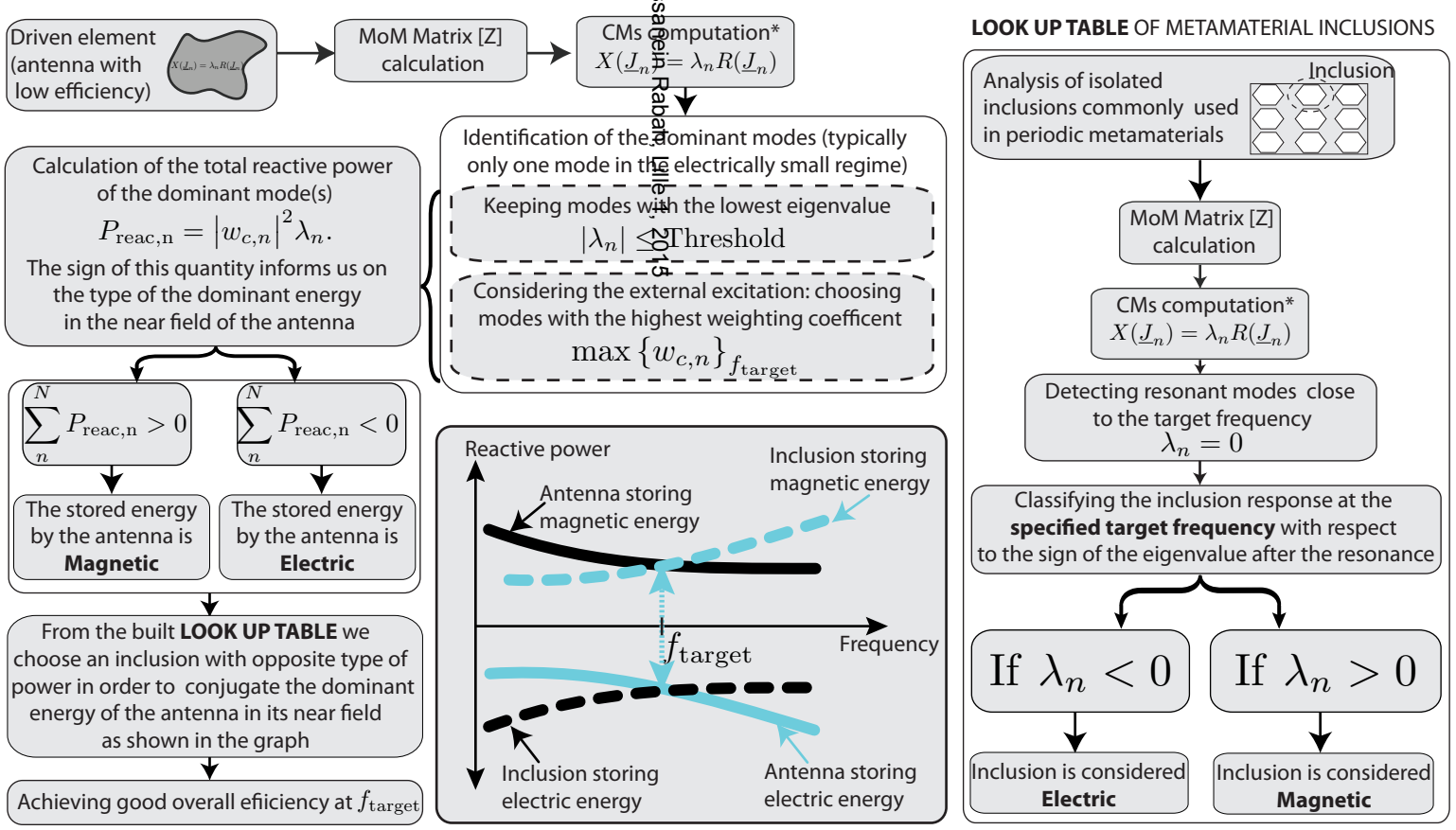

* The CMA tool in FEKO can be used to solve the eigenvalue problem.

FIGURE 5.3: **Design workflow for enhancing the efficiency of antennas using metamaterial inclusion based on the theory of characteristic modes.**

Thèse de Mhamad Hassanein Rabah, Lille 1, 2015

5.3 Modal Study of Metamaterial Inspired Antennas

In this section, the proposed methodology will be followed in order to analyse the metamaterial inspired ESAs proposed in [6]. This analysis will help to validate the workflow suggested in Fig. 5.3.

A metamaterial inspired antenna is a system composed of two parts: the radiator and the inclusion. We split the system into these two parts and study the modal currents on each of the radiator, the inclusion and then the overall system. This will provide the physical insight for the interaction between the radiator and the metamaterial inclusion.
Since EZ antennas are electrically small antennas [6], considering the first current modes should be sufficient. In this study we consider only the first three current modes.

5.3.1 Modal Study of 2D Electric Based Antennas

The basic idea of the 2D electric-based antenna is that a 2D meander line is positioned in very close proximity to the monopole antenna, approximately $\lambda_0/275$. It provides a large inductance, which again allows the combined system to form an RLC resonator. Another valid explanation for the properties of the inductance can be made if one visualises each electrically-small copper strip as a transmission line terminated in a short circuit.

5.3.1.1 Isolated Monopole

The monopole alone does not radiate because it suffers from stored reactive energy (electrical length $\approx \lambda_0/30$). Therefore, any of the eigencurrents on the monopole will not be resonating. To show that, eigenvalues in Eq. (3.13) are calculated and shown in Fig. 5.4 (a). Regardless of their signs, the first three eigenvalues are very high. This explains why the used thresholds are so high (order of 10^6). For the sake of clarity, the characteristic angles (eigenangles) are calculated using Eq. (3.14). They are shown in Fig. 5.4 (b). The first and third modes store electric energy over all the frequencies, since their characteristic angles ϕ_1 and ϕ_3 are equal to 270°. The second mode has a magnetic behaviour and stores magnetic energy within the targeted frequency band since ϕ_2 is equal to 90°.
The profiles of the first three eigencurrents of the monopole are shown in Fig. 5.5. Indeed, a dipole-like profile can be seen for modes storing electrical energy (modes 1

© 2015 Tous droits réservés. doc.univ-lille1.fr

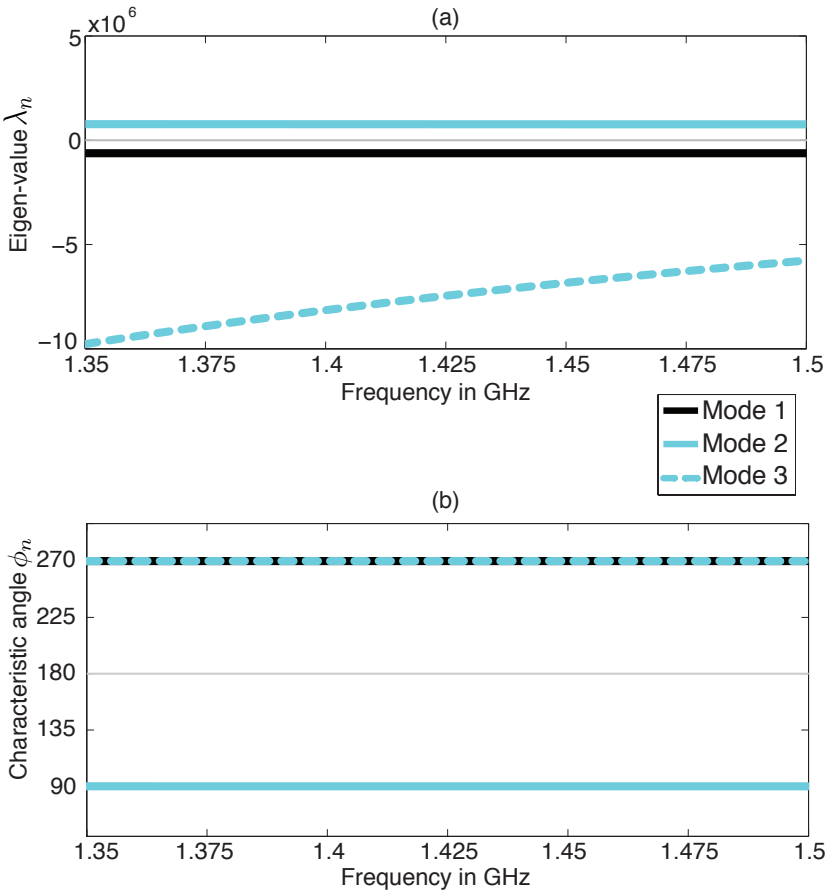

FIGURE 5.4: **Calculated eigenvalues (a), and eigenangles (b), of an isolated monopole. Any of the eigenvalues approaches zero since the modes are non-resonant in the studied frequency band. For the same reason, any characteristic angles cross the 180° line.**

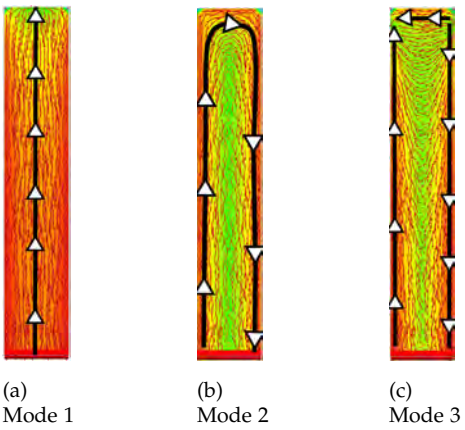

FIGURE 5.5: **Profiles of the first three eigencurrents of an isolated monopole (2D view). The monopole is perpendicular to an infinite ground plane. The same scale is used for all modes.**

and 3), and a loop-like profile for the second mode which is storing magnetic energy. Note that the monopole is excited with an edge voltage source via an infinite ground

© 2015 Tous droits réservés.

plane as depicted in Fig. 5.6. In order to know which mode is the most influenced by such an excitation, we calculate the modal excitation coefficient in Eq. (3.18). Fig. 5.6 shows the first three modal excitation coefficients.

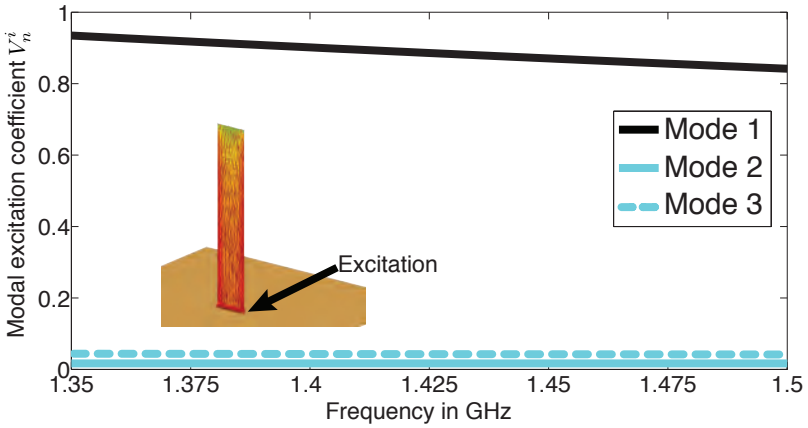

FIGURE 5.6: **Modal excitation coefficient V_n^i of the first three modes of an isolated monopole: the considered excitation here is an edge voltage source as depicted. The first mode is the most influenced by this excitation because of the mode configuration. Indeed the excitation is placed at the maximum surface current of this mode.**

The first mode is the most reactive to the considered excitation while the two others have $V_{2,3}^i$ close to zero. This means that the later modes are not excited by the voltage source for a such configuration. In practice, the first mode will be the dominant mode on the monopole when the antenna system is fed by such an excitation. This explains why the meander line helps the monopole to radiate. In fact, the electric energy stored by the dominant first mode of the monopole is conjugated by the meander line which behaves like an ϵ_r negative medium. In order to prove that, we investigate the current modes of an isolated meander line.

5.3.1.2 Isolated Meander Line

The meander line is considered as a resonant metamaterial inclusion at the operating frequency. Unlike the monopole, the eigenvalues of the structure are small and cross zero at the resonance. The eigenvalues of the first three eigencurrents on the meander line are shown in Fig. 5.7. The threshold used here is 5.10^5.

The first current mode of the meander line resonates at 1.481 GHz since its eigenvalue is equal to zero at this frequency (eigenangle equals 180°). Whereas, the second mode stores magnetic energy and the third one stores electric energy over the whole frequency band. The profiles of the first three eigencurrents flowing on the meander line are shown in Fig. 5.8.

© 2015 Tous droits réservés.

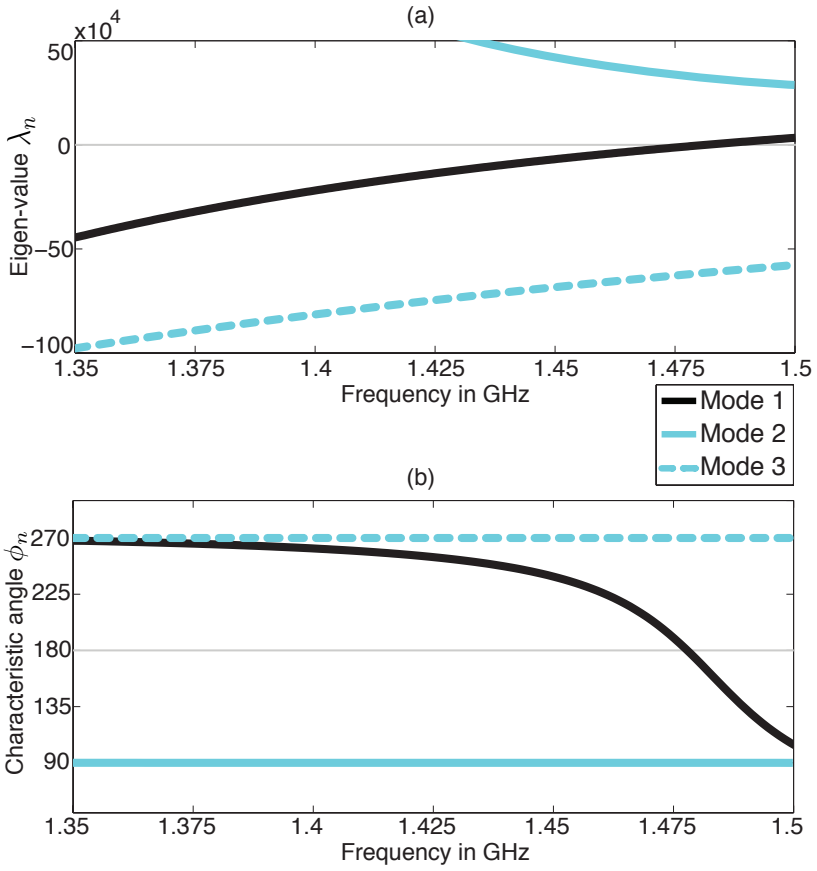

FIGURE 5.7: **Calculated eigenvalues (a), and eigenangles (b), of an isolated meander line. The first eigenvalue cross zero at the first resonance while the second mode has a high positive eigen value and the third mode has a high negative eigenvalue. For the same reason, the first characteristic angle cross the 180° line at 1.481 GHz which is the resonance of the first mode.**

The first eigencurrent flows from one end to the other of the meander as if following the path. The second eigencurrent seems to be flowing on both edges of each meander line with opposite flowing direction. The third mode present the same behaviour as the second one but both modes are out of phase.

5.3.1.3 Monopole and Meander Line

An advantage of computing characteristic modes using the MoM method is that the coupling between two separate objects can be included into the impedance matrix [Z]. Then, this generates a new eigenvalue problem which derives a new set of modified eigen-vectors taking into account the coupling between both objects. The characteristic modes have been computed for the whole antenna system (monopole and meander line). The eigenvalues of the first three eigencurrents are shown in Fig. 5.9.

© 2015 Tous droits réservés.

Thèse de Mhamad Hassanein Rabah, Lille 1, 2015

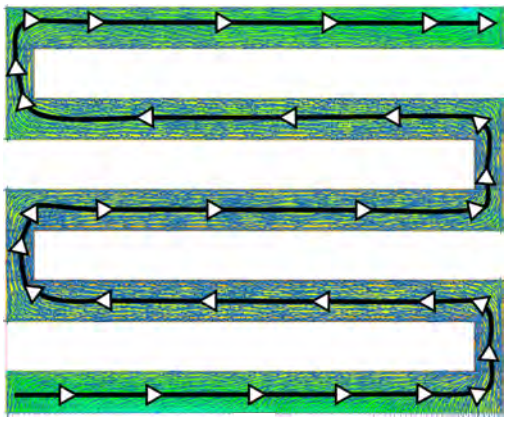

(a) Mode 1

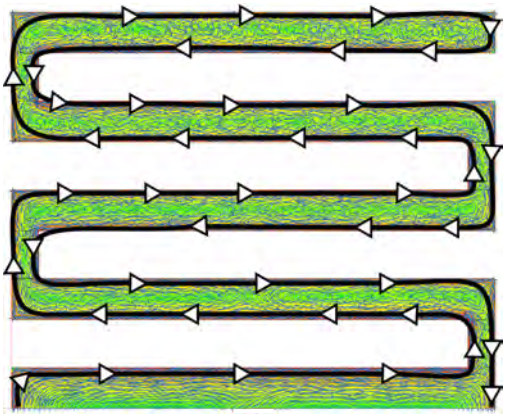

(b) Mode 2

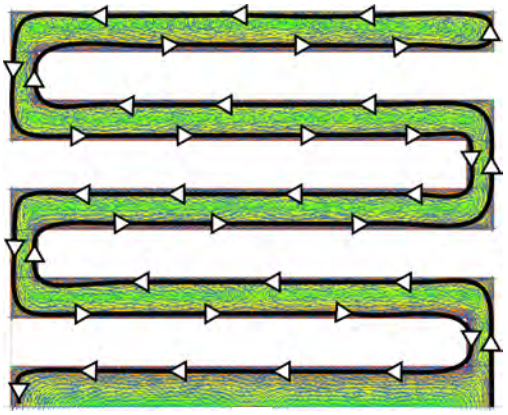

(c) Mode 3

FIGURE 5.8: **Profiles of the first three eigencurrents of an isolated meander line. The first eigencurrent go straight following the meander line, similarly to a current in a coil. The second eigencurrent follow a path with two way direction, which will push the resonance toward higher frequencies. The third mode presents the same profile as the second one but they are out of phase.**

Fig. 5.9 shows that the eigenvalues behaviour of the antenna system is almost identical to that of the isolated meander line. It is believed that the antenna will follow the resonance of the first mode since it is the only mode contributing to the radiation (see eigenangles in Fig. 5.9). However, in order to demonstrate this, we calculate the modal weighting coefficient $w_{c,n}$ from Eq. (3.18). The coefficient of the antenna system (monopole+meander line) are normalized and shown in Fig. 5.10. The normalization consists in adjusting the amplitude of the source such that the highest coefficient equals to 1.

© 2015 Tous droits réservés. doc.univ-lille1.fr

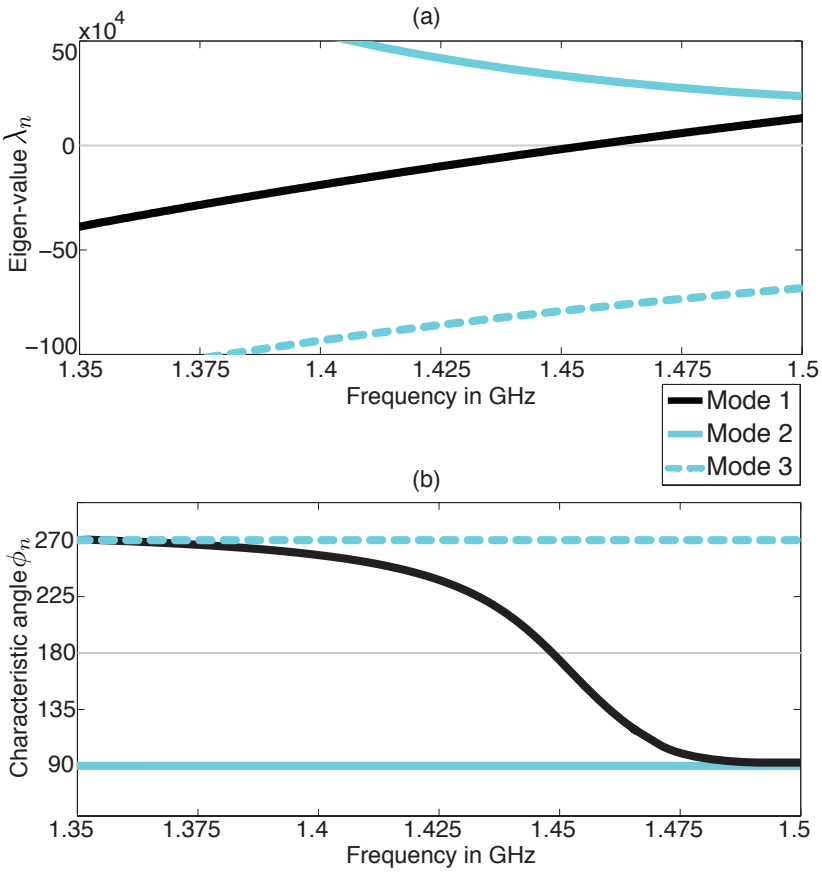

FIGURE 5.9: **Calculated eigenvalues (a), and eigenangles (b), of the system composed of the monopole and the meander line. The first eigenvalue crosses zero at the first resonance 1.442 GHz. This could also be seen from the first characteristic angle which crosses the 180° line at the same frequency. The second and third modes have high positive and negative eigenvalues, respectively. Both are bad radiators.**

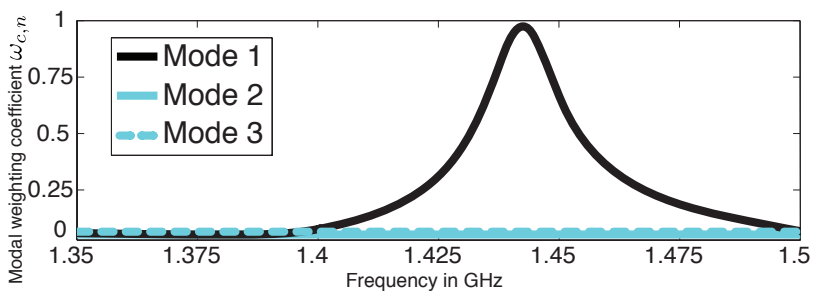

FIGURE 5.10: **Normalized modal weighting coefficients [from Eq. (3.18)] for the first three eigencurrents of the meander line and monopole together: the first mode has the higher coefficient because it meets the resonance condition and has high modal excitation coefficient (Fig. 5.6).**

Fig. 5.10 proves that the only resonating/radiating mode on the antenna system is mode 1. Moreover, it will be next demonstrated that this dominant mode carries the majority of the power injected into the structure.

© 2015 Tous droits réservés.

To show the impact of the meander line on the first eigenmode of the monopole, we make a zoom close to the resonance on the eigenvalues for both cases as shown in Fig. 5.11.

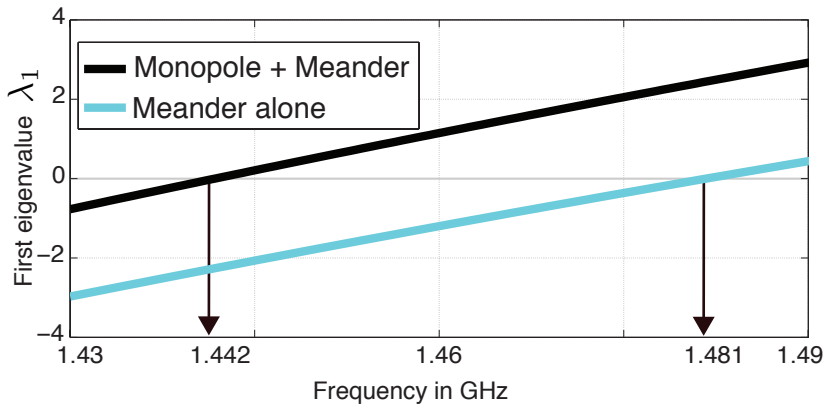

FIGURE 5.11: **Comparison of the first eigenvalue of the antenna system and the meander line alone. The isolated meander has a higher resonance than the system of monopole and meander. The difference is slight and is estimated to be 1%.**

The first resonance (mode 1) of the system (monopole + meander line) occurs at 1.442 GHz while that of the isolated meander is at 1.481 GHz. The frequency downshift is about 1%.

It is clear that the resonance behaviour of the monopole with the meander line follows that of an isolated meander since it is the resonating element in the system. The slight shift is due to the coupling between the monopole and the meander line. Note that as in the reference paper [6], the antenna resonance is about 1.373 GHz while the resonance frequency found with the modal analysis is 1.442 GHz. This difference can be due to the fact that the substrate having a relative permittivity $\epsilon_r = 2.2$ used in [6] for mechanical support purposes was neglected here.

The profile of the first eigencurrent on the monopole and the meander line together is shown in Fig. 5.12.

The first eigencurrent on the meander presents the same profile as the one found for an isolated meander line: it flows from one to the other end of the meander as if following the path. This is not the case of the monopole where the current tries to emulate that of the meander. It is this new current configuration on the monopole which induces radiation due to the current maxima in the vicinity of the meander line giving rise to resonance in the monopole. Furthermore, the frequency downshift of the mode resonance could be explained by the extended length of the current path on the monopole instead of a straight line, as in the case of Fig. 5.5(a).

© 2015 Tous droits réservés.

Thèse de Mhamad Hassanein Rabah, Lille 1, 2015

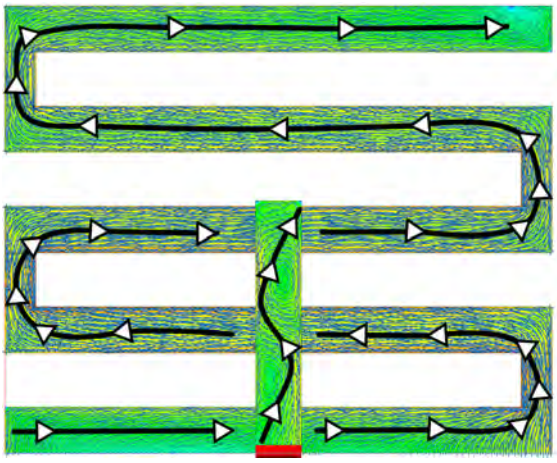

FIGURE 5.12: **First eigencurrent profile of a monopole associated to a meander line: the profile on the meander remains unchanged from when it is isolated. The current profile on the monopole is modified compared to an isolated one, and seems to follow the paths of the meander line.**

5.3.1.4 Power and Quality Factor Calculations for the 2D Antenna

The analysis presented above and the proposed methodology in Section 5.2 are based on the fact that only the dominant modes in the structure should be considered, and that metamaterial inspired antenna presented yet is a single-mode antenna. To validate this, a comparison between the modal analysis and classical full wave simulation of the total current using ANSYS HFSS commercial software [129] is presented. First, we compare the amount of power carried per mode to the power injected in the structure. Fig. 5.13 shows the total power transmitted to the structure.

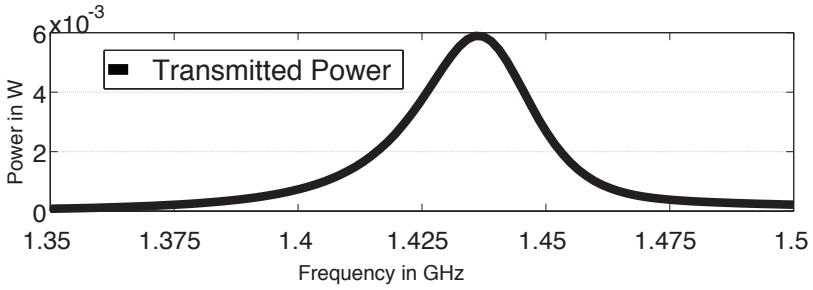

FIGURE 5.13: **Full wave simulation: transmitted power to the structure. This power represents the power generated by the voltage source and transmitted to the monopole + meander line antenna system. The peak value is 6 mW.**

The curve in Fig. 5.13 represents the power transmitted from the voltage source to the antenna system (monopole + meander line). The maximum absorbed power is 6 mW. The importance of this value is to compare it to the modal powers calculated with equations (3.22) and (3.20) and to show how the power is distributed over

© 2015 Tous droits réservés. doc.univ-lille1.fr

the modes. Fig. 5.14 shows the modal active and reactive power for the first three eigencurrents of the monopole when associated to the meander line.

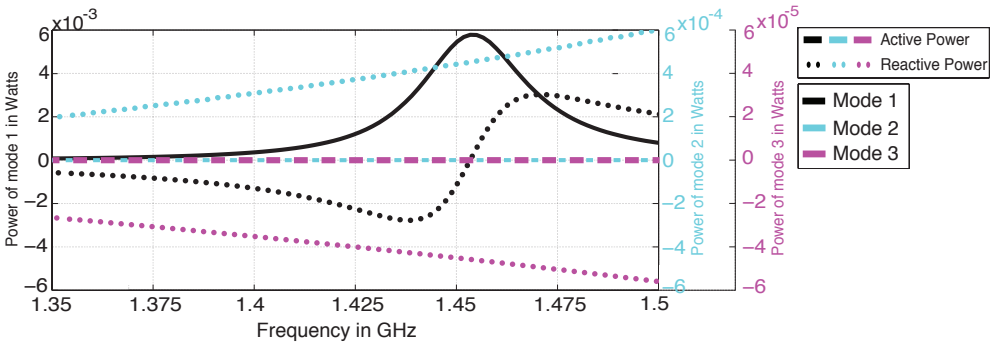

FIGURE 5.14: **Modal active and reactive powers from Eq. (3.22) and (3.20), respectively, of the first three characteristic modes of the monopole associated to the meander line.**

Because of the large difference between modal power values, 3 scales were used. It is shown from Fig. 5.14 that radiated power for mode 1 rises to a maximum value of 5.8 mW at the resonance while the reactive power crosses zero from negative (electric power) to positive (magnetic power). This is the typical behaviour of a resonance, as described in [6]. Mode 2 presents nearly zero radiated power and a positive reactive power is of the order of 10^{-4} mW over all the frequencies. Mode 3 also has zero radiated power and presents the opposite behaviour since it has negative reactive power within the whole frequency band which is of the order of 10^{-5} . When comparing Fig. 5.14 and Fig. 5.13, it can be deduced that more than 98 % of the transmitted power has been carried and radiated by the first mode at its resonance frequency. This approves the fact that mode 1 is the predominant mode contributing to the radiation of the antenna and then it is the mode that drives the overall behaviour of the system.

Also, the investigation of the antenna (monopole + meander line) quality factor is presented. Authors in [6] have used a quality factor ratio Q_{ratio} to compare the performances of the antennas and to take into consideration the matching and the radiation efficiency. Dividing by Chu's expression normalises the calculated quality factor with respect to the lower bound.

In this chapter, we adopt the same Q_{ratio} expression using the modal quality factors proposed in Section 4.4 and that from Eq. (4.10) as follows:

$$Q_{\text{ratio}} = \frac{Q_{\omega_0}}{Q_{\text{Chu}}}, \tag{5.3}$$

where

© 2015 Tous droits réservés.

Thèse de Mhamad Hassanein Rabah, Lille 1, 2015

$$Q_{\text{Chu}} = \left(\frac{1}{ka} + \frac{1}{(ka)^3}\right) \times RE \tag{5.4}$$

and

$$Q_{\omega_0} = \begin{cases} \frac{2}{FBW_{-3\text{dB}}} & \text{From the reflexion coefficient issued from full wave simulation [53, Eq. 91].} \\ Q_{\text{tot}} & \text{Modal quality factors using Eq. (4.25) based on the eigenvalues.} \\ Q_{Z,\text{tot}} & \text{Sum of quality factors in Eq. (4.10) based on the modal form of the input impedance expression [53].} \end{cases} \tag{5.5}$$

RE is the radiation efficiency, $f_0 = \omega_0/2\pi$ is the resonance frequency, and $FBW_{-3\text{dB}}$ is the half-power matched VSWR fractional bandwidth [53]. Q_{ω_0} is calculated from equations (4.24), (4.25) and (4.10) when characteristic modes are involved, and depend on a specific number of modes N. The radiation efficiency of the mode can be calculated from the eigenvalues of the considered modes [67, Eq. 44]. However, RE is assumed to be 1 since at the resonance the eigenvalue is equal to zero.
Table 5.1 shows a comparison of calculated quality factors using Q_{ratio} expressions.

TABLE 5.1: **Comparison between calculated quality factors of a 2D Electric Based Antenna (Monopole+Meander Line), based on modal and classical expressions.**

Used equation	N	ka	**FBW (%)**	Q_{chu}	Q_{ratio}
Full wave simulation [6]	–	0.497	4.079	10.16	5.35
Eq. (4.24)	1	0.522	2.3	8.95	5.08
Eq. (4.24) and (4.25)*	1,2,3	0.502	1.85	9.9	5.38
Eq. (4.10)	1	0.522	2.66	8.95	5.11
Eq. (4.10) and (4.12)*	1,2,3	0.502	3.6	9.9	5.45

* When N modes are considered, the antenna resonance frequency is used as center frequency for the calculation of ka.

Obviously, the values of Q_{ratio} issued from different equations are very close to 5.35 which is the reference value in [6]. In table 5.1 the FBW (%) of modes has been calculated from the modal quality factors using Eq. (4.11). The differences of computed FBWs can be due to the design sensitivity to the ka product and to the mismatch. In fact, when only the first mode is considered, the obtained values with Eq. (4.24) and (4.10) are 5.08 and 5.11 respectively. These values approach the total quality factor, which shows that the modal quality factor of mode 1 is close to the total quality factor

© 2015 Tous droits réservés. doc.univ-lille1.fr

Thèse de Mhamad Hassanein Rabah, Lille 1, 2015

since the studied structure is electrically small [67, 126]. Furthermore, the accuracy increases when considering modes 2 and 3 using Eq. (4.25).

5.3.2 Modal Study of 3D Magnetic Based Antennas

The main idea in the 3D magnetic-based antenna is that the magnetic energy stored by the semi-loop antenna is conjugated using a capacitively-loaded loop (CLL). The CLL can be seen as a capacitor with a very small spacing between the two plates $(0.03\ mm)$. This small distance is at the origin of the narrow bandwidth of the antenna [6].

5.3.2.1 Isolated Semi-Loop

The semi-loop antenna does not radiate alone because its electrical size is too small ($\approx \lambda/520$). None of the eigencurrents on the loop will resonate as shown by the characteristic angles in Fig. 5.15.

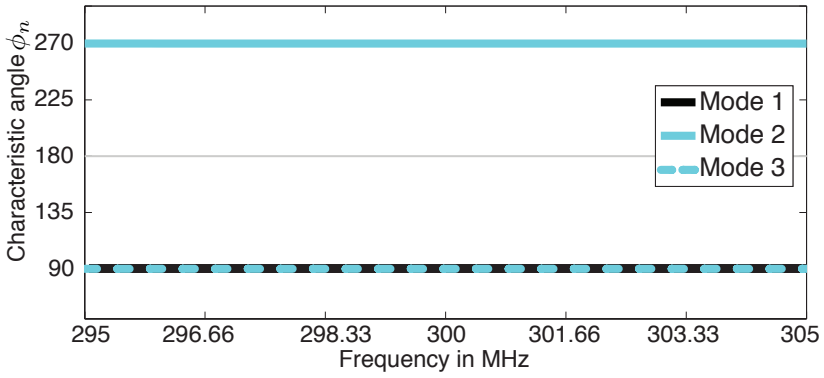

FIGURE 5.15: **Calculated eigenangles of an isolated semi-loop. Any of the characteristic angles cross the 180° line, since the modes are non-resonant in the studied frequency band.**

The first and third modes store magnetic energy over all the frequencies, since their characteristic angles ϕ_1 and ϕ_3 are equal to 90°. The second mode has an electric behaviour within the operating frequency band since ϕ_2 is equal to 270°.
The profiles of the first two eigencurrents flowing on the semi-loop are shown in Fig. 5.16. The typical configuration of magnetic and electric currents on a loop are represented by modes 1 and 2, respectively. The third mode is not shown on Fig. 5.16 since it presents the same profile as mode 1 with an opposite phase.
The semi-loop is excited with a wire voltage source via an infinite ground plane, as depicted in Fig. 5.17. As done for the 2D antenna, we calculate the modal excitation

© 2015 Tous droits réservés. doc.univ-lille1.fr

Thèse de Mhamad Hassanein Rabah, Lille 1, 2015

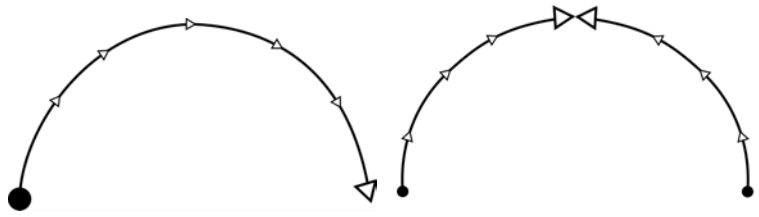

(a) Mode 1 (b) Mode 2

FIGURE 5.16: **Profiles of the first two eigencurrent of an isolated semi-loop (2D view). The loop is mounted on an infinite ground plane.**

coefficient in Eq. (3.18) in order to know which mode is predominant with such an excitation. Fig. 5.17 shows the first three modal excitation coefficients.

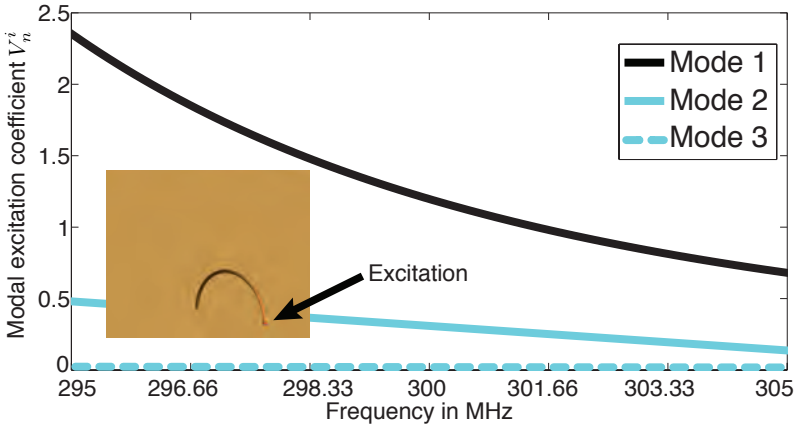

FIGURE 5.17: **Modal excitation coefficient V_n^i of the first three modes of an isolated semi-loop: the considered excitation here is a wire port as depicted. The first mode is the most excited with a such excitation because of the mode configuration. Indeed the excitation is not placed at the maximum of the mode, then V_1^i is not the maximum at 300 MHz.**

Unlike the studied 2D monopole, the first modal excitation coefficient of the semi-loop antenna decreases faster with respect to the frequency. This mode is the most sensitive to the considered excitation. Mode 2 has a lower coefficient value, while V_3^i is nearly zero. The first mode will be the dominant mode on the semi-loop when the antenna system is fed by such an excitation. Combining this information with the resonance condition, the modal weighting coefficient of this mode comfirms this observation (Fig. 5.22). Furthermore, this explains why the CLL makes the semi-loop radiates. In fact, the magnetic energy stored by the dominant first mode of the semi-loop is conjugated by CLL which behaves like an μ_r negative medium. In order to prove that, we investigate the current modes of an isolated CLL.

© 2015 Tous droits réservés. doc.univ-lille1.fr

5.3.2.2 Isolated Capacitively-Loaded Loop

The CLL is considered a resonant metamaterial inclusion. Thus, unlike the semi-loop, the first eigenvalues of the structure are small and cross zero at the resonance. The eigenvalues of the first two eigencurrents on the CLL are shown in Fig. 5.18 with a threshold of 10^4.

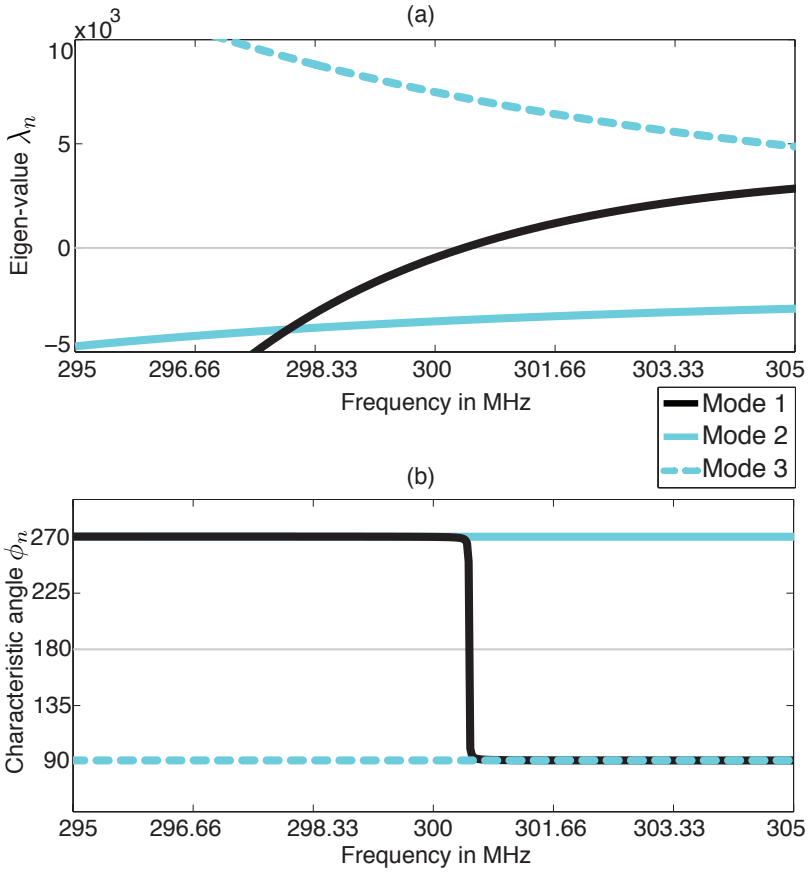

FIGURE 5.18: **Calculated eigenvalues (a), and eigenangles (b), of an isolated CLL. The first eigenvalue crosses zero at the first resonance while the second mode has a high negative eigenvalue and the third mode has a high positive eigenvalue. For the same reason, the first characteristic angle crosses the 180° line at 301 MHz which is the resonance of the first mode.**

The first current mode of the CLL resonates at 301.35 MHz since its eigenvalue cross zero at this frequency ($\phi_1 = 180°$). It passes from electric to magnetic energy storage: this is the required behaviour to make the semi-loop antenna resonate. Whereas, the second mode stores electric energy and the third one stores magnetic energy over the whole frequency band. The profiles of the first two eigencurrents flowing on the CLL are shown in Fig. 5.19.

© 2015 Tous droits réservés.

Thèse de Mhamad Hassanein Rabah, Lille 1, 2015

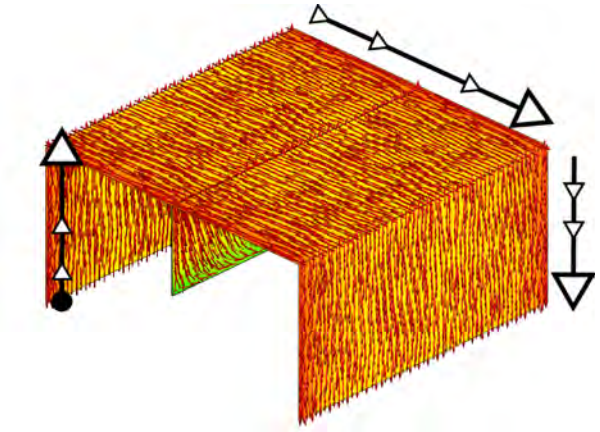

(a) Mode 1

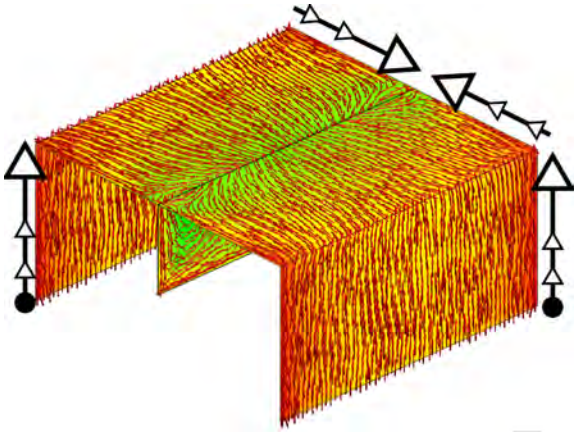

(b) Mode 2

FIGURE 5.19: **Profiles of the first two eigencurrent of a CLL (3D view). The CLL is mounted on an infinite ground plane.**

The first eigencurrent flows from one end of the CLL to the other as following the path. This configuration creates two opposite surface currents at the gap of the CLL. In fact this mode makes a current loop with the ground plane. This mode is believed to match the semi-loop antenna at 301.35 MHz. The second mode is symmetrical with respect to the vertical axis. The current flows from both CLL ends resulting in two surface currents at the gap flowing in the same direction.

5.3.2.3 Semi-Loop with a Capacitively-Loaded Loop

The characteristic modes have been computed for the entire antenna system (Semi-Loop and Capacitively-Loaded Loop). The profiles of modes 1 and 2 are shown in Fig. 5.20.

© 2015 Tous droits réservés. doc.univ-lille1.fr

Thèse de Mhamad Hassanein Rabah, Lille 1, 2015

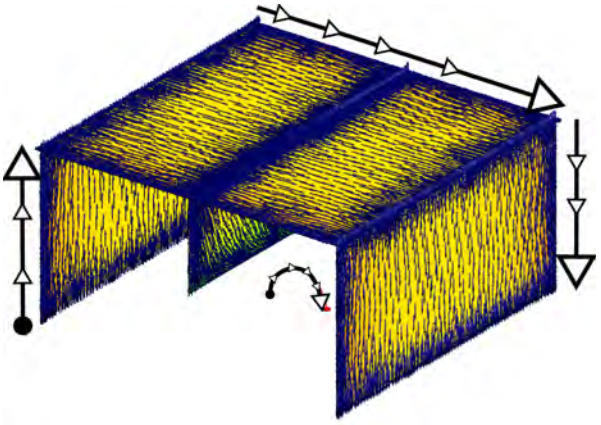

(a) Mode 1

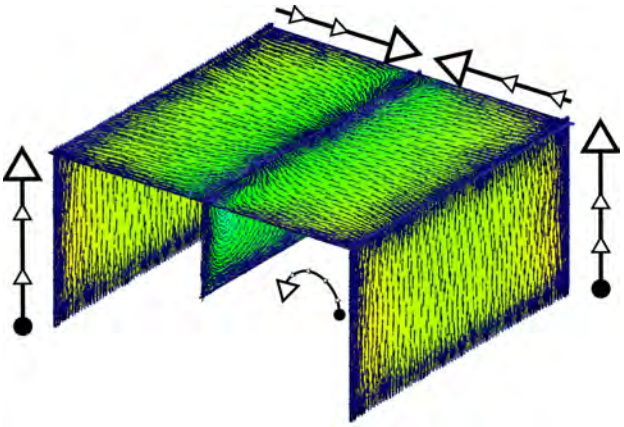

(b) Mode 2

FIGURE 5.20: **Profiles of the first two eigencurrent of a CLL+ semi-loop antenna (3D view). The system is mounted on an infinite ground plane (not shown on the figure).**

The profile of mode 1 over the 3D antenna system combines both first modes of the isolated semi-loop and CLL. The second mode is a combination of the third mode and second mode of the semi-loop and the CLL, respectively. However, since the CLL is the only resonant element, then, the system will follow it. This can be further seen from the first eigenvalue of the system, with a zoom close to the resonance in Fig. 5.21.

It is obvious that both the antenna system and the isolated CLL present the same behaviour for the first eigenvalue. The resonant frequencies are almost identical. The first resonance of the antenna occurs at 299.69 MHz while that of the isolated CLL is at 301.35 MHz.
Contrarily to the 2D case, there is no frequency shift between the antenna reflection coefficient in Fig. 2.14 and the first eigenvalue in Fig. 5.21. This is because there is no substrate to be neglected here and the only assumption is the infinite ground plane. The agreement between Fig. 2.14 and Fig. 5.21 justifies this assumption.

© 2015 Tous droits réservés. doc.univ-lille1.fr

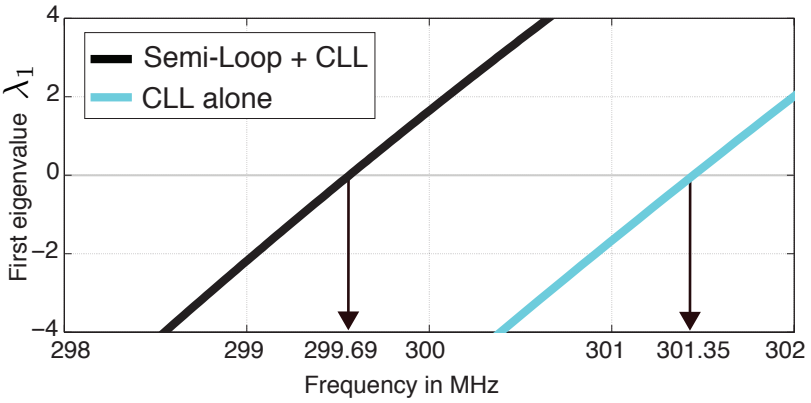

FIGURE 5.21: **Comparison of the first eigenvalue of the antenna system and an isolated CLL inclusion. The CLL alone has a slightly higher resonance than the system. The difference is very small and is estimated to be 0.55%.**

The second eigenvalue of the antenna system is not shown in Fig. 5.21 since it presents the same non resonant behaviour as in Fig. 5.18. Nevertheless, the second mode had a remarkable reaction for the considered excitation (Fig. 5.17), but does not contribute to the total antenna response. This can be demonstrated by calculating the modal weighting coefficients of the antenna.

The coefficients of the first three modes flowing on the 3D antenna are shown in Fig. 5.22.

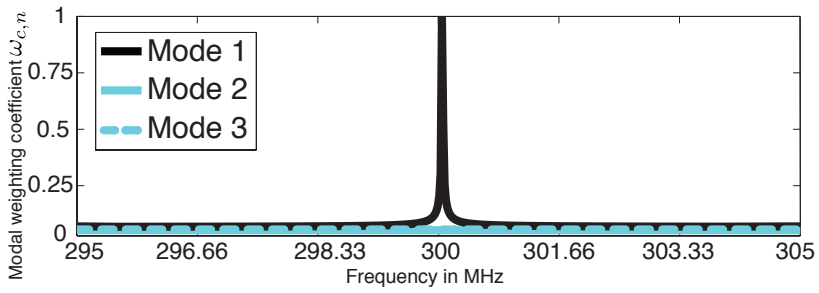

FIGURE 5.22: **Normalized modal weighting coefficients (from Eq. (3.18)) for the first three eigencurrents of the semi-loop and the CLL together: the first mode has the higher coefficient because it meets the resonance condition and has considerable high modal excitation coefficient (Fig. 5.17). The two higher modes have $w_{c,1 \text{ and } 2}$ close to zero since they only store energy.**

Fig. 5.22 proves that the only resonating/radiating mode on the antenna system is mode 1. Furthermore, as done for the 2D design, we demonstrate using modal powers that this dominant mode carries the majority of the power injected into the structure.

© 2015 Tous droits réservés.

5.3.2.4 Power and Quality Factor Calculations for the 3D Antenna

Our aim in this paragraph is to demonstrate how the power absorbed by the antenna is distributed over the characteristic modes. The total power transmitted to the structure is shown on Fig. 5.23.

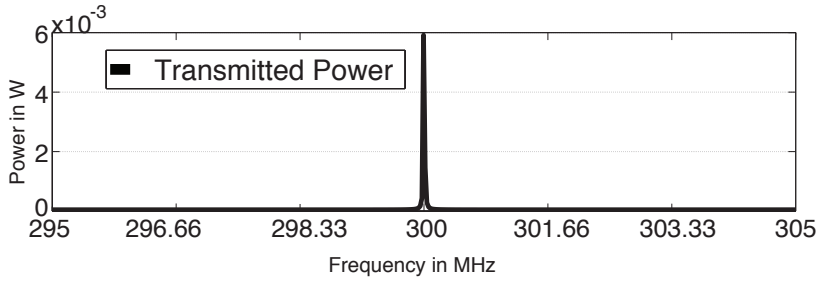

FIGURE 5.23: **Full wave simulation: transmitted power to the structure. This power represents the power generated by the voltage source and transmitted to the semi-loop + CLL antenna system. The peak value is 6 mW.**

The power in Fig. 5.23 represents the transmitted power from the voltage source to the antenna system (semi-loop + CLL). The maximum absorbed power is 6 mW. Fig. 5.24 shows the modal active and reactive power for the first three modes of the semi-loop associated to the CLL.

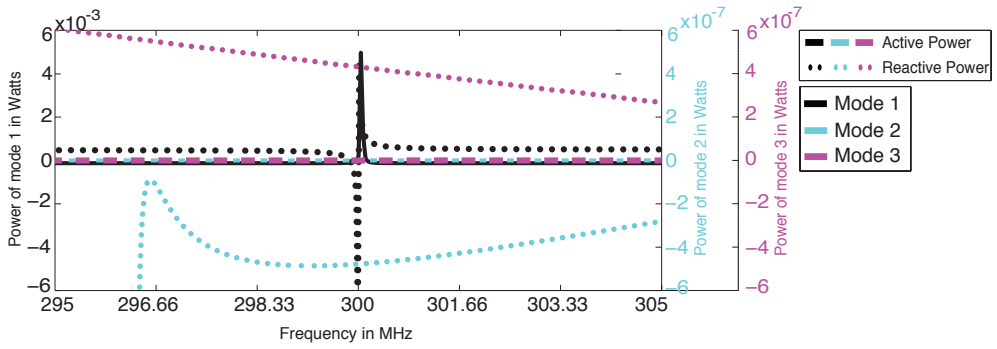

FIGURE 5.24: **Modal active and reactive power from Eq. (3.22) and (3.20), respectively, of the first three characteristic modes of the semi-loop associated to the capacitively-loaded loop.**

The power carried by the first mode has the order of 10^{-3} Watts, while for modes 2 and 3 the power is of the order of $10^{-7.}$ Watts. Among the three scales, one can deduce that powers carried by modes 2 and 3 can be neglected with respect to mode 1.

Moreover, it is shown from Fig. 5.24 that radiated power for mode 1 rises to a maximum (5 mW) at 300 MHz (mode resonance 299.69 MHz). The reactive power

© 2015 Tous droits réservés.

Thèse de Mhamad Hassanein Rabah, Lille 1, 2015

crosses zero from positive (magnetic power) to negative (electric power) and then is positive again.

Mode 2 presents nearly zero radiated power and a negative reactive power. Mode 3 has also zero radiated power and presents the opposite behaviour because it has positive reactive power within the whole frequency band since it is a magnetic mode. When comparing Fig. 5.24 and 5.23, it can be deduced that more than 91.5 % of the transmitted power has been carried and radiated by the first mode at its resonance frequency. This is in agreement with the fact that only mode 1 is the mode contributing to the radiation of the antenna and it is the predominant mode of the overall system.

It should be noticed that in the studied 3D antenna, 100 % of the transmitted power has not been collected by the first three modes. This is due to the imperfections in the orthogonality of the modes. Indeed, theoretical characteristic modes are orthogonal, but when they are computed from the impedance matrix, the later should be symmetrical to obtain orthogonal modes. The used solver (FEKO) enforces the symmetricy condition of the matrix and results in such inaccuracies. This limitation is further detailed in Section 5.4. Moreover, to compare the results with other conventional methods we investigate the antenna Q factor.

Table 5.2 compares the calculated quality factors using Q_{ratio} expressions. Same expressions as Section 5.3.1.4 were used.

TABLE 5.2: **Comparison between calculated quality factors of a 3D Magnetic Based Antenna (Semi-Loop+CLL), based on modal and classical expressions.**

Used equation	N	ka	**FBW (%)**	Q_{chu}	Q_{ratio}
Full wave simulation [6]	–	0.1110	0.04	738.26	6.68
Eq. (4.24)	1	0.1117	0.046	726	5.91
Eq. (4.24) and (4.25)*	1,2,3	0.0744	0.2	244	4.05
Eq. (4.10)	1	0.1117	0.045	726	6.1
Eq. (4.10) and (4.12)*	1,2,3	0.0744	0.15	244	5.45

* When N modes are considered, the antenna resonance frequency is used as center frequency for the calculation of ka.

A good agreement between different Q_{ratio} is obtained. For instance, when considering only mode 1, the difference between the reference Q (6.68) and the modal one is about 0.77 when using Eq. (4.24), and 0.58 when using Eq. (4.10). Unlike the case of 2D electric based antenna, this difference increases when considering 3 modes instead of mode 1.

Theoretically, the higher the number of considered modes, the greater the accuracy

© 2015 Tous droits réservés. doc.univ-lille1.fr

Thèse de Mhamad Hassanein Rabah, Lille 1, 2015

of the solution. Nevertheless, this is not the case and could be predicted from modal powers calculated in previous paragraph. In fact, this is mainly due to numerical problem induced by the non-orthogonality of the modes. However, the accuracy of the calculated quality factor values using the proposed modal approach prove to be acceptable and satisfying. Furthermore, this could be also due to the narrow bandwidth of the design, and the high sensitivity to the *ka* product.

5.4 Discussion

The modal study of the 2D electric based antenna and 3D magnetic based antenna proved to provide very useful information by solving only the eigenvalue problem. The separated study of the driven element and the parasitic inclusion allowed us to define the modes responsible for the overall system behaviour. Furthermore, we were able to define the antenna quality factor without a prior knowledge on the feeding. This is an appealing feature of the modal approach because it presents a huge advantage over other expressions in terms of simplicity and ability to calculate Q for an arbitrary shape without the need to define a particular excitation. However, in the proposed study a good agreement between the modal based quality factor and the conventional Q was achieved for the 2D electric based antenna.

In the case of the 3D magnetic based antenna, there was a larger gap between quality factors based on characteristic modes and reference value [6]. This results from a numerical issue. In fact, unlike the 2D antenna, in the 3D antenna we have used two different types of mesh: the loop is modelled as wire segments while the CLL is modelled using RWG triangular surface meshes [93]. This results in a non-symmetrical impedance matrix [Z]. Meanwhile, it has been demonstrated in [81] that the impedance matrix must be totally symmetric in order to obtain totally orthogonal modes. Then, modes 1, 2 and 3 in the 3D magnetic based antenna are not totally orthogonal, thus, both active and reactive powers have not been distributed correctly over the modes. However, to increase the accuracy of the Q calculations, the same type of meshes should be used. For instance, instead of using wire segments, the semi-loop can be modelled as small cylinders with triangular meshes. This can increase the symmetry of the impedance matrix, while resulting in harder mode tracking [97].

The analysis of the EZ antennas using the metrics proposed by the methodology workflow in Fig. 5.3 provides a new dimension for the analysis of metamaterial inspired antennas. In fact, this has approved two main points. Dominant modes have been identified using the thresholds on the eigenvalues and the maximum modal

© 2015 Tous droits réservés. doc.univ-lille1.fr

Thèse de Mhamad Hassanein Rabah, Lille 1, 2015

weighting coefficients. We demonstrated that the total injected power has been collected by the dominant characteristic mode(s) selected with respect to these criteria. The Q factor values calculated using the modal based approach and the conventional classical approach have demonstrated a good agreement.
It has also been demonstrated that matching the driven element requires a MTM inclusion with opposite type of stored energy in the near field. This in order to conjugate the reactive power of the driven element. This was the case of the CLL with the semi-loop antenna and the meander line with the monopole antenna. However, other inclusions presenting the same behaviour could also be considered.

5.5 Conclusion

We presented in this chapter a new methodology for the synthesis of metamaterial inspired antennas. This methodology is based on the analysis of particular characteristic modes of the antenna and the metamaterial inclusion. These particular characteristic modes are selected with respect to their resonance conditions and their sensitivity to a particular external excitation. We further applied this methodology on existing metamaterial inspired designs known as EZ antennas [6]. The Q_{ratio} has been used to compare results from the presented approach and the common one. Good agreement between the modal based Q factor and the conventional one was achieved for the 2D electric based and 3D magnetic based antennas.

© 2015 Tous droits réservés. doc.univ-lille1.fr

Chapter 6

Design of a Spectrum Sensing Antenna Using TCM

6.1 Introduction

In this chapter, we present a novel extremely-wide-band antenna dedicated for underlay CR used for spectrum sensing operations. The antenna presented is based on designs proposed for UWB systems. These include various printed antennas with different shapes and enhanced bandwidths. The shapes of the printed antennas can be rectangular [130, 131], triangular-ring [132, 133], circular [134], annular-ring [135], fractal [136], and elliptical [38, 39, 137]. The monopole antenna chosen is an elliptical one, because it offers more resonating modes at lower frequencies and hence the variation of its elliptical ratio provides an additional degree of freedom for impedance matching.

We will use TCM to optimize the antenna in order to meet spectrum sensing requirements taking into account both constraints: bandwidth and radiation pattern stability. The design workflow consists of three parts: the first part is related to the feeding system and ground plane, while the second one deals with the radiator using TCM. Finally, the efficiency of the antenna is improved at low frequencies using the methodology proposed in the Chapter 5. For this purpose a MTM inclusion is selected and associated to the antenna in order to enhance its radiation characteristics in its electrically small regime.

© 2015 Tous droits réservés. doc.univ-lille1.fr

Thèse de Mhamad Hassanein Rabah, Lille 1, 2015

6.2 Bandwidth Enhancement of a Spectrum Sensing Antenna Using TCM

In general, bandwidth enhancement is obtained by exciting higher-order modes on the monopole, which results in a radiation pattern instability over the whole frequency range. However, when miniaturising the disk of the monopole, higher-order modes are naturally excited at higher frequencies. Whereas to excite these higher-order modes at low frequencies, further manipulation of the disk feeding is required. Authors in [132] and [134], explain how a parametric study allows the determination of the optimal values for an elliptical disc feeding system in terms of lowest matched frequency and total bandwidth. Fig. 6.1 shows the schematic of an optimized miniaturized design.

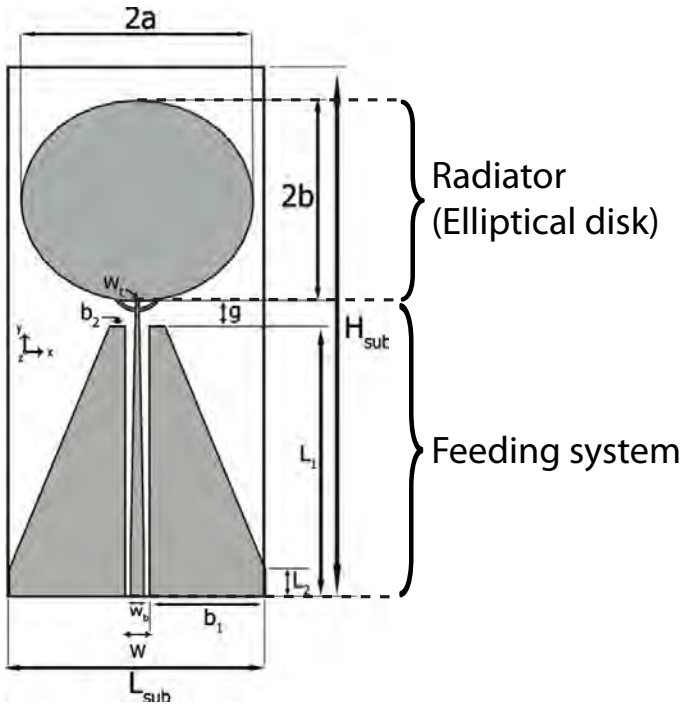

FIGURE 6.1: **Miniaturized antenna configuration: optimized feeding system based on a CPW transmission line with a triangular ground plane.**

The proposed design is composed of two main parts: the radiator and the feeding system. Optimal parameters for both geometries are given in Table 6.1.

The main parameters to reduce the antenna size are the disk dimensions. This could be seen obviously in Table 6.1. The variation of the radiator size changes the input impedance. This impedance results from the contribution of different intrinsic impedances of the weighted current modes. The weighting coefficients [Eq. 3.18)]

© 2015 Tous droits réservés. doc.univ-lille1.fr

Thèse de Mhamad Hassanein Rabah, Lille 1, 2015

TABLE 6.1: **Dimensions of the miniaturized antenna [mm]**

H_{sub}	L_{sub}	a	b	L_1	L_2
68	33	15	13	35	3.5
b_1	b_2	W	w_b	w_t	g
15	2	3.15	1.7	0.35	3.28

depend on the excitation. In the targeted frequency band, the first six modes will be considered as efficient radiators.

These modes present capacitive impedance [10] as can be seen from the sign of the first six eigenvalues shown in Fig. 6.2.

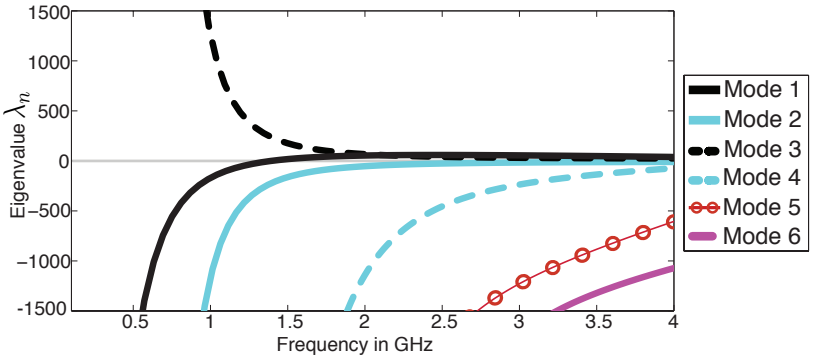

FIGURE 6.2: **First six eigenvalues of the considered EWB antenna over the band 0−4 GHz.**

Except for the third mode, all characteristic modes over the disk present a capacitive behaviour since their eigenvalues are negative. As shown in Fig 6.1, a tapered transmission line is used in order to match the disk total input impedance. This matching occurs thanks to the compensation of the electric energy stored by the disk with the magnetic nature of the tapered transmission line. The line access have a $w_b = 1.7\ mm$ and $W = 3\ mm$ to guarantee an input impedance of 50 Ω. Another advantage of using a CPW line are to keep the design on a single layer, and to reduce dispersion at higher frequencies. At the end of the CPW line, a trident feed is used to excite the radiator in 3 equidistant points in order to increase the number of excited modes and to decrease the cut-off frequency of the first modes. To show this, Fig. 6.3 compares the impact of the trident feed on the eigenvalues of the first two characteristic modes.

© 2015 Tous droits réservés. doc.univ-lille1.fr

Thèse de Mhamad Hassanein Rabah, Lille 1, 2015

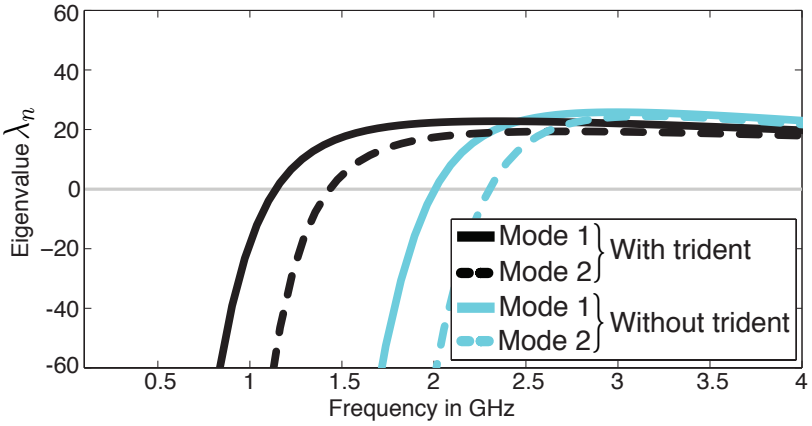

FIGURE 6.3: **Impact of the trident feed on the first two eigenvalues of the monopole.**

The presence of the trident structure at the circumference of the disk has shifted down the resonance frequency of the modes having current density flowing in its vicinity. The semi-ring structure impacts mainly the first two modes of which the eigenvalues are shown in Fig. 6.3. This is due to the path taken by the surface currents, as shown in Fig. 6.4.

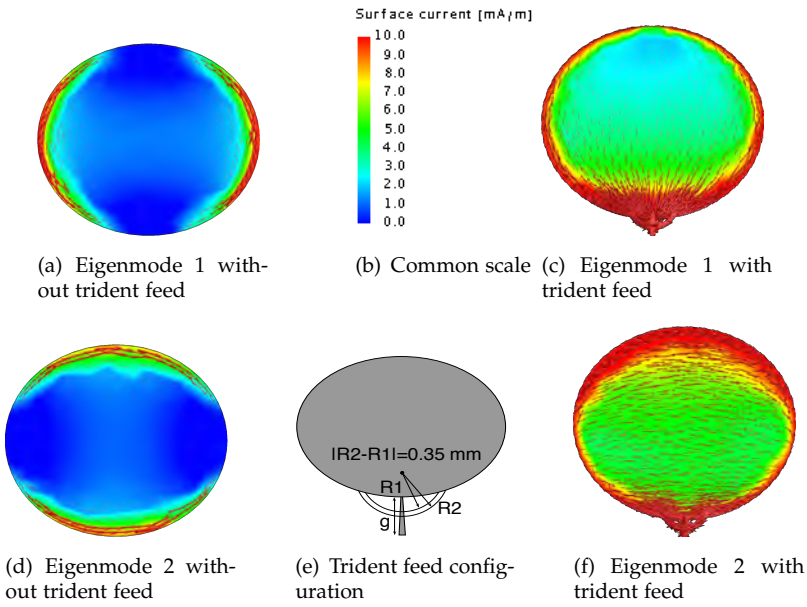

(a) Eigenmode 1 without trident feed

(b) Common scale

(c) Eigenmode 1 with trident feed

(d) Eigenmode 2 without trident feed

(e) Trident feed configuration

(f) Eigenmode 2 with trident feed

FIGURE 6.4: **Trident feed configuration and the surface current densities of the first two eigencurrents at 1 GHz. The first two current modes present higher current peripheral at their maxima (the circumference of the disk) when the trident feed is used, thus modes become better radiators at the corresponding frequency.**

The maxima of the first two current modes (horizontal and vertical modes) are concentrated at the peripheral of the disk. Then, the current path of these modes are longer when they pass through the semi-ring. This results in a matching at lower

© 2015 Tous droits réservés. doc.univ-lille1.fr

Thèse de Mhamad Hassanein Rabah, Lille 1, 2015

frequencies especially when the antenna becomes electrically small; Thus enhancing the radiation phenomena of these modes.

The radii and width of the ring also impact the impedance matching. The distance g between the tapered line and the monopole has a critical role in the matching. Numerical optimization of these parameters needs to be done in parallel because they are strongly related. The optimal values of g is 3.28 mm and of the ring width $|R_2 - R_1|$ is 0.35 mm.

The triangular shaped ground plane was selected to reduce the coupling with the radiator.

This feeding system results in a good matching from 0.65 GHz to 12 GHz as shown in Fig. 6.5. Simulated[1] VSWR ≤ 2 extends from 650 MHz to 12 GHz.

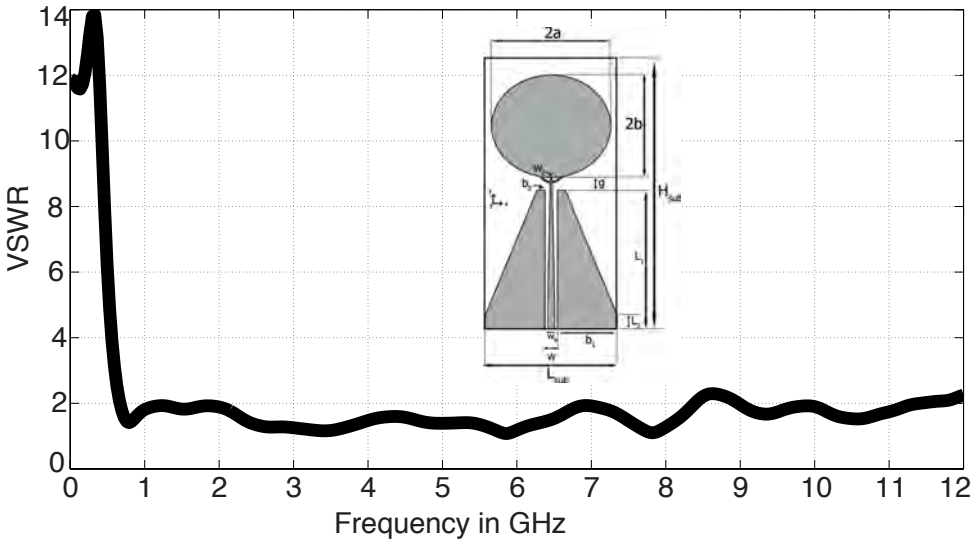

FIGURE 6.5: **Simulated VSWR proposed EWB antenna before modifying the radiator.**

Despite the good matching, the radiation pattern is not stable over all the frequency band. Figure 6.6 shows the power pattern in the YZ plane of the described antenna (without slot).

Since the antenna is dedicated to a spectrum sensing application, a stable and omnidirectional power pattern is required. This instability does not occur for the power pattern in the XZ plane (not shown).

Investigated surface currents at these higher frequencies have shown that the distortion in the YZ plane occurs at 5.6 GHz and 7.5 GHz. This is due to the higher modes

[1]Simulations have been done using CST Microwave Studio [138] and FEKO [8].

© 2015 Tous droits réservés. doc.univ-lille1.fr

Thèse de Mhamad Hassanein Rabah, Lille 1, 2015

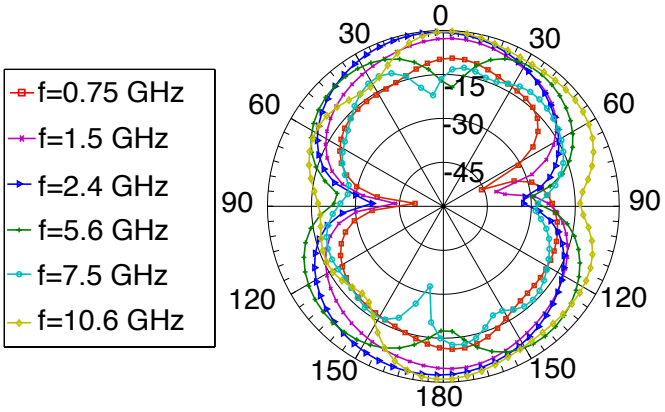

FIGURE 6.6: **Power pattern (YZ plane) for the described antenna without the V-shaped slot at different frequencies within the matched frequency band.**

of the disk, that become active at the mentioned frequencies (small eigenvalues). The TCM is used here to investigate these higher order modes and control their radiation behaviour, and forces them to keep a monopole like radiation pattern.

6.3 Power pattern stability enhancement of a spectrum sensing antenna using TCM

The disk is small for miniaturization purposes. This causes the excitation of higher order modes on the radiator. It is found that the dip at 7.5 GHz is caused by the radiation of the sixth mode, as shown in Fig. 6.7(b), which is resonant at this frequency (corresponding eigenvalue $\lambda_6 = 0.125$).

Since this active mode presents two nulls in the surface current, a dip in the main radiation pattern axis is produced. The solution is to trap the current between these two nulls at the corresponding frequency, and to create a maximum in the center of the disk. This trap is achieved with a V-shaped slot resonating at 7.5 GHz, as shown in Figures 6.7(a) and 6.8. The most important feature of this type of slots is that it does not affect the radiation behaviour of the first five modes. The total radiation pattern in the YZ plane at 7.5 GHz and at the other frequencies are shown in Fig. 6.9.

Introducing the $\lambda/2$ V-shaped slot in the middle of the radiator results in an obvious impact on the power patterns. When comparing Figures 6.9 and 6.6 one can see how the dips have been remarkably reduced. Another advantage of using the V-shape slot is that it doesn't affect the matching of the antenna. Fig. 6.10 shows a comparison for the VSWR with and without slot.

© 2015 Tous droits réservés. doc.univ-lille1.fr

Thèse de Mhamad Hassanein Rabah, Lille 1, 2015

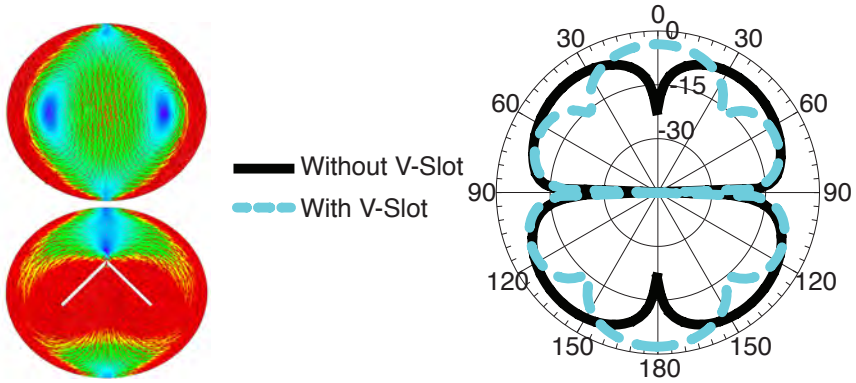

(a) Current density (b) Radiation pattern in the YZ plane

FIGURE 6.7: **V-shaped slot impact on the 6th current mode at 7.5 GHz: the dip in the main radiation axis is due to the low surface current density in the center of the disk. The V-shaped slot creates a new current maximum in the center instead of the two nulls. This results in a maximum in the main radiation axis.**

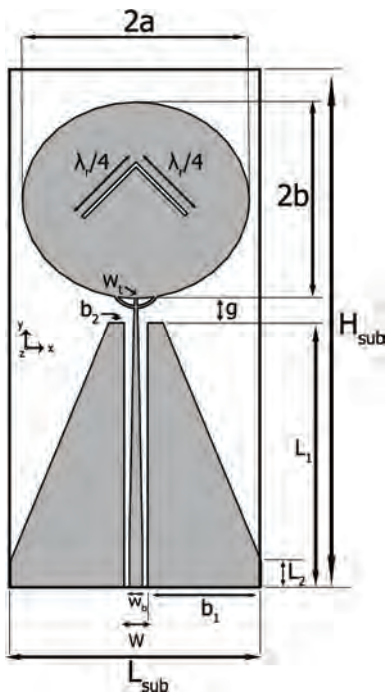

FIGURE 6.8: **Miniaturized antenna configuration: optimized feeding system based on a CPW transmission line with a triangular ground plane, and an optimized slotted radiator for power pattern stabilisation.**

Indeed, the matching of the antenna is quasi stable after modifying the shape of the radiator.

© 2015 Tous droits réservés. doc.univ-lille1.fr

Thèse de Mhamad Hassanein Rabah, Lille 1, 2015

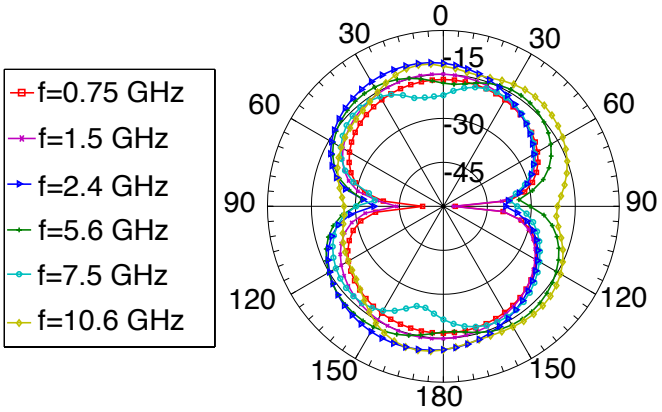

FIGURE 6.9: **Power pattern (YZ plane) for the described antenna with the V-shaped slot at different frequencies within the matched frequency band.**

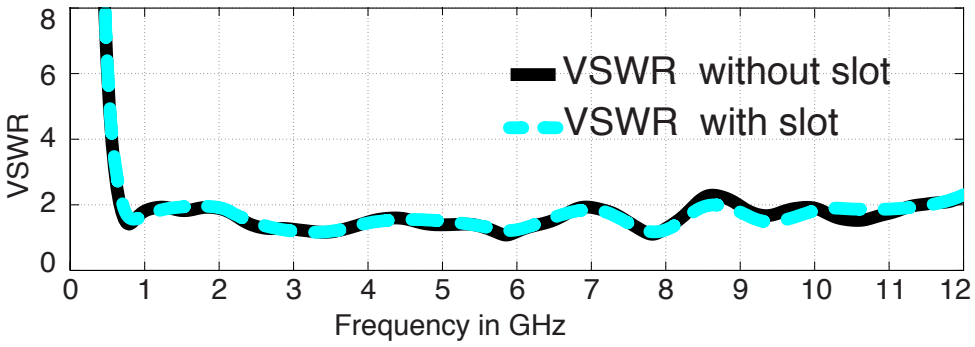

FIGURE 6.10: **Simulated VSWR comparison for the proposed EWB antenna with and without V-Slot.**

6.3.1 Experimental Results and Discussion: Part 1

To validate the numerical results, a prototype of the proposed antenna is printed on an 0.787 mm thick Teflon substrate ($\epsilon = 3.2, \tan(\delta) = 0.0002$), as shown in the inset of Fig. 6.11.

Fig. 6.11 shows a comparison between the simulated and measured S_{11} parameters of the fabricated antenna (with V-shaped slot). The return loss value is less than -10 dB from 0.67 GHz to 12 GHz. This confirms the numerical results shown before and proves that the slot does not affect the matching of the antenna. Therefore, the total radiation pattern in the YZ plane is very stable over the whole frequency range, as shown in Fig. 6.9. This is further confirmed by measured radiation patterns in Fig. 6.12 for both YZ and XZ planes. A very good stability is observed over the matched frequency bands. These measurement results are in agreement with simulated radiation patterns shown in Fig. 6.9 (YZ plane). Small dips in the measured patterns are due to imperfections in the measurement setup in the anechoic chamber, as shown in

© 2015 Tous droits réservés. doc.univ-lille1.fr

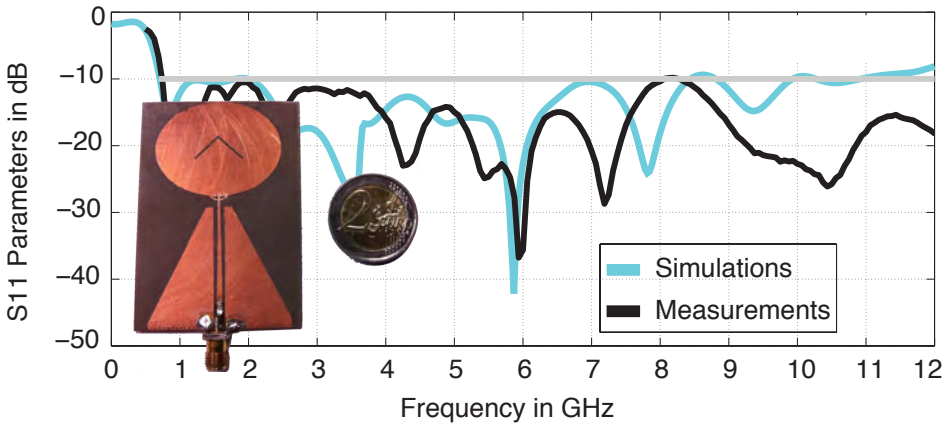

FIGURE 6.11: **Comparison between simulated and measured S_{11} parameters for the proposed antenna printed on an 0.787 mm thick Teflon substrate ($\epsilon = 3.2, tan(\delta) = 0.0002$).**

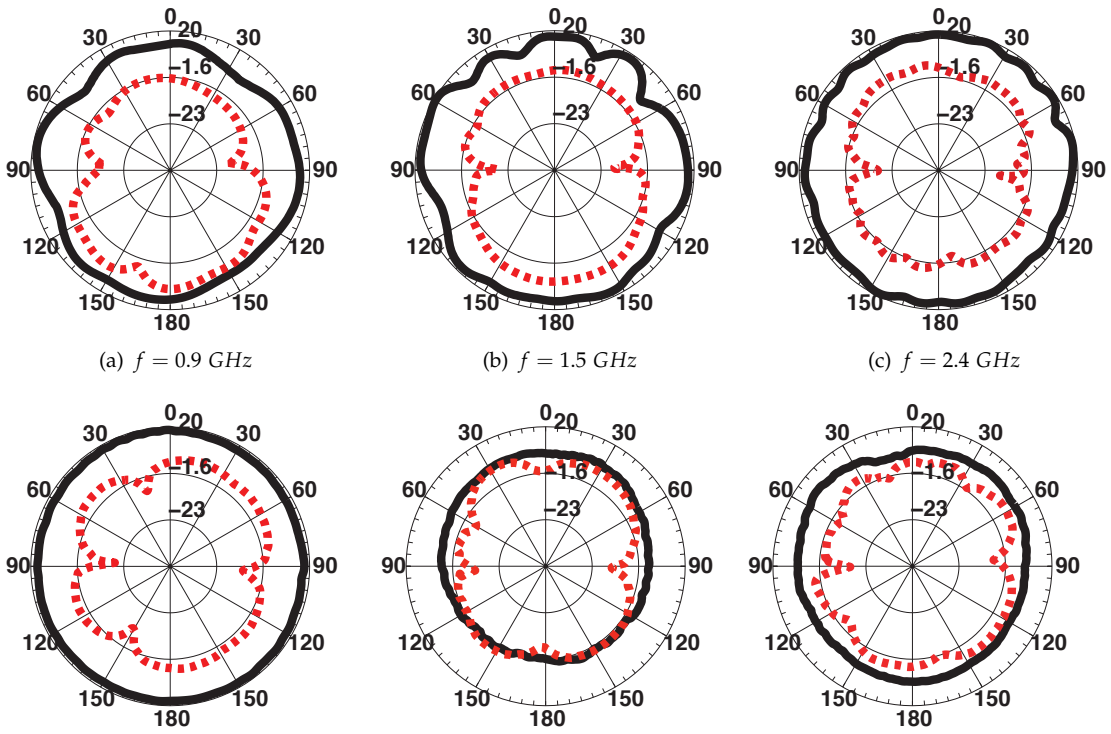

(a) $f = 0.9\ GHz$ (b) $f = 1.5\ GHz$ (c) $f = 2.4\ GHz$

(d) $f = 5.6\ GHz$ (e) $f = 7.8\ GHz$ (f) $f = 10.6\ GHz$

FIGURE 6.12: **Measured radiation pattern of the fabricated antenna in the XZ plane (—), and YZ plane (−−), over the matched frequency band.**

Fig. 6.13. Power patterns at frequencies lower than 0.9 GHz could not be measured because of the chamber dimensions [12].

© 2015 Tous droits réservés.

Thèse de Mhamad Hassanein Rabah, Lille 1, 2015

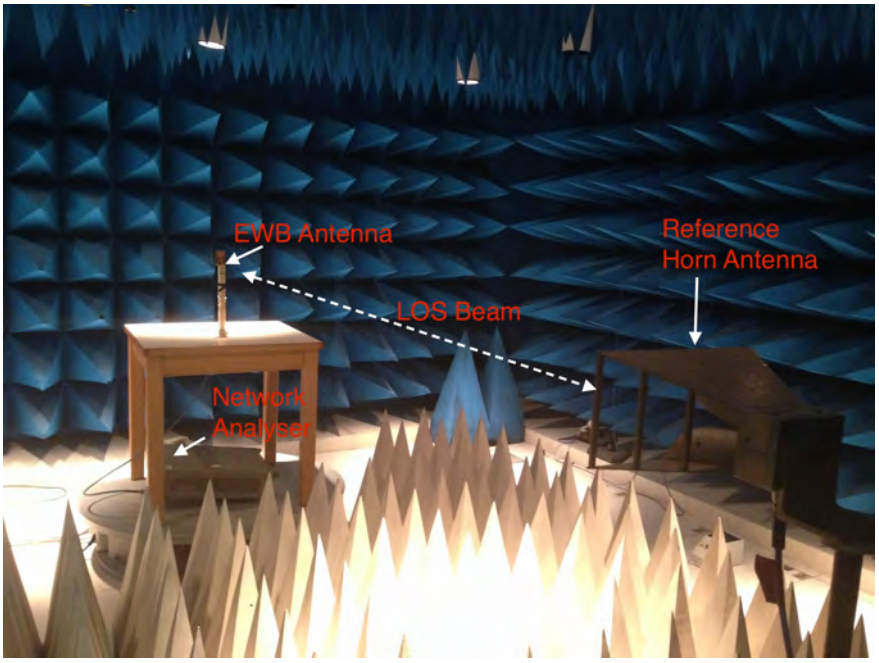

FIGURE 6.13: **Measurements setup of the power pattern of the proposed EWB antenna in the anechoic chamber [12].**

6.4 Efficiency Enhancement With Metamaterials: EWB-MTM Antenna

The efficiency of the antenna proposed in Fig. 6.8 is presented in Table 6.2. It oscillates between 25% and 87%. These values of the efficiency in Table 6.2 are expected since

TABLE 6.2: **Efficiency of the proposed miniature EWB antenna.**

Frequency (GHz)	0.9	1.5	2.4	3.1	5.6	10.5
Efficiency (%)	25	30	57	85	81	87

they increase with the frequency. The bigger the electrical size of the antenna, the higher the efficiency.

The present EWB antenna suffers from its low electrical size (0.07λ at 650 MHz). Thus, to improve the efficiency in this band, we refer to the methodology proposed in Chapter 5. We use the modal analysis applied to metamaterial inspired antennas, in order to find an adequate MTM inclusion to be associated to the antenna. This inclusion will be from the LUT of metamaterial inclusions (Section 5.2.3).

First, we must answer the question illustrated in Fig. 6.14. Which inclusion should we use ?

© 2015 Tous droits réservés. doc.univ-lille1.fr

Thèse de Mhamad Hassanein Rabah, Lille 1, 2015

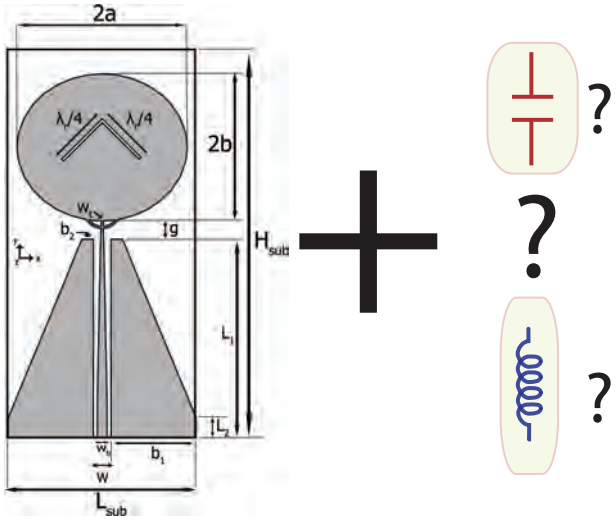

FIGURE 6.14: **Schematic of the EWB antenna illustrating the question of searching the right metamaterial inclusion at a specific frequency (in our case 600 MHz), wether it should be inductive or capacitive ?**

Should we add a capacitive metamaterial inclusion or an inductive one ? This question was simple to answer in the case of classical antenna (monopole, loop). Neverhteless, it is not evident to find the answer when we deal with complex structures or arbitrary shaped antenna, such as the proposed EWB antenna.

6.4.1 CMA of the EWB Antenna

First, a threshold of 500 is used in Fig. 6.15 to identify the modes to be considered within the electrically small regime [$0 - 1.5$ GHz ($0 < ka < 1$)].

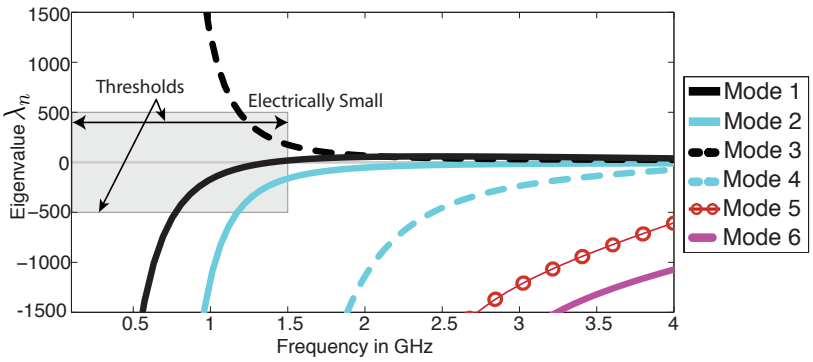

FIGURE 6.15: **First six eigenvalues of the considered EWB antenna over the band 0−4 GHz. A threshold of 500 is applied on the eigenvalues in order to limit the number of the considered modes within the electrically small regime.**

The first three modes are selected by the selection box shown in Fig. 6.15. The first mode resonates around 1 GHz, while the others resonate outside the selection

© 2015 Tous droits réservés. doc.univ-lille1.fr

Thèse de Mhamad Hassanein Rabah, Lille 1, 2015

box. Therefore, in the electrically small regime, modes 1 and 2 store electric energy while mode 3 stores magnetic energy. The type of dominant energy stored in the near field of the antenna is determined quantitatively by calculating the sum of the modal powers of the first three modes using Eq. (5.2), as presented in Section 5.2.

This power is calculated at the target frequency. It is chosen to be 600 MHz ($ka \approx 0.5$) for two reasons:

1. Decreasing the least operating frequency, hence spreading out the bandwidth.
2. Increasing the total efficiency at the lowest matched frequency (600 MHz).

The total power $P_{\text{reac, tot}}$ from the first three modes at 600 MHz with a voltage source of 1 Volt is calculated as follows:

$$P_{\text{reac, tot}} = P_{\text{reac},1} + P_{\text{reac},2} + P_{\text{reac},3} = |\omega_{c,1}|^2\lambda_1 + |\omega_{c,2}|^2\lambda_2 + |\omega_{c,3}|^2\lambda_3 = -30 \text{ mW}$$

The negative sign means that the dominant energy in the near field of the antenna at 600 MHz is electric. In other words, the antenna needs +30 mW of magnetic power to resonate. Thus, the next step consists of searching for an inclusions which stores magnetic energy in its near field at 600 MHz.

6.4.2 Searching For the Right Inclusion

The adequate MTM inclusion is selected from the LUT of metamaterial inclusions as presented in Section 5.2. We fed this table with many inclusions (commonly used in periodic metamaterial mediums), including SRR, BC-SRR, EC-SRR, CLL, Meander line, Jerusalem Cross, S-shape, Double-can, V-shape, etc.

Meanwhile, there exists many inclusions providing a magnetic behaviour at 600 MHz, while adjusting the geometrical dimensions. However, regarding the configuration of the EWB antenna in Fig 6.8, the elected inclusion is a modified version of the split ring resonator studied in Chapter 3. It consists of an elliptical loop as shown in Fig. 6.16.

The elliptical shape has been chosen for two reasons. First to fit the perimeter of the elliptical disk while keeping the initial size of the antenna. Second, to have a longer current path flowing on the loop, thus, decreasing its resonance frequency as much as possible. For the same reason we use a substrate with higher permittivity in order to bring the first resonance of the loop at 600 MHz. The loop is printed over

© 2015 Tous droits réservés. doc.univ-lille1.fr

Thèse de Mhamad Hassanein Rabah, Lille 1, 2015

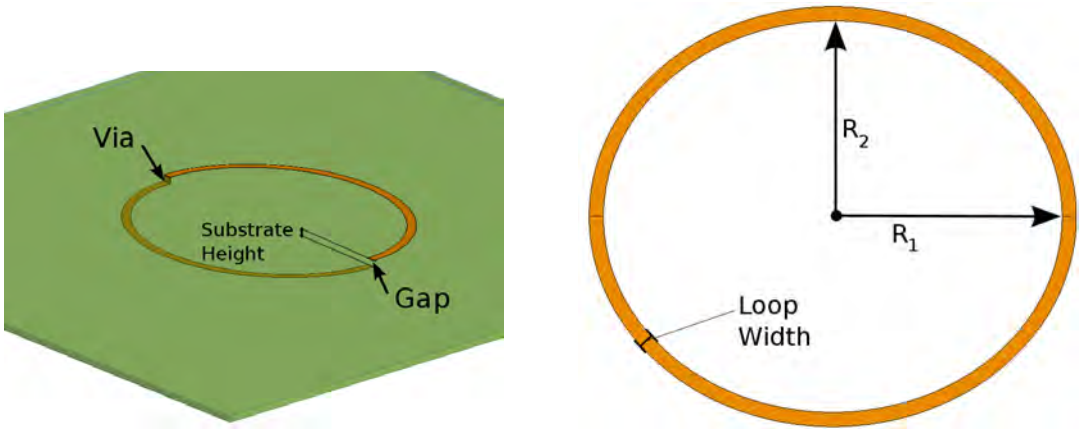

(a) 3D View (b) 2D View

FIGURE 6.16: **Schematic of a split ring composed of 2 elliptical semi-loops printed over both faces of a dielectric substrate, and connected via the substrate. The substrate has a thickness of 1.5 mm and relative permittivity of ϵ_r=10.7. The dimensions in mm are: R_1=17.595, R_2=16.15 and the loop width equals to 1.105 mm.**

both substrate faces. It is divided onto two semi-loops connected via the substrate. The gap between both loop ends equals the substrate height. These dimensions are tuned in order to make the loop resonate at the desired frequency.

The CMA of the elliptical loop shows that it presents the same magnetic mode J_0 as the BC-SRR[2] studied in Chapter 3. To investigate this feature, we calculate the the first four characteristic modes. Eigenvalues are shown in Fig. 6.17. The first mode

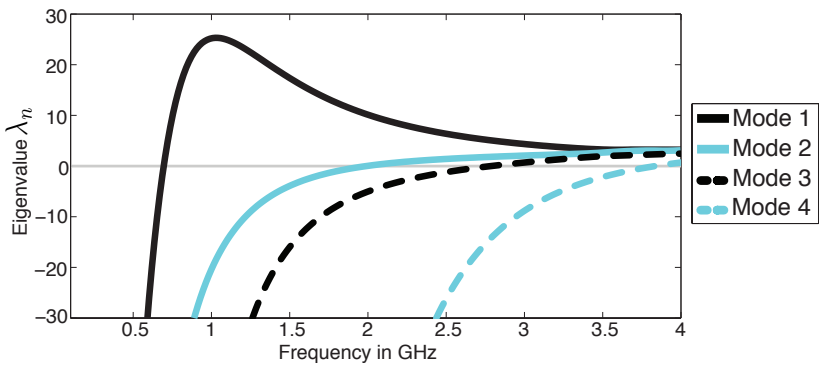

FIGURE 6.17: **First four eigenvalues of an elliptical loop printed over both substrate faces.**

resonates at 600 MHz and stores magnetic energy after its resonance. This mode is identical to the first mode in a BC-SRR in Chapter 3, where the magnetic polarizability is expressed in terms of the first eigenvalue (Fig. 3.4). Higher order modes (2, 3 and 4) present the typical behaviour of an electrical mode, as found in Chapter 3 (Fig. 3.3). However, they do not present the same current profile. These modes become active at

[2]In this chapter the first mode in the loop is indexed J_1.

© 2015 Tous droits réservés. doc.univ-lille1.fr

Thèse de Mhamad Hassanein Rabah, Lille 1, 2015

higher frequencies (for example mode 2 resonates at 1.8 GHz) and do not have a high impact on the overall loop response at 600 MHz.

Next, we associate the elliptical loop (Fig. 6.16) to the EWB antenna by aligning the centers of both the loop and the disk. The new design is then called EWB-MTM inspired antenna and shown in Fig. 6.18.

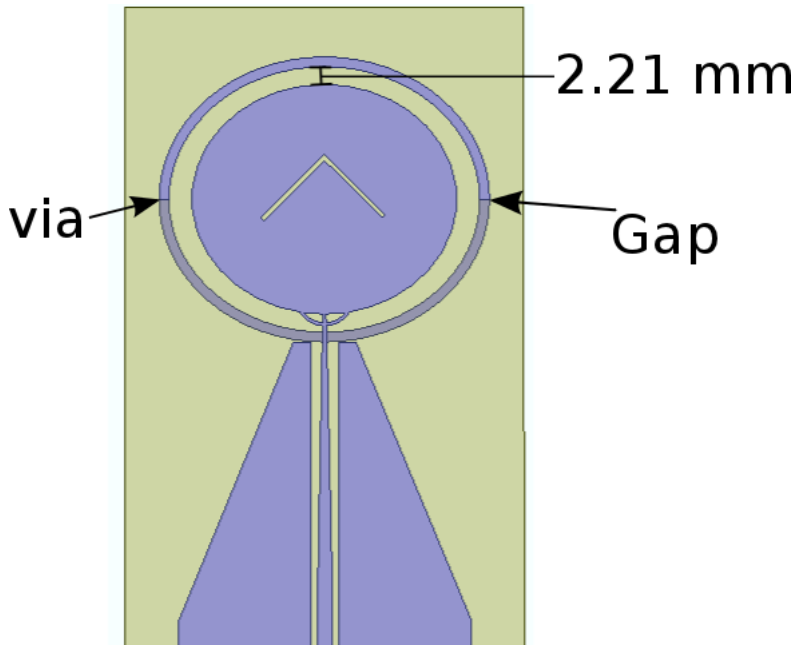

FIGURE 6.18: **New configuration of the EWB-MTM inspired antenna.**

The distance between the loop and the disk control the coupling between both structures. In the present design, this distance has been chosen to be the double of the loop gap, hence it measures 2.210 mm.

Fig. 6.19 shows the first four eigenvalues of the new EWB-MTM inspired antenna in the frequency range 0.2−1 GHz.

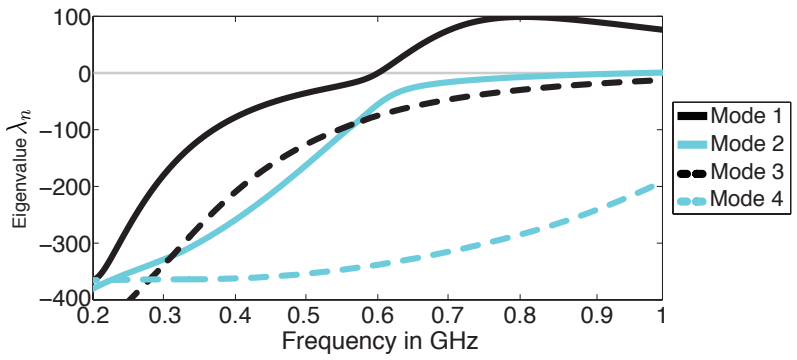

FIGURE 6.19: **First four eigenvalues of the considered EWB antenna associated with an elliptical loop in Fig. 6.16.**

© 2015 Tous droits réservés.

doc.univ-lille1.fr

Thèse de Mhamad Hassanein Rabah, Lille 1, 2015

The first eigenvalue crosses zero at 600 MHz compared to 1 GHz for the EWB antenna alone. This is because the entire system (EWB+Loop) follows the behaviour of the first mode of the loop at the targeted frequency (600 MHz).

The resulting curve of the first eigenvalue seems to be a combination of the first eigenvalues of the EWB antenna and the loop. This phenomenon disappears progressively when getting far from the first resonance. The loop behaviour is mainly dominant at 600 MHz.

Mode 2 is also influenced by the loop since it is an electrical mode and its resonance frequency is shifted down from 1.8 GHz to 1 GHz. The magnetic mode of the EWB antenna in Fig. 6.2 has disappeared from the studied frequency band. This is because the presence of the loop has increased its eigenvalue (not shown within the selected window $-400 < \lambda < 100$). Higher order modes are less impacted by the loop and maintain the same phenomenon at higher frequencies.

To visualise the impact of the loop on the first current mode, Figures 6.20 (a) and 6.20 (c) show the first eigencurrent profile without and with the loop, respectively. The

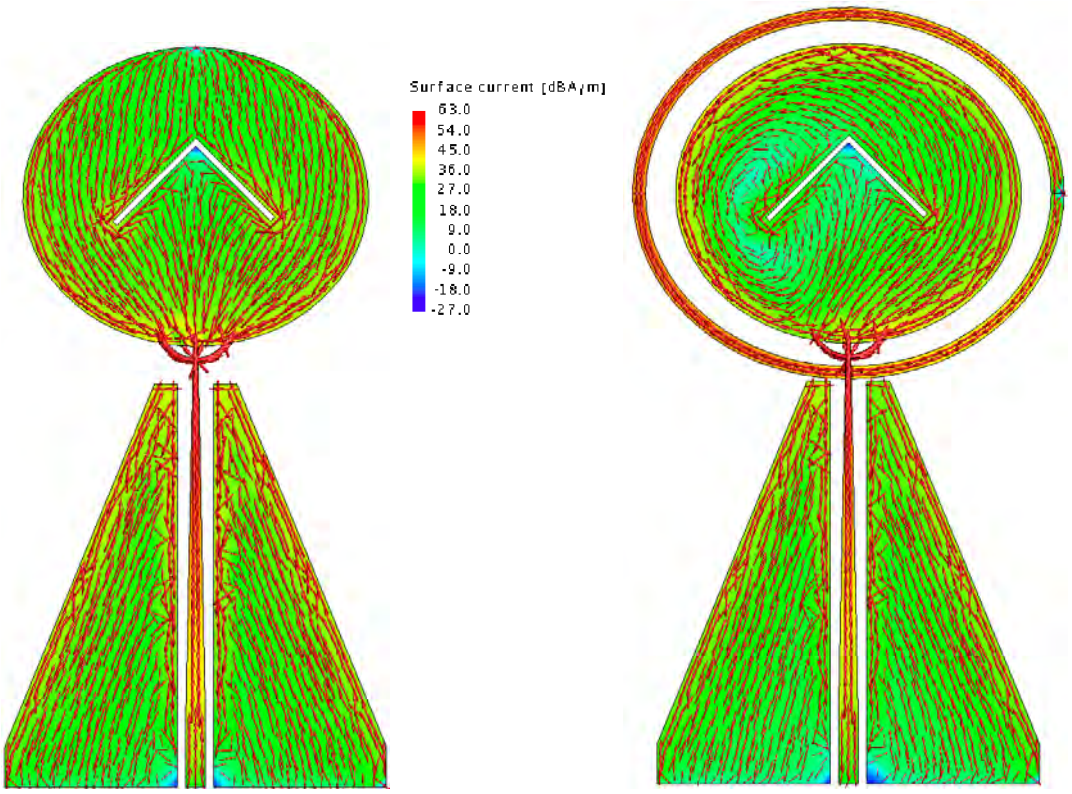

(a) Isolated EWB (b) Common scale (c) EWB + Elliptical Loop

FIGURE 6.20: **Impact of the loop on the first eigencurrent (J_1) profile at 600 MHz. The presence of the the loop makes the first eigencurrent emulating the same path of the current flowing on the loop.**

© 2015 Tous droits réservés. doc.univ-lille1.fr

Thèse de Mhamad Hassanein Rabah, Lille 1, 2015

impact of the elliptical loop on the first eigencurrent can be seen clearly in Fig. 6.20. As predicted, modifying the geometry modifies the profiles of the modes. Instead of flowing between the vertices of the elliptical disk, the current follows a circular path as it is emulating the same path of current flowing on the loop. This is due to the magnetic nature of the first mode of the loop. Furthermore, the current configuration over the feeding system is unchanged since there is no interaction between it and the loop.

6.4.3 Experimental Results and Discussion: Part 2

As a proof of concept, a prototype of the new modified EWB-MTM inspired antenna has been fabricated[3]. The picture of the fabricated prototype is shown in Fig. 6.21. Simulations and measurements of the reflexion coefficient are shown in Fig. 6.22.

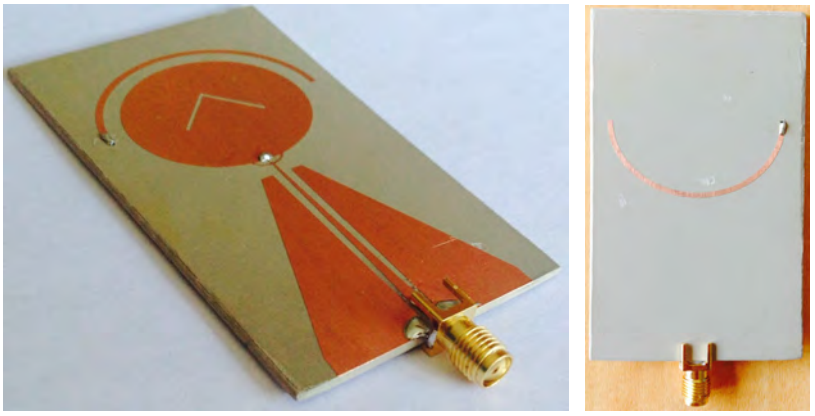

(a) Top (b) Bottom

FIGURE 6.21: **Prototype of the modified EWB-MTM inspired antenna printed over Arlon10 substrate with relative permittivity $\epsilon_r = 10.7$, $tan(\delta) = 0.0023$ and height of 1.55 mm.**

Introducing the elliptical loop causes a clear resonance in the reflexion coefficient of the EWB antenna system (cyan curve) at 600 MHz. This frequency is exactly the same as that of the first mode resonance of the isolated elliptical loop. This agrees with the expectation of the workflow proposed in Section 5.3.1.

[3]The substrate of the initial EWB antenna has been modified: the relative permittivity ϵ_r has been increased from 3.2 to 10.7. The aim of this modification is to decrease the electrical size of the loop. Also to enhance the coupling between the inclusion and the antenna. Albeit, the substrate height is extended from 0.787 mm to 1.55 mm in order to compensate the variation of ϵ_r in order to keep the same matching. This guarantees that the antenna keeps the same bandwidth as achieved over the low permittivity substrate.

© 2015 Tous droits réservés. doc.univ-lille1.fr

Thèse de Mhamad Hassanein Rabah, Lille 1, 2015

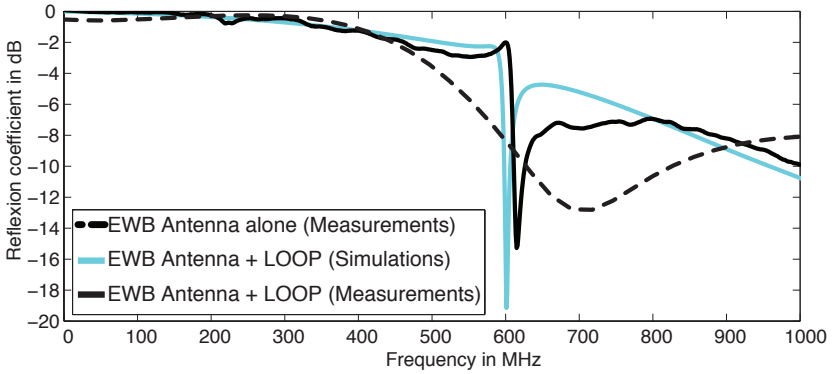

FIGURE 6.22: **Comparison between simulation and measurement of the reflexion coefficient of the EWB antenna with and without the metamaterial loop inclusion.**

When comparing the dashed black curve (EWB alone) and the cyan curve (EWB+LOOP) in Fig. 6.22, one can see a significant enhancement in terms of lowest matched frequency at -10 dB. In fact the lowest matched frequency is shifted down from 670 MHz to 600 MHz. The mismatch between 700 MHz and 900 MHz can be due to the anti-resonance phenomenon of the inclusion.

Fig. 6.23 shows a comparison between the simulated and measured S_{11} of the EWB-MTM inspired antenna over a lager bandwidth ($0 - 18$ GHz). The EWB-MTM

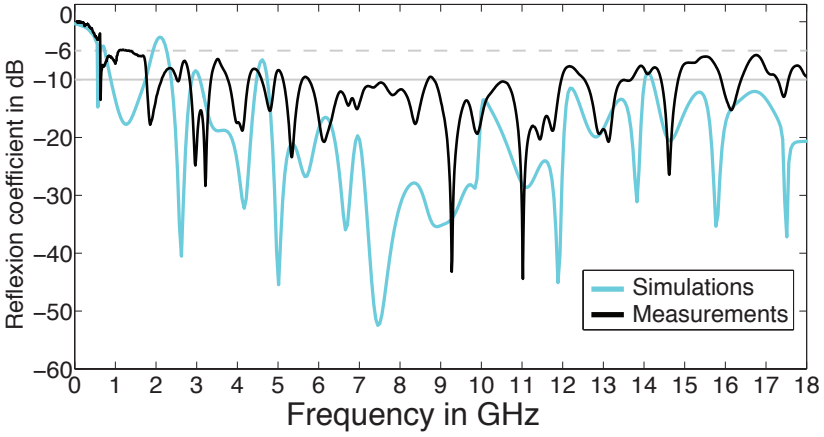

FIGURE 6.23: **Comparison between simulation and measurement of the reflexion coefficient of the EWB-MTM inspired antenna over the band 0–18 GHz**

inspired antenna presents an extremely wide bandwidth with acceptable matching. In fact, the presence of the loop has altered the reflexion coefficient (higher than -10 dB) at the following upper frequencies: 1.8 GHz, 3.2 GHz, 12 GHz and 15 GHz. This because of the higher-order resonances of the loop (i.e. 1.8 GHz for mode 2) and the coupling between the loop and the disk at higher frequencies. However, if only a $S_{11} \leq -6$ dB reflexion coefficient is required (typical for spectrum sensing), the antenna proves to cover a bandwidth extending from $0.6 - 18$ GHz.

© 2015 Tous droits réservés. doc.univ-lille1.fr

Thèse de Mhamad Hassanein Rabah, Lille 1, 2015

Fig 6.23 shows a reasonable agreement between the simulation and measurements of the reflexion coefficient. The slight frequency shifting can be due to the non consideration of the coaxial cable in simulations, and cable imperfections. The measurements setup is shown in Fig. 6.24

FIGURE 6.24: **Measurements setup of the reflexion coefficient of the EWB-MTM Inspired antenna.**

Moreover, with a -6 dB level, Fig. 6.22 shows that the antenna without the loop will presents a lower matched frequency. However, this does not mean that the EWB alone presents better performances. And this can also be adjusted by re-optimising the feeding system dimensions (tapered line and trident feed) in presence of the loop. To show the advantage of using the loop we investigate the radiation characteristics of both antennas at 600 MHz. We compare the EWB-MTM inspired antenna with an EWB antenna over the same type of substrate[4]. Fig. 6.25 shows a polar representation of the realized gain in the XZ plane with and without the metamaterial inclusion.

The metamaterial inclusion enhances significantly the realized gain of the antenna at 600 MHz. This enhancement is around 10 dB averaged over all the angles in the XZ plane. The maximum realized gain of the EWB-MTM inspired antenna is about 0.582 (-3.16 dBi) at 600 MHz while the calculated directivity is around 0.85 (-0.7 dB). This means that the antenna presents $\approx$ 56.4% of radiation efficiency which is excellent regarding its total dimensions.

[4]The substrate of the initial EWB antenna has been modified: the relative permittivity ϵ_r has been increased from 3.2 to 10.7. The aim of this modification is to decrease the electrical size of the loop.

© 2015 Tous droits réservés. doc.univ-lille1.fr

Thèse de Mhamad Hassanein Rabah, Lille 1, 2015

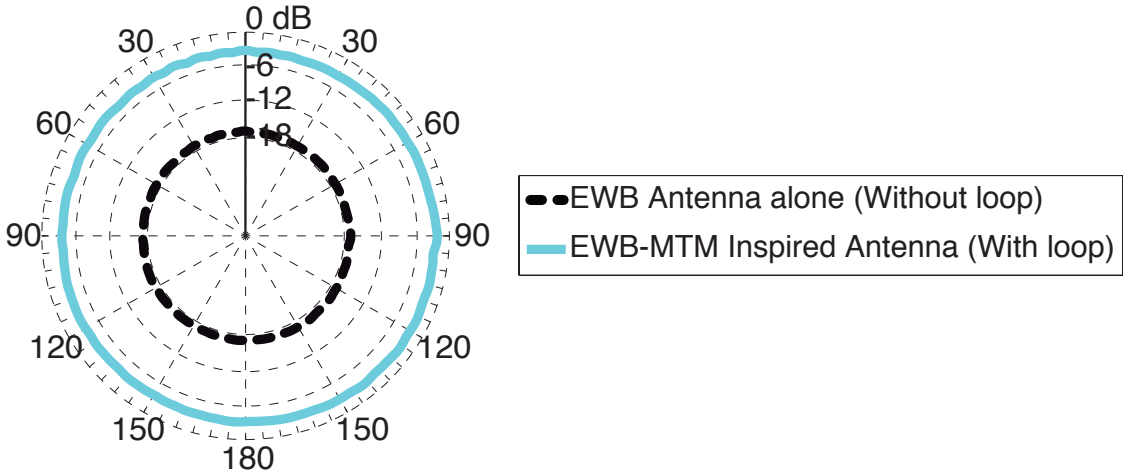

FIGURE 6.25: **Comparison of the realized gain of the EWB antenna in the XZ plane, with and without the metamaterial inclusion at 600 MHz. The average difference over all the angles is about 10 dB.**

Table 6.3 presents a comparison between different radiation performances achieved by the EWB-MTM inspired antenna.

TABLE 6.3: **Comparison of the radiation performances of the EWB antenna alone and the MTM Inspired EWB antenna.**

Design	Peak Directivity		Peak Realized Gain		Radiation Efficiency
	Linear	dB scale	Linear	dB scale	
EWB Antenna alone	0.14	−8.53	0.021	−16.7	**15** %
EWB-MTM Inspired Antenna	0.85	−0.7	0.482	−3.16	**56.4** %

Table 6.3 shows two important improvements in terms of directivity and realized gain [55]. The directivity is increased of 0.71 and the realized gain of 0.461. This means that an enhancement of the matching together with radiation efficiency has been achieved. This results into an increase of $\approx$ 45% of the antenna total efficiency.

Furthermore, when comparing the present antenna to the designs shown in Chapter 2 (Table 2.2), one can deduce that the present antenna exhibits a higher bandwidth/size ratio among all the previously published ones.

Moreover, we believe that the present analysis can be applied for other types of monopole antennas since CMA can be performed regardless of the geometry. Therefore, an antenna shape optimisation methodology based on CMA can be used. Fig. 6.26 shows a diagram giving an overview of the methodology used in this chapter for enhancing the bandwidth, power pattern stability and efficiency at low frequencies. This diagram can be applied to other antennas with performances suffering from their electrical size.

© 2015 Tous droits réservés. doc.univ-lille1.fr

Thèse de Mhamad Hassanein Rabah, Lille 1, 2015

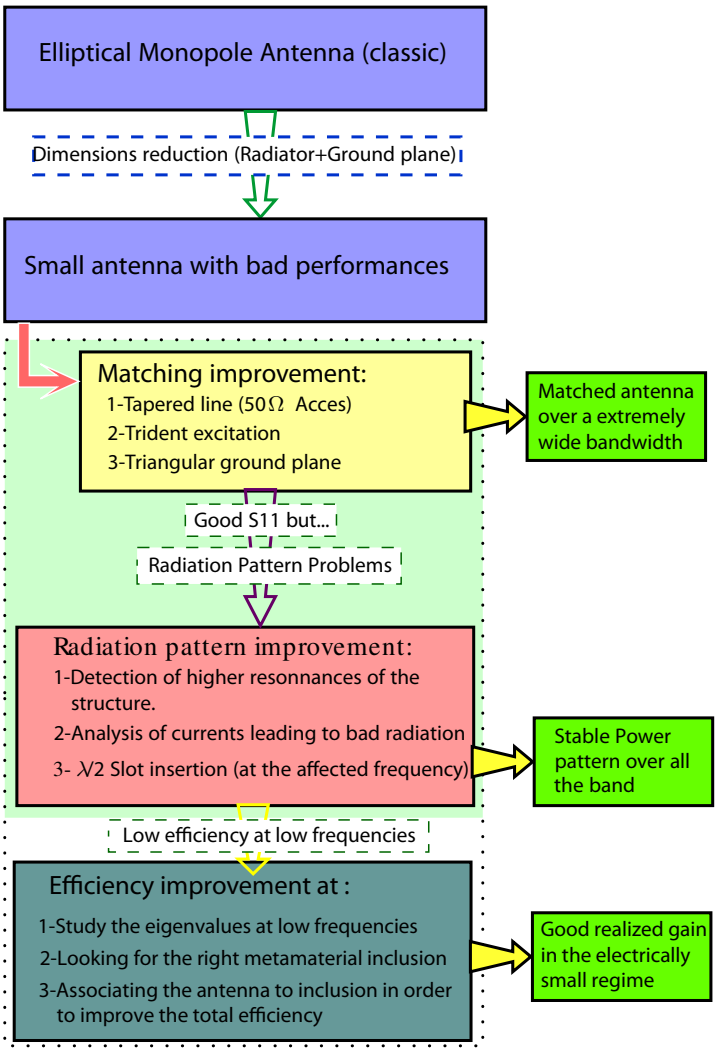

FIGURE 6.26: **Design methodology for the enhancement of the bandwidth, radiation pattern and efficiency of a planar monopole antenna.**

6.5 Conclusion

In this chapter, the design, simulation, optimization and measurements of an EWB-MTM inspired antenna have been presented. A technique to improve the performances after miniaturization has been proposed and validated. The theory of characteristic modes was used to analyze and optimize the excitation and multimodal radiation of the monopole antenna. The total efficiency of the antenna has been improved by using the methodology proposed in Chapter 5; for the analysis of metamaterial-inspired antennas. This methodology uses a database of inclusions built using CMA. An inclusion from this database is then associated to the EWB antenna in order to conjugate its reactive energy in the near field when it is electrically small.

The performances of the EWB-MTM inspired antenna described in this chapter

© 2015 Tous droits réservés. doc.univ-lille1.fr

Thèse de Mhamad Hassanein Rabah, Lille 1, 2015

are compared to a reference antenna proposed in [39]. The smallest operating frequency is 600 MHz (matched at -10 dB), for the antenna presented, compared to 1.07 GHz for the reference antenna. The measured $S_{11} \leq -6$ dB extends over a bandwidth from $0.61 - 18$ GHz. Moreover, the total dimensions of the proposed antenna are $73 \times 46\ mm^2$ whereas the reference antenna has total dimensions of $124 \times 110\ mm^2$. The proposed antenna surface is four times smaller than the reference one. The achieved antenna efficiency at 600 MHz equals 56.4%, which is considered excellent given its small electrical size ($0.146 \times 0.09\lambda_l$). Moreover, the antenna radiation patterns remain stable and omnidirectional in both planes over the whole frequency band. This confirms that this antenna is a good candidate for spectrum sensing applications in the context of cognitive radio systems.

© 2015 Tous droits réservés. doc.univ-lille1.fr

Chapter 7

Conclusions and Future Work

7.1 Main Contributions of the Thesis

This thesis has dealt with the use of metamaterials and the theory of characteristic modes in the design and analysis of antennas for future telecommunication systems. The goal was to overcome some physical limitations governing these antennas, namely when they are electrically small. The main contributions of this work are listed as follows:

- **Defining main challenges in antenna design for CR systems and the associated physical limitations.** A summary on the recent advances in the literature on this subject is reported.
- **Defining new metrics based on the theory of characteristic modes to describe a metamaterial based medium behaviour, such as an artificial magnetic medium.** The theory of characteristic modes has been proposed as a tool and shown to be suitable for the design and analysis of antennas when associated to metamaterials. As an example, new metrics have been presented and validated for equivalent magnetic mediums, namely between split-ring resonators and reactive impedance substrate.
- **A new approach for evaluating the quality factor of an arbitrary shaped antenna surrounded by metamaterials without any prior knowledge on the excitation.** A new method for the evaluation the Q factor of arbitrary shaped antennas is presented. This method consists of calculating the antenna quality factor using only the eigenvalues of the structure. It is shown to be more accurate when the antenna is electrically small. A modal study of a small patch antenna

© 2015 Tous droits réservés. doc.univ-lille1.fr

Thèse de Mhamad Hassanein Rabah, Lille 1, 2015

over conventional and metamaterial substrates has shown good agreement with other numerical and analytical approaches. Furthermore, an arbitrary shaped antenna shaped as the IFSTTAR institute name has been designed to operate in the electrically small regime. The quality factor of this antenna has been calculated using the proposed approach and proven to approach the quality factor calculated using the input impedance expression of Yaghjian-Best formula.

- **New systematic technique to enhance an antenna efficiency at low frequencies, via metamaterial inclusions.** A new methodology for using metamaterial inclusion with antennas in order to improve the efficiency is presented. This provides a smart technique to search the right metamaterial inclusion and putting it in the vicinity of an arbitrary-shaped antenna in order to conjugate the reactive energy in the antenna near field.

- **Novel antenna design for spectrum sensing applications.** A proof of concept consisting into an extremely wideband antenna associated to a metamaterial inclusion has been presented. The presented antenna is a very good candidate for CR underlay systems. Moreover, the agreement between simulations and measurements validates the proposed methodology.

7.2 Some Limitations

The work presented in this thesis is mainly based on the modal decomposition of the surface current on an antenna through the theory of characteristic modes. This theory has been used in different fields of antenna design, including the synthesis and evaluation of the performances of antennas. Nevertheless, some features of the proposed work are limited by the range of applications or computational constraints. These limitations can be listed as follows:

- **Limitation on the Q factor calculation using the modal concept to the electrically small regime.** This limitation is due to the fact that the total defined quality factor is based on a superposition of eigenvalues instead of modal energies. However, the proposed method remains accurate for $ka > 1$ when the number of main contributor modes still close to 1. Furthermore, the proposed method reformulation remains simpler and the calculation is faster.

- **Modes orthogonality in 3D structures.** Theoretically characteristic modes are purely orthogonal mutually. Due to numerical limitation -and losses- characteristic modes can be non orthogonal within a frequency range. In fact, unlike

© 2015 Tous droits réservés. doc.univ-lille1.fr

Thèse de Mhamad Hassanein Rabah, Lille 1, 2015

the 2D antenna, in the 3D antenna we usually use two different types of mesh. The surface RWG triangles and another type which usually segments for wire modelling. This results in a non-symmetrical impedance matrix [Z] and modal coupling. However, to increase the accuracy of calculations, the same type of meshes is recommended.

- **Mode tracking problem in very complex structures**. One of the drawbacks of using characteristic modes as entire domain-basis functions in the MoM formulation is that characteristic modes depend upon frequency. This dependency should be taken into account to get to accurate results, especially at the highest frequencies. Thus, characteristic modes need to be obtained and stored for each frequency under analysis, and then tracked with respect to the frequency. However, there are many tracking algorithms for this problem. These algorithms require finer meshing which goes up to $\lambda/100$ for very complex structures. This increases the computation time.

7.3 Further Work

The present work opens the doors to many fields in applied electromagnetics, including metamaterials. Since the systems scale is decreasing constantly, the miniaturization challenge is very appealing for researchers in the field of antennas. The theory of characteristic modes can be further investigated in antenna miniaturization as well as in isolation between antennas [139]. Nonetheless, characteristic modes can be calculated within any frequency range, then, exploiting TCM in the THz domain (including photonics and nano antennas) will be an interesting topic for us in the near future. Furthermore, because of its unique dependency on the shape, the present work based on TCM can be applied to cloaking and RCS reduction/maximisation problems. Moreover, we believe that the present work can introduce new prospects in electromagnetic compatibility through the mode isolation concept to minimise crosstalk.

Since the theory of characteristic modes has been revisited in 2007, it became the centre of interest of a big number of research teams around the world. This is why we believe that TCM will be the most suitable systematic antenna design tool, especially when associated to artificial materials such as metamaterials.

© 2015 Tous droits réservés. doc.univ-lille1.fr

Bibliography

[1] Mohammed Al-Husseini, Karim Kabalan, Ali El-Hajj, and Christos Christodoulou, "Cognitive Radio: UWB Integration and Related Antenna Design", in *New Trends in Technologies: Control, Management, Computational Intelligence and Network Systems*, Meng Joo, Ed. Sciyo, November 2010.

[2] Richard W. Ziolkowski and Aycan Erentok, "Metamaterial-based efficient electrically small antennas", pp. 2113–2130.

[3] H. Mosallaei and K. Sarabandi, "Magneto-dielectrics in electromagnetics: concept and applications", *IEEE Transactions on Antennas and Propagation*, vol. 52, no. 6, pp. 1558–1567, 2004.

[4] P.M.T. Ikonen, Stanislav I Maslovski, C.R. Simovski, and S.A Tretyakov, "On artificial magnetodielectric loading for improving the impedance bandwidth properties of microstrip antennas", *IEEE Transactions on Antennas and Propagation*, vol. 54, no. 6, pp. 1654–1662, June 2006.

[5] H. Mosallaei and K. Sarabandi, "Antenna miniaturization and bandwidth enhancement using a reactive impedance substrate", *IEEE Transactions on Antennas and Propagation*, vol. 52, no. 9, pp. 2403 – 2414, September 2004.

[6] A. Erentok and R.W. Ziolkowski, "Metamaterial-Inspired Efficient Electrically Small Antennas", *IEEE Transactions on Antennas and Propagation*, vol. 56, no. 3, pp. 691–707, 2008.

[7] A. Erentok, P.L. Luljak, and R.W. Ziolkowski, "Characterization of a volumetric metamaterial realization of an artificial magnetic conductor for antenna applications", *IEEE Transactions on Antennas and Propagation*, vol. 53, no. 1, pp. 160–172, 2005.

[8] *FEKO, www.feko.info*.

[9] D.J. Ludick, E. Lezar, and U. Jakobus, "Characteristic mode analysis of arbitrary electromagnetic structures using FEKO", in *2012 International Conference on Electromagnetics in Advanced Applications (ICEAA)*, pp. 208–211.

© 2015 Tous droits réservés. doc.univ-lille1.fr

Thèse de Mhamad Hassanein Rabah, Lille 1, 2015

[10] E. Antonino-Daviu, M. Cabedo-Fabres, M. Gallo, M. Ferrando-Bataller, and M. Bozzetti, "Design of a multimode MIMO antenna using characteristic modes", in *3rd European Conference on Antennas and Propagation, 2009. EuCAP 2009*, March 2009, pp. 1840 –1844.

[11] L. J. Chu, "Physical Limitations of Omni-Directional Antennas", *Journal of Applied Physics*, vol. 19, no. 12, pp. 1163, 1948.

[12] "Telice: Moyen d'essais CEM website: http://telice.univ-lille1.fr (online version septembre 2015)".

[13] J.Mitola, *J. Mitola, ìCognitive Radio an Integrated Agent Architecture for Software Defined Radio,î PhD thesis, KTH Royal Institute of Technology, Stockholm, Sweden, 2000.*, PhD thesis, Royale institute of technology(KTH), Stockholm, Sweden.

[14] J. Mitola, "Cognitive radio for flexible mobile multimedia communications", in *(MoMuC '99) 1999 IEEE International Workshop on Mobile Multimedia Communications, 1999*, 1999, pp. 3–10.

[15] B. Le D. Maldonado, "Cognitive radio applications to dynamic spectrum allocation: a discussion and an illustrative example", pp. 597 – 600, 2005.

[16] M. A. Stuchly, *Modern Radio Science 1999*, Wiley, September 1999.

[17] Jacques Palicot, *Radio Engineering: From Software Radio to Cognitive Radio*, John Wiley & Sons, January 2013.

[18] Ying-Chang Liang, Kwang-Cheng Chen, G.Y. Li, and P. Mahonen, "Cognitive Radio Networking and Communications: An Overview", *IEEE Transactions on Vehicular Technology*, vol. 60, no. 7, pp. 3386 –3407, September 2011.

[19] M. Cabedo-Fabres, E. Antonino-Daviu, A. Valero-Nogueira, and M.F. Bataller, "The Theory of Characteristic Modes Revisited: A Contribution to the Design of Antennas for Modern Applications", *IEEE Antennas and Propagation Magazine*, vol. 49, no. 5, pp. 52 –68, October 2007.

[20] M. Vogel, G. Gampala, D. Ludick, U. Jakobus, and C.J. Reddy, "Characteristic Mode Analysis: Putting Physics back into Simulation", *IEEE Antennas and Propagation Magazine*, vol. 57, no. 2, pp. 307–317, April 2015.

[21] Yuandan Dong and T. Itoh, "Metamaterial-Based Antennas", *Proceedings of the IEEE*, vol. 100, no. 7, pp. 2271–2285, July.

[22] R. C. Hansen and Mary Burke, "Antennas with magneto-dielectrics", *Microwave and Optical Technology Letters*, vol. 26, no. 2, pp. 75–78, 2000.

© 2015 Tous droits réservés. doc.univ-lille1.fr

Thèse de Mhamad Hassanein Rabah, Lille 1, 2015

[23] R.W. Ziolkowski and A. Erentok, "At and below the chu limit: passive and active broad bandwidth metamaterial-based electrically small antennas", *IET Microwaves, Antennas Propagation*, vol. 1, no. 1, pp. 116–128, 2007.

[24] Divitha Seetharamdoo, Ronan Sauleau, Kouroch Mahdjoubi, and Anne-Claude Tarot, "Effective parameters of resonant negative refractive index metamaterials: Interpretation and validity", *Journal of Applied Physics*, vol. 98, no. 6, pp. 063505, September 2005.

[25] Y. Tawk, M. Bkassiny, G. El-Howayek, S.K. Jayaweera, K. Avery, and C.G. Christodoulou, "Reconfigurable front-end antennas for cognitive radio applications", *IET Microwaves, Antennas Propagation*, vol. 5, no. 8, pp. 985–992, 2011.

[26] P.S. Hall, P. Gardner, and A. Faraone, "Antenna Requirements for Software Defined and Cognitive Radios", *Proceedings of the IEEE*, vol. 100, no. 7, pp. 2262–2270, 2012.

[27] P.S. Hall, P. Gardner, J. Kelly, E. Ebrahimi, M.R. Hamid, F. Ghanem, F.J. Herraiz-Martinez, and D. Segovia-Vargas, "Reconfigurable antenna challenges for future radio systems", in *3rd European Conference on Antennas and Propagation, 2009. EuCAP 2009*, March 2009, pp. 949 –955.

[28] Y. Hur, J. Park, W. Woo, K. Lim, C.-H. Lee, H.S. Kim, and J. Laskar, "A wideband analog multi-resolution spectrum sensing (MRSS) technique for cognitive radio (CR) systems", in *2006 IEEE International Symposium on Circuits and Systems, 2006. ISCAS 2006. Proceedings*, 2006, pp. 4 pp.–.

[29] J. Laskar, R. Mukhopadhyay, Y. Hur, C.-H. Lee, and K. Lim, "Reconfigurable RFICs and modules for cognitive radio", in *2006 Topical Meeting on Silicon Monolithic Integrated Circuits in RF Systems, 2006. Digest of Papers*, 2006, pp. 4 pp.–.

[30] H. Harada, "A Software Defined Cognitive Radio Prototype", in *IEEE 18th International Symposium on Personal, Indoor and Mobile Radio Communications, 2007. PIMRC 2007*, 2007, pp. 1–5.

[31] P. Gardner, M.R. Hamid, P.S. Hall, J. Kelly, F. Ghanem, and E. Ebrahimi, "Reconfigurable Antennas for Cognitive Radio: Requirements and Potential Design Approaches", in *2008 Institution of Engineering and Technology Seminar on Wideband, Multiband Antennas and Arrays for Defence or Civil Applications*, 2008, pp. 89–94.

[32] J.S. McLean, "A re-examination of the fundamental limits on the radiation Q of electrically small antennas", *IEEE Transactions on Antennas and Propagation*, vol. 44, no. 5, pp. 672–, 1996.

© 2015 Tous droits réservés. doc.univ-lille1.fr

Thèse de Mhamad Hassanein Rabah, Lille 1, 2015

[33] Y. Tawk, J. Costantine, K. Avery, and C.G. Christodoulou, "Implementation of a Cognitive Radio Front-End Using Rotatable Controlled Reconfigurable Antennas", *IEEE Transactions on Antennas and Propagation*, vol. 59, no. 5, pp. 1773–1778, 2011.

[34] E. Erfani, J. Nourinia, C. Ghobadi, M. Niroo-Jazi, and T.A. Denidni, "Design and Implementation of an Integrated UWB/Reconfigurable-Slot Antenna for Cognitive Radio Applications", *IEEE Antennas and Wireless Propagation Letters*, vol. 11, pp. 77–80, 2012.

[35] G. Augustin and T. A. Denidni, "An Integrated Ultra Wideband/Narrow Band Antenna in Uniplanar Configuration for Cognitive Radio Systems", *IEEE Transactions on Antennas and Propagation*, vol. 60, no. 11, pp. 5479 –5484, November 2012.

[36] Yvan Duroc and Ali Imran, "UWB Antennas: Design and Modeling", in *Ultra Wideband*, Boris Lembrikov, Ed. Sciyo, August 2010.

[37] K.P. Ray and Y. Ranga, "Ultrawideband Printed Elliptical Monopole Antennas", *IEEE Transactions on Antennas and Propagation*, vol. 55, no. 4, pp. 1189 –1192, April 2007.

[38] Jianjun Liu, K.P. Esselle, S.G. Hay, and Shunshi Zhong, "Achieving Ratio Bandwidth of 25:1 From a Printed Antenna Using a Tapered Semi-Ring Feed", *IEEE Antennas and Wireless Propagation Letters*, vol. 10, pp. 1333 –1336, 2011.

[39] Jianjun Liu, Shunshi Zhong, and K.P. Esselle, "A Printed Elliptical Monopole Antenna With Modified Feeding Structure for Bandwidth Enhancement", *IEEE Transactions on Antennas and Propagation*, vol. 59, no. 2, pp. 667 –670, February 2011.

[40] M. Al-Husseini, Y. Tawk, C.G. Christodoulou, K.Y. Kabalan, and A. El-Hajj, "A reconfigurable cognitive radio antenna design", in *2010 IEEE Antennas and Propagation Society International Symposium (APSURSI)*, 2010, pp. 1–4.

[41] Y. Tawk and C.G. Christodoulou, "A New Reconfigurable Antenna Design for Cognitive Radio", *IEEE Antennas and Wireless Propagation Letters*, vol. 8, pp. 1378 –1381, 2009.

[42] Jie-Bang Yan and J.T. Bernhard, "Implementation of a Frequency-Agile MIMO Dielectric Resonator Antenna", *IEEE Transactions on Antennas and Propagation*, vol. 61, no. 7, pp. 3434–3441, July 2013.

© 2015 Tous droits réservés. doc.univ-lille1.fr

Thèse de Mhamad Hassanein Rabah, Lille 1, 2015

[43] Shou Hui Zheng, XiongYing Liu, and M.M. Tentzeris, "Optically controlled reconfigurable band-notched UWB antenna for cognitive radio systems", *Electronics Letters*, vol. 50, no. 21, pp. 1502–1504, October 2014.

[44] H. Rajagopalan, J.M. Kovitz, and Y. Rahmat-Samii, "MEMS Reconfigurable Optimized E-Shaped Patch Antenna Design for Cognitive Radio", *IEEE Transactions on Antennas and Propagation*, vol. 62, no. 3, pp. 1056–1064, March 2014.

[45] R. Hussain and M.S. Sharawi, "A Cognitive Radio Reconfigurable MIMO and Sensing Antenna System", *IEEE Antennas and Wireless Propagation Letters*, vol. 14, pp. 257–260, 2015.

[46] X. L Liang, S.-S. Zhong, W. Wang, and F.-W. Yao, "Printed annular monopole antenna for ultra-wideband applications", *Electronics Letters*, vol. 42, no. 2, pp. 71–72, 2006.

[47] Tan-Phu Vuong, Anthony Ghiotto, Yvan Duroc, and Smail Tedjini, "Design and characteristics of a small U-slotted planar antenna for IR-UWB", *Microwave and Optical Technology Letters*, vol. 49, no. 7, pp. 1727–1731, 2007.

[48] Xiao-Rong Yan, Shun-Shi Zhong, and Xiao-Rong Tang, "Compact printed monopole antenna with extremely wide bandwidth", in *IET Conference on Wireless, Mobile and Sensor Networks, 2007. (CCWMSN07)*, December 2007, pp. 337 –339.

[49] F. Keshmiri, R. Chandra, and C. Craeye, "Design of a UWB antenna with stabilized radiation pattern", in *IEEE Antennas and Propagation Society International Symposium, 2008. AP-S 2008*, July 2008, pp. 1–4.

[50] T. Aboufoul, A. Alomainy, and C. Parini, "Reconfiguring UWB Monopole Antenna for Cognitive Radio Applications Using GaAs FET Switches", *IEEE Antennas and Wireless Propagation Letters*, vol. 11, pp. 392–394, 2012.

[51] E.J.B. Rodrigues, H.W.C. Lins, and A.G. D'Assuncao, "Reconfigurable circular ring patch antenna for UWB and cognitive radio applications", in *2014 8th European Conference on Antennas and Propagation (EuCAP)*, April 2014, pp. 2744–2748.

[52] J.L. Volakis, Chi-Chih-Chen, Ming Lee, B. Kramer, and D. Psychoudakis, "Miniaturization methods for narrowband and ultrawideband antennas", in *IEEE International Workshop on Antenna Technology: Small Antennas and Novel Metamaterials, 2005. IWAT 2005*, March 2005, pp. 119 – 121.

© 2015 Tous droits réservés. doc.univ-lille1.fr

Thèse de Mhamad Hassanein Rabah, Lille 1, 2015

[53] A.D. Yaghjian and S.R. Best, "Impedance, bandwidth, and Q of antennas", *IEEE Transactions on Antennas and Propagation*, vol. 53, no. 4, pp. 1298–1324, April 2005.

[54] M. Gustafsson, M. Cismasu, and B. L G Jonsson, "Physical Bounds and Optimal Currents on Antennas", *IEEE Transactions on Antennas and Propagation*, vol. 60, no. 6, pp. 2672–2681, 2012.

[55] Constantine BALANIS, *Antenna Theory , analysis and design*, John Wiley & Sons, Inc., 2005.

[56] Viktor G Veselago, "THE ELECTRODYNAMICS OF SUBSTANCES WITH SIMULTANEOUSLY NEGATIVE VALUES OF ϵ AND Îij", vol. 10, no. 4, pp. 509–514.

[57] J.B. Pendry, A. J. Holden, D. J. Robbins, and W. J. Stewart, "Magnetism from conductors and enhanced nonlinear phenomena", vol. 47, no. 11, pp. 2075–2084.

[58] D. R. Smith, Willie J. Padilla, D. C. Vier, S. C. Nemat-Nasser, and S. Schultz, "Composite Medium with Simultaneously Negative Permeability and Permittivity", *Physical Review Letters*, vol. 84, no. 18, pp. 4184–4187, May 2000.

[59] Eric Lheurette, Seetharamdoo Divitha, and Sauviac. Bruno, *Metamaterials and wave control Chapter3: Metamaterials for Non-Radiative Microwave Functions and Antennas.*, 2013.

[60] Christian Sohl, Mats Gustafsson, and Gerhard Kristensson, "Physical limitations on broadband scattering by heterogeneous obstacles", vol. 40, no. 36, pp. 11165.

[61] C. Sohl, M. Gustafsson, and G. Kristensson, "Physical limitations on antennas #x2014; isoperimetric inequalities and the effect of metamaterials", in *19th International Conference on Applied Electromagnetics and Communications, 2007. ICECom 2007*, pp. 1–5.

[62] Richard W. Ziolkowski and Student Member, "Application of double negative materials to increase the power radiated by electrically small antennas", pp. 2626–2640.

[63] M. Karkkainen, Murat Ermutlu, S. Maslovski, P. Ikonen, and Sergei Tretyakov, "Numerical simulations of patch antennas with stacked split-ring resonators as artificial magnetic substrates", in *IEEE International Workshop on Antenna Technology: Small Antennas and Novel Metamaterials, 2005. IWAT 2005*, pp. 395–398.

[64] X. Begaud and A.C. Lepage, "Wideband low profile antennas and metamaterials", in *Microwave Optoelectronics Conference (IMOC), 2011 SBMO/IEEE MTT-S International*, October 2011, pp. 406–411.

© 2015 Tous droits réservés. doc.univ-lille1.fr

Thèse de Mhamad Hassanein Rabah, Lille 1, 2015

[65] J.J. Adams and J.T. Bernhard, "A Modal Approach to Tuning and Bandwidth Enhancement of an Electrically Small Antenna", *IEEE Transactions on Antennas and Propagation*, vol. 59, no. 4, pp. 1085–1092, April 2011.

[66] M. Capek, P. Hazdra, and J. Eichler, "A method for the evaluation of radiation q based on modal approach", vol. 60, no. 10, pp. 4556–4567.

[67] J.L.T. Ethier and D.A. McNamara, "Antenna Shape Synthesis Without Prior Specification of the Feedpoint Locations", *IEEE Transactions on Antennas and Propagation*, vol. 62, no. 10, pp. 4919–4934, October 2014.

[68] Miloslav Capek, Lukas Jelinek, Guy A. E. Vandenbosch, and Pavel Hazdra, "A Scheme for Stored Energy Evaluation and a Comparison with Contemporary Techniques", *arXiv:1403.0572 [physics]*, March 2014.

[69] Jonathan Ethier, Eric Lanoue, and Derek McNamara, "MIMO handheld antenna design approach using characteristic mode concepts", *Microwave and Optical Technology Letters*, vol. 50, no. 7, pp. 1724–1727, 2008.

[70] R. Martens and D. Manteuffel, "Systematic design method of a mobile multiple antenna system using the theory of characteristic modes", *IET Microwaves, Antennas Propagation*, vol. 8, no. 12, pp. 887–893, September 2014.

[71] M. Bouezzeddine and W.L. Schroeder, "Parametric study on capacitive and inductive couplers for exciting characteristic modes on CPE", in *2014 8th European Conference on Antennas and Propagation (EuCAP)*, pp. 2731–2735.

[72] R. Garbacz and R. Turpin, "A generalized expansion for radiated and scattered fields", *IEEE Transactions on Antennas and Propagation*, vol. 19, no. 3, pp. 348 – 358, 1971.

[73] R. Harrington and J. Mautz, "Theory of characteristic modes for conducting bodies", *IEEE Transactions on Antennas and Propagation*, vol. 19, no. 5, pp. 622 – 628, September 1971.

[74] Roger F. Harrington, J.R. Mautz, and Yu Chang, "Characteristic modes for dielectric and magnetic bodies", *IEEE Transactions on Antennas and Propagation*, vol. 20, no. 2, pp. 194–198, 1972.

[75] J.R. Mautz and Roger F. Harrington, "Modal analysis of loaded n-port scatterers", vol. 21, no. 2, pp. 188–199.

[76] Roger F. Harrington and J.R. Mautz, "Control of radar scattering by reactive loading", *IEEE Transactions on Antennas and Propagation*, vol. 20, no. 4, pp. 446–454, July 1972.

© 2015 Tous droits réservés. doc.univ-lille1.fr

Thèse de Mhamad Hassanein Rabah, Lille 1, 2015

[77] M. Capek, P. Hamouz, P. Hazdra, and J. Eichler, "Implementation of the Theory of Characteristic Modes in MATLAB", *IEEE Antennas and Propagation Magazine*, vol. 55, no. 2, pp. 176–189, 2013.

[78] E. Safin and D. Manteuffel, "Reconstruction of the Characteristic Modes on an Antenna Based on the Radiated Far Field", *IEEE Transactions on Antennas and Propagation*, vol. 61, no. 6, pp. 2964–2971, June 2013.

[79] *Yikai Chen, Chao-Fu Wang, Characteristic Modes: Theory and Applications in Antenna Engineering- Wiley, 2015*.

[80] Ethier Jonathan, *Antenna Shape Synthesis Using Characteristic Mode Concepts*, PhD thesis, Ottawa-Carleton Institute for Electrical and Computing Engineering School of Electrical Engineering and Computer Science Faculty of Engineering University of Ottawa, Canada, 2012.

[81] Roger F. Harrington and J.R. Mautz, "Computation of characteristic modes for conducting bodies", *IEEE Transactions on Antennas and Propagation*, vol. 19, no. 5, pp. 629–639, 1971.

[82] Roger F. Harrington, *Field Computation by Moment Methods*, Oxford University Press, USA, 1993.

[83] T.E. Gilles, C. Craeye, and M. Piette, "E-MFIE Formulation for Arbitrary PEC Sheets", *IEEE Transactions on Antennas and Propagation*, vol. 60, no. 8, pp. 3744–3753, August 2012.

[84] Edmund K. Miller, *Integral Equation Solutions of Three-dimensional Scattering Problems*, MB Assoc., 1970.

[85] T.K. Wu and L.L Tsai, "Scattering from Arbitrarily-Shaped Lossy Dielectric Bodies of Revolution, Radio Sci., Vol. 12, No. 5, 1977, pp. 709-718. [51)".

[86] P. Yla-Oijala and M. Taskinen, "Efficient formulation of closed-form Green's functions for general electric and magnetic sources in multilayered media", *IEEE Transactions on Antennas and Propagation*, vol. 51, no. 8, pp. 2106–2115, August 2003.

[87] I.-Ting Chiang and Weng Cho Chew, "A Coupled PEC-TDS Surface Integral Equation Approach for Electromagnetic Scattering and Radiation From Composite Metallic and Thin Dielectric Objects", *IEEE Transactions on Antennas and Propagation*, vol. 54, no. 11, pp. 3511–3516, November 2006.

© 2015 Tous droits réservés. doc.univ-lille1.fr

Thèse de Mhamad Hassanein Rabah, Lille 1, 2015

[88] X. Dardenne and C. Craeye, "Method of Moments Simulation of Infinitely Periodic Structures Combining Metal With Connected Dielectric Objects", *IEEE Transactions on Antennas and Propagation*, vol. 56, no. 8, pp. 2372–2380, August 2008.

[89] D. Tihon, V. Sozio, N.A. Ozdemir, M. Albani, and C. Craeye, "Efficient numerical analysis of 3d periodic metamaterials: Multilayer approach and eigenmode analysis", in *2015 9th European Conference on Antennas and Propagation (EuCAP)*, April 2015, pp. 1–5.

[90] H. Alroughani, J.L.T. Ethier, and D.A. McNamara, "Observations on computational outcomes for the characteristic modes of dielectric objects", in *2014 IEEE Antennas and Propagation Society International Symposium (APSURSI)*, pp. 844–845.

[91] Nilufer A. Ozdemir and Christophe Craeye, "An integral-equation method using interstitial currents devoted to the analysis of multilayered periodic structures with complex inclusions", *arXiv:1408.3826 [physics]*, August 2014, arXiv: 1408.3826.

[92] Sergey Makarov, *Antenna and EM Modeling with Matlab*, Wiley-Interscience, 1 edition edition.

[93] S.M. Rao, D. Wilton, and A.W. Glisson, "Electromagnetic scattering by surfaces of arbitrary shape", *IEEE Transactions on Antennas and Propagation*, vol. 30, no. 3, pp. 409–418, May 1982.

[94] D. Seetharamdoo, *Étude des métamatériaux à indice de réfraction négatif : paramètres effectifs et applications antennaires potentielles*, PhD thesis, Université de Rennes I, Rennes, France, 2006.

[95] R.T. Maximidis, C.L. Zekios, T.N. Kaifas, E.E. Vafiadis, and G.A. Kyriacou, "Characteristic mode analysis of composite metal-dielectric structure, based on surface integral equation/moment method", in *2014 8th European Conference on Antennas and Propagation (EuCAP)*, pp. 2822–2826.

[96] H. Alroughani, J.L.T. Ethier, and D.A. McNamara, "On the classification of characteristic modes, and the extension of sub-structure modes to include penetrable material", in *2014 International Conference on Electromagnetics in Advanced Applications (ICEAA)*, pp. 159–162.

[97] D.J. Ludick, U. Jakobus, and M. Vogel, "A tracking algorithm for the eigenvectors calculated with characteristic mode analysis", in *2014 8th European Conference on Antennas and Propagation (EuCAP)*, pp. 569–572.

© 2015 Tous droits réservés. doc.univ-lille1.fr

Thèse de Mhamad Hassanein Rabah, Lille 1, 2015

[98] P. Hamouz M. Capek, P. Hazdra and J. Eichler, "A Method for tracking characteristic numbers and vectors", *Progress In Electromagnetics Research B, Vol. 33, 115-134, 2011.*

[99] N. Surittikul and R.G. Rojas, "Time domain method of characteristic modes for the analysis/design of reconfigurable antennas", in *2005 IEEE Antennas and Propagation Society International Symposium*, vol. 2B, pp. 585–588 vol. 2B.

[100] Ricardo Marqués, Francisco Medina, and Rachid Rafii-El-Idrissi, "Role of bianisotropy in negative permeability and left-handed metamaterials", *Physical Review B*, vol. 65, no. 14, pp. 144440, April 2002.

[101] Sergei Tretyakov, *Analytical modeling in applied electromagnetics*, Artech House, Boston, 2003.

[102] Robert E. Collin and Francis J. Zucker, *Antenna theory: Chapter 11 : The loop antenna for transmission and reception par Ronold W. King.*, McGraw Hill Book Company, 1969.

[103] Ari Sihvola, "Dielectric polarization and particle shape effects", vol. 2007, pp. e45090.

[104] Yang Hao and Raj Mittra, *FDTD Modeling of Metamaterials: Theory and Applications*, Artech House, 1 edition edition.

[105] James R. James and P.S. Hall, *Handbook of Microstrip Antennas*, P. Peregrinus, 1989.

[106] A.K. Skrivervik, J.-F. Zürcher, O. Staub, and J.R. Mosig, "PCS antenna design: the challenge of miniaturization", *IEEE Antennas and Propagation Magazine*, vol. 43, no. 4, pp. 12–27, August 2001.

[107] J. McLean and R. Sutton, "Optimum core parameters for an electrically-small TE1 (loop) mode antenna with an inhomogeneous magneto-dielectric core", in *Antennas and Propagation Conference (LAPC), 2010 Loughborough*, November 2010, pp. 281–284.

[108] L. Kempel, B. Shanker, J. Xiao, and Stephen W. Schneider, "Radiation by a magneto-dielectric loaded patch antenna", in *Antennas Propagation Conference, 2009. LAPC 2009. Loughborough*, November 2009, pp. 745–748.

[109] F. Bilotti, L. Di Palma, D. Ramaccia, A. Toscano, L. Vegni, D. Ates, and E. Ozbay, "Extracting power from sub-wavelength apertures by using electrically small resonators: Phenomenology, modeling, and applications", in *Antennas and Propagation Conference (LAPC), 2012 Loughborough*, November 2012, pp. 1–4.

© 2015 Tous droits réservés. doc.univ-lille1.fr

Thèse de Mhamad Hassanein Rabah, Lille 1, 2015

[110] M. RABAH, D. Seetharamdoo, M. Berbineau, and A. de Lustrac, "New metrics for artificial magnetism from metal-dielectric metamaterial based on the theory of characteristic modes", vol. PP, no. 99, pp. 1–1.

[111] H.A. Wheeler, "Fundamental limitations of small antennas", vol. 35, no. 12, pp. 1479–1484.

[112] R.C. Hansen and R.E. Collin, "A New Chu Formula for Q", *IEEE Antennas and Propagation Magazine*, vol. 51, no. 5, pp. 38–41, October 2009.

[113] H.L. Thal, "New Radiation Limits for Spherical Wire Antennas", *IEEE Transactions on Antennas and Propagation*, vol. 54, no. 10, pp. 2757–2763, October 2006.

[114] M. Capek, L. Jelinek, and P. Hazdra, "On the Functional Relation Between Quality Factor and Fractional Bandwidth", *IEEE Transactions on Antennas and Propagation*, vol. 63, no. 6, pp. 2787–2790, June 2015.

[115] M. Gustafsson, C. Sohl, and G. Kristensson, "Illustrations of new physical bounds on linearly polarized antennas", *Antennas and Propagation, IEEE Transactions on*, vol. 57, no. 5, pp. 1319–1327, May 2009.

[116] Mats Gustafsson, Christian Sohl, and Gerhard Kristensson, "Physical limitations on antennas of arbitrary shape", *Proceedings of the Royal Society A: Mathematical, Physical and Engineering Science*, vol. 463, no. 2086, pp. 2589–2607, October 2007.

[117] Daniel Sjoberg, "Variational principles for the static electric and magnetic polarizabilities of anisotropic media with perfect electric conductor inclusions", *Journal of Physics A: Mathematical and Theoretical*, vol. 42, no. 33, pp. 335403, 2009.

[118] J. Chalas, K. Sertel, and J.L. Volakis, "Q limits for arbitrary shape antennas using characteristic modes", in *2012 6th European Conference on Antennas and Propagation (EUCAP)*, March 2012, pp. 1672–1673.

[119] A. Krewski, "Systematic design of multiport antennas for MIMO-enabled mobile wireless terminals. Ph.D dissertation. Universitaẗ Duisburg-Essen 2014.".

[120] M. Capek, L. Jelinek, P. Hazdra, and J. Eichler, "The Measurable Q Factor and Observable Energies of Radiating Structures", *IEEE Transactions on Antennas and Propagation*, vol. 62, no. 1, pp. 311–318, January 2014.

[121] Brandan Thomas Strojny, *Excitation and Analysis of Characteristic Modes on Complex Antenna Structures*, Phd. thesis from the ohio state university, 2011.

[122] "EMCoS, www.emcos.com".

© 2015 Tous droits réservés. doc.univ-lille1.fr

Thèse de Mhamad Hassanein Rabah, Lille 1, 2015

[123] E.A. Elghannai and R.G. Rojas, "Study of the total Q of antennas in terms of modal Qn provided by Characteristic Modes Theory", in *2014 IEEE Antennas and Propagation Society International Symposium (APSURSI)*, July 2014, pp. 49–50.

[124] Khaled Ahmad Obeidat, *Design Methodology for Wideband Electrically Small Antennas (ESA) Based on the Theory of Characteristic Modes (CM)*, PhD thesis, The Ohio State University, 2010.

[125] P. Hazdra, M. Čapek, P. Hamouz, and M. Mazánek, "Advanced modal techniques for microstrip patch antenna analysis", in *ICECom, 2010 Conference Proceedings*, September 2010, pp. 1–6.

[126] M.H. Rabah, D. Seetharamdoo, and M. Berbineau, "Modal study of electrically small patch antennas on dielectric, magnetic and reactive impedance metamaterial substrates", in *Antennas and Propagation Conference (LAPC), 2014 Loughborough*, pp. 545–548.

[127] C. Niamien, S. Collardey, A. Sharaiha, and K. Mahdjoubi, "Compact Expressions for Efficiency and Bandwidth of Patch Antennas Over Lossy Magneto-Dielectric Materials", *IEEE Antennas and Wireless Propagation Letters*, vol. 10, pp. 63–66, 2011.

[128] P.M.T. Ikonen, K.N. Rozanov, AV. Osipov, P. Alitalo, and S.A Tretyakov, "Magnetodielectric Substrates in Antenna Miniaturization: Potential and Limitations", *IEEE Transactions on Antennas and Propagation*, vol. 54, no. 11, pp. 3391–3399, November 2006.

[129] "ANSYS HFSS www.ansys.com".

[130] Chan Hwang See, H.I Hraga, R.A Abd-Alhameed, N.J. McEwan, J.M. Noras, and P.S. Excell, "A Low-Profile Ultra-Wideband Modified Planar Inverted-F Antenna", *IEEE Transactions on Antennas and Propagation*, vol. 61, no. 1, pp. 100–108, January 2013.

[131] C.-C. Chen E. Yetisir, "Low-Profile UWB 2-Port Antenna With High Isolation", *Antennas and Wireless Propagation Letters, IEEE*, vol. 13, pp. 55–58, 2014.

[132] Tharaka Dissanayake, Karu Esselle, and Yuehe Ge, "A printed triangular-ring antenna with a 2:1 bandwidth", *Microwave and Optical Technology Letters*, vol. 44, no. 1, pp. 51–53, 2005.

[133] Yuan-Ming Cai, Ke Li, Ying-Zeng Yin, and Wei Hu, "Broadband Circularly Polarized Printed Antenna With Branched Microstrip Feed", *IEEE Antennas and Wireless Propagation Letters*, vol. 13, pp. 674–677, 2014.

© 2015 Tous droits réservés. doc.univ-lille1.fr

Thèse de Mhamad Hassanein Rabah, Lille 1, 2015

[134] Jianxin Liang, C.C. Chiau, Xiaodong Chen, and C.G. Parini, "Study of a printed circular disc monopole antenna for UWB systems", *IEEE Transactions on Antennas and Propagation*, vol. 53, no. 11, pp. 3500 – 3504, November 2005.

[135] Yu-Jiun Ren and Kai Chang, "An Annual Ring Antenna for UWB Communications", *IEEE Antennas and Wireless Propagation Letters*, vol. 5, no. 1, pp. 274 –276, December 2006.

[136] M. Naser-Moghadasi, R.A Sadeghzadeh, T. Sedghi, T. Aribi, and B.S. Virdee, "UWB CPW-Fed Fractal Patch Antenna With Band-Notched Function Employing Folded T-Shaped Element", *IEEE Antennas and Wireless Propagation Letters*, vol. 12, pp. 504–507, 2013.

[137] Y. Lu, Y. Huang, Y.C. Shen, and H.T. Chattha, "A further study of planar UWB monopole antennas", in *Antennas Propagation Conference, 2009. LAPC 2009. Loughborough*, November 2009, pp. 353 –356.

[138] *CST Microwave studio, www.cst.com*.

[139] M. Ayoub, "Metamaterial-Inspired Isolation Technique for Antennas: Systematic Design through Characteristic Mode Theory", Master thesis, French Institute of Science and Technology (IFSTTAR), September 2015.

© 2015 Tous droits réservés. doc.univ-lille1.fr